Study on the electrical properties of single- and multi-layer graphene nanoribbons for next generation nanoelectronics

著者	Pandey Reetu Raj
その他のタイトル	次世代ナノエレクトロニクスを志向した単層及び多層グラフェンナノリボンの電気特性に関する研究
学位授与年度	平成29年度
学位授与番号	17104甲生工第295号
URL	http://hdl.handle.net/10228/00006408

Study on the electrical properties of single- and multi-layer graphene nanoribbons for next generation nanoelectronics

A Dissertation Submitted
in Partial Fulfillment of the requirement
for the award of the Degree of

DOCTOR OF PHILOSOPHY

Submitted by
Reetu Raj Pandey

Under the Supervision of
Prof. Hirofumi Tanaka

Department of Human Intelligence Systems
Graduate School of Life Science and Systems Engineering
Kyushu Institute of Technology

March, 2017

ABSTRACT

Graphene nanoribbon (GNR) is a narrow strip of carbon atoms which has exceptional properties and are being exploited for various applications, such as in semiconductor electronics, solar cells, and sensors. However, the realization of GNR based devices still needs an extensive research to achieve the commercial specifications. This research is mainly emphasized on the synthesis of high-quality GNR from double-walled carbon nanotubes (DWNTs) and fabrication of field effect transistor (FET) devices. Moreover, the electrical transport properties were also investigated for single-layer GNR (sGNR), multi-layer GNR with and without adsorption of molecular nanoparticles. The electrical transport properties of GNR device was tuned to semiconducting with the adsorption of molecular nanoparticles.

This study demonstrates a simple and fast approach to band gap formation in sGNR using Hexaazatriphenylenehexacarbonitrile (HAT-CN6). In this process, sGNRs were synthesized by unzipping of DWNTs followed by casting the solution of HAT-CN6. HAT-CN6 on GNR forms self-assembled nanoparticle and the adsorption of nanoparticles was confirmed by AFM observation. Further, the electric property of pristine sGNR device and the device with HAT-CN6 were measured using point-contact current imaging (PCI-) AFM and also with the FET device. Thus, the adsorbed nanoparticles on sGNR forms the electron trapping sites which result in a neck-like structure of sGNR near the adsorbed region of the molecular nanoparticle. The neck region working similar to narrow width GNR (< 10 nm) allows the charge carriers passing through. Such a narrow sGNR has lateral confinement of charge carrier around the neck region hence the device turns to semiconducting. The activation energy of pristine sGNR and the sGNR with HAT-CN6 were calculated by the results of temperature change measurement as about 1.5 meV and 52 meV,

respectively. The pristine sGNR has very low activation energy as compared to the device with HAT-CN6. Thus, the device with HAT-CN6 has a large transition from semimetallic to semiconducting property. The device could have various possible application in future electronics industry due to its semiconducting property.

Moreover, the study also explains the fabrication of multi-layer GNR (mGNR) field effect transistor (FET) and control of its electrical property with the adsorption of the flat molecular nanoparticle. The stacked mGNR device shows the similar performance to the sGNR device due to lower inter layer coupling. Inter layer interaction was supposed to be lower since the turbostratic stacking of GNR was formed with CVD growth process. Next, HAT-CN6 were casted on the mGNR device to alter the electronic property of GNR. Thus, the adsorbed nanoparticles form the charge carrier trapping sites on mGNR and the channel width was narrowed due to the nanoparticles on GNR. Hence, the charge carriers are confined in a narrow channel and the device is in a transition state from semimetallic to semiconducting, which is similar to narrow width GNR. The on/off ratio and mobility of mGNR-FET device was also improved with the adsorption of the nanoparticle. The fabricated mGNR-FET device has wide area of semiconductor electronics applications in the semiconductor industry.

Furthermore, X- and Y-type junctions were also fabricated using GNRs obtained by unzipping of DWNTs. The junction of the synthesized GNR shows semiconducting property whereas the other part shows the semimetallic property. The semiconducting property at the junction was supposed to be due to change in lattice orientation at the junction of two GNRs. Such a junction can have great interest for the device and wiring application in the semiconductor industry. The semiconducting property in the several X-type junctions of wide GNRs (greater than 10 nm) was investigated.

ACKNOWLEDGEMENT

The completion of this thesis represents the opportunity to remember numerous individuals who have influenced my attitude towards the progress of research. I would like to acknowledge my debt to my professors, family, and friends.

First and foremost, I would like to thank my supervisor, Prof. Hirofumi Tanaka, for the endless hours of help, suggestions, ideas and advice during the development of the thesis and research. His continuous guidance, constructive suggestions and wholehearted supervision throughout the progress of this work, makes this thesis to be materialized. I am highly indebted to him for giving me an opportunity to work under him and for his support and suggestions. His enthusiasm, inspiration, and great efforts to explain things clearly and simply, helped a lot for me.

I would also like to express my gratitude to Prof. Takashi Morie, Associate Prof. Shyam S. Pandey, Associate Prof. Hakaru Tamukoh, Dr. Amin TermehYousefi from Kyushu Institute of Technology (Kyutech) and Dr. Masanori Eguchi from Fuzzy Logic Systems Institute for their kind encouragements, necessary advice and valuable suggestions for the success of my work.

I am also very thankful to Prof. Yoshihiro Kobayashi and Asst. Prof. Ryota Negishi of Osaka University for their kind collaboration and time to time suggestions for the improvement of research. At the same time, I would like to thank all of the office members from Kyutech for their kind support, cooperation and encouragement during the course of the work.

Above all, I would like to thank my friends Dr. Ajay Kumar Barnwal, Faisal Budiman and all other lab mates who gave me endless support and provided me with an opportunity to reach this far with my studies. Their constant encouragement has always helped me to walk over all the hurdles. It's just not possible to express my gratitude and indebtedness towards them in words.

Last but not least, I would like to honor special thanks to my father, Kameshwar Prasad Pandey, mother Malti Devi Pandey, my wife Jyoti Pandey and brother Brikh Raj Pandey, who have supported me throughout my life. I would also like to express my true gratitude and love to my wife for her greatness, support, and encouragement since she came into my life.

Table of Contents

CHAPTER 1

Introduction

1.1 Introduction to graphene

A single atomic layer of graphite known as graphene has gained wide attention due to its intrinsic high electrical conductivity, large surface area, excellent mechanical strength, flexibility, and exceptional catalytic properties. These properties of graphene have been already investigated theoretically before 60-70 years,[1, 2] but graphene was supposed to be thermodynamically unstable at room temperature.[3] The first isolated graphene was observed by Geim and Novoselov. It is still an early stage of commercial production of graphene, and an intensive research continues to investigate new techniques that can be applied to make it available at industrial scale. There has been an intense research going on and an enormous number of publications on graphene-based nanomaterials to explore and tackle the challenges for numerous applications of graphene. Graphite is the source of graphene which is the combination of an infinite 3-D crystal. It is stacked layers of graphene that interact with each layer weakly through van der Waals force. Graphite can be obtained naturally in an abundant amount and can be synthesized artificially by thermolytic processes, such as the production of highly oriented pyrolytic graphite. In spite of mechanical exfoliation to obtain single-layer graphene, there are several other techniques. Some of the techniques to obtain the graphene are epitaxial technique, solution-based graphene, and substrate-based with chemical vapor deposition (CVD) grown graphene.[4]

This new class of material graphene has opened the wide range of research possibility in low-dimensional physics. It is conceptually a new class of materials with one atomic thick layer. Single-

layer graphene might be one of the thinnest material has ever been observed. The simplest technique that makes the production of graphene easy was the way of spotting the single-layer graphene among the thicker flakes and was obtained by Geim and Novoselov. Observing the single-layer of graphene was the biggest task at the very first stage. One atomic thick layer of graphene are usually invisible but it changes the color of SiO_2 at the top of the wafer which makes it visible and can be measured. The mother of graphene and it's all forms are shown in **Figure 1.1.**

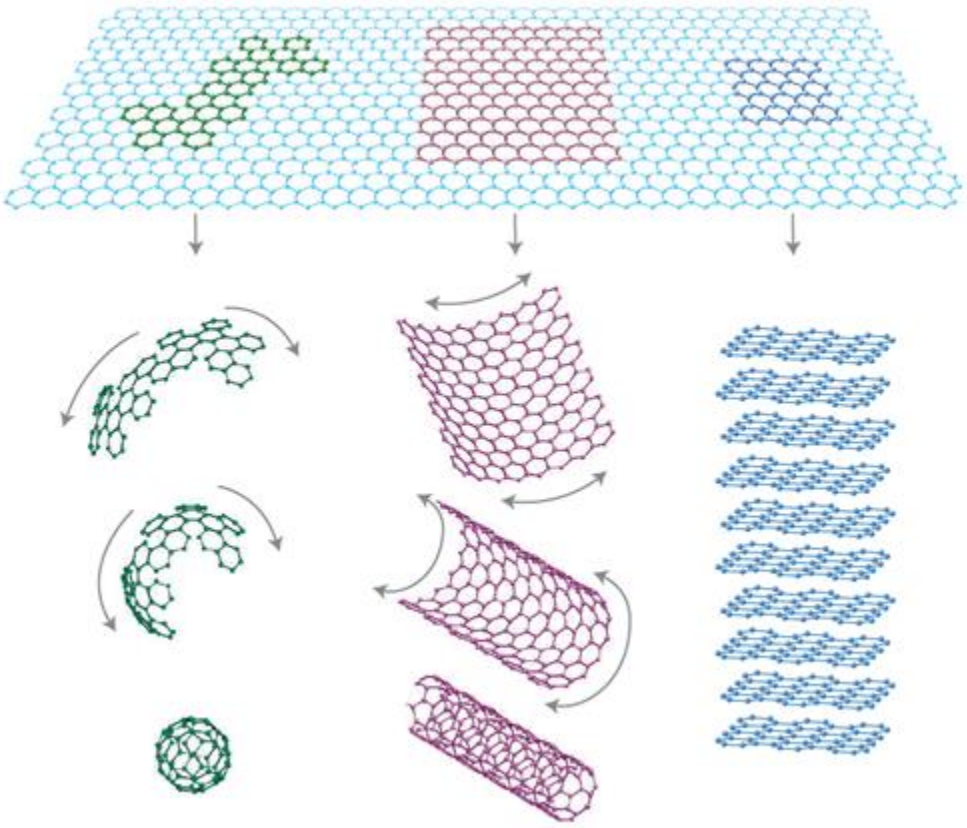

Figure 1.1 Mother of all graphitic forms, a basic building block to form 0D fullerene, 1D nanotube and stacked 3D graphite.[5]

The electrical property of graphene is semimetallic with zero band gap and can be named as zero band gap semiconductor. In comparison with most of the materials, charge carrier transport property of graphene is different. The velocity of charge carriers remains constant throughout the

bands and does not decrease at the top of the valence band and the bottom of the conduction band, unlike other material. It has a high conductivity which makes it suitable for wiring, interconnects or transistor applications. It is an inert material which makes it possible to obtain on a large area with low defect densities and low electronic scattering rates.[5] Therefore, graphene literally exhibits exceptionally high carrier mobility, offering the tantalizing possibility of all-carbon electronics,[6, 7] including spintronics,[8, 9] chemical and biological sensing,[10, 11] nanoelectromechanical systems[12] and energy storage.[13]

1.2 Introduction to graphene nanoribbon

Over the past few years, graphene has gained wide attention among the all known materials with large potential applications in material science,[14] nanoelectronics,[5] nanophotonics and nanomechanics. It is an exceptional material with carrier mobility of 25000 cm^2 $V^{-1}s^{-1}$ which enables the advancement in electronics with the fabrication of transistors having smaller channel resistance compared to their Si counterparts.[15] However, many of the electronics applications are handicapped due to special confinement of graphene, the zero band gap, and semimetallic behavior. The zero band gap of graphene limits the room temperature operation of transistors and remains the challenging topic. Numerous effort has been made to introduce the band gap in graphene by various methods but the device performance is not well improved.[16] Some theoretical and experimental results suggest that the strip of graphene less than 10 nm width can be used to open the bandgap in graphene for electronic device applications, but it has the limitation of edge state control which contributes the bandgap formation.[17] It has also been reported that the band gap of graphene nanoribbons (GNRs) is inversely proportional to the ribbon width which is due to quasi-one-dimensional carrier confinement in narrow width GNRs. The electronic property of quasi-one-dimensional structure of GNRs makes it different from that of its counterpart

graphene (2-D material). Thus, GNR becomes one of the important candidate materials for the next generation semiconductor electronics possessing various applications like transistors, sensors and the optoelectronics devices. The methods to obtain GNR is discussed in the following section.

1.3 Recent progress in GNR synthesis

Graphene nanoribbon is a narrow width strip of graphene which has attracted wide attention among the researchers due to its potential applications in various fields. The focus on GNR is made due to some limitation of graphene, in spite of very high carrier mobility in graphene. It cannot be used for room temperature application of transistors due to its zero band gap. Whereas the band gap in GNR can be obtained by various engineering steps, like doping with foreign molecules, forming nanomesh in the graphene sheet, cutting down graphene sheet to narrow width GNR and many other methods. Thus, the narrow width GNR can be very useful in semiconductor technology for transistor and wiring applications. Especially the semiconductor industry is in high demand of new material to replace the silicon technology as it is approaching the limit of miniaturization. Width-dependent energy gap of GNR[18] was reported by Melinda et al. which is shown in **Figure 1.2**.

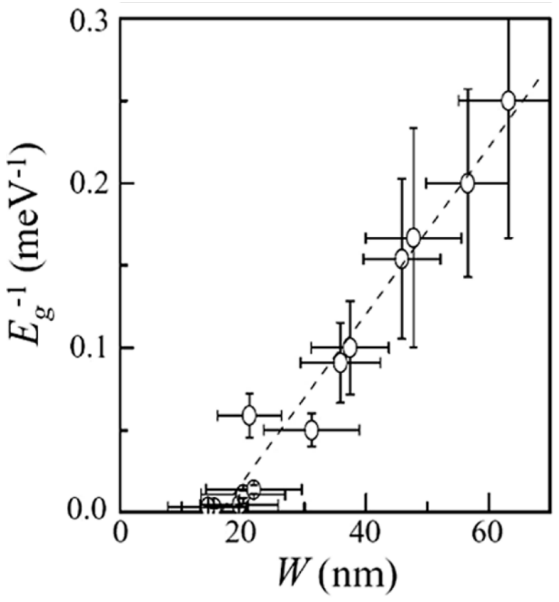

Figure 1.2 Reciprocal of energy gap E_g as a function of width of GNR.[18]

It suggests that energy gap of GNR device is disproportional to the width of GNR, which means as the width decreases the energy gap increases. Thus, narrow width GNR has high energy gap and can be used for semiconductor device applications.

Furthermore, the edge of GNR also has great impact on the electronic property of GNR. Depending on the obtained edge structure of GNR through various process steps, the nanoribbon can be defined as an armchair (A) GNRs or zigzag (Z) GNRs. Moreover, the electronics property of two types GNRs differs depending upon the nanoribbon width and its shape. It has already been theoretically predicted that both AGNRs and ZGNRs has bandgap inversely proportional to the nanoribbon width.[19, 20] Apart from the above two types of GNR, there is also other type of nanoribbon known as chiral GNR and the electronics property of such GNR depends on the cutting angle. Chiral GNR has the combination of both types of edge structures that is AGNR and ZGNR.

Some of the synthesis approach to obtain GNR are discussed below in brief. However, in spite of rapid development in research and technology, it still remains the challenging topic to achieve high quality controlled edge structure of GNR. In this step, there is various research going on to obtain GNRs with the carbon nanotubes (CNTs) through several methods like using lithographic approach,[18, 21, 22] chemical[23-25] or sonochemical[26] approaches. However, it is difficult to obtain high yield GNRs with smooth edges structures and controllable width. Hence, the researchers are trying to find the suitable technique to unzipping CNTs which can produce high-quality GNRs. Some of the methods to synthesize GNRs are discussed below.

1.4 Methods to obtain GNR

The GNR can be obtained with various methods like nanotomy, epitaxial growth of GNR and CVD growth. All these methods are basically divided into two main categories, top-down and

bottom-up approaches as shown in **Figure 1.3**. Both of them are discussed briefly in the respective sections.

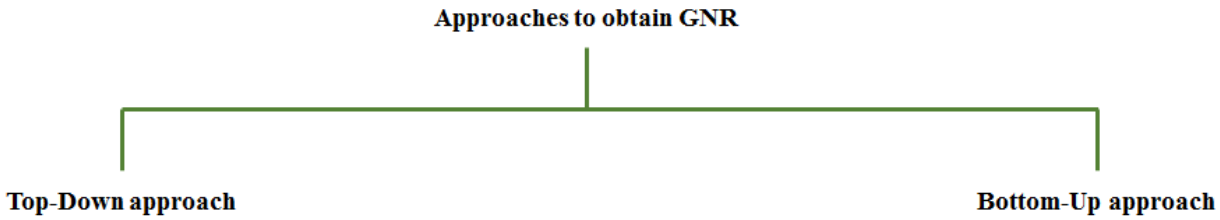

Figure 1.3 Approaches to obtaining the GNR

1.4.1 Top-down approach

Top-down approach is a process to obtain the precise segment of material starting with the big module. In this research top-down approach refers to obtain GNRs with the graphene or CNTs which is "mother" of GNR. There are various methods involved to obtain GNRs through the top-down approach. It can be obtained by precisely cutting the graphene sheet to GNR,[21] sonochemical method,[26] nanowire lithography approach,[27] cutting of graphene in nanoscale using nickel nanoparticles[23, 28] or a diamond knife cutting[29] and unzipping of carbon nanotubes.[30, 31] Some of the top-down methods to obtain GNRs are discussed below in brief.

1.4.1.1 Unzipping double-walled carbon nanotubes

In our group, we are successfully able to unzip double-walled carbon nanotubes (DWNTs) via sonication process. In this process, the defects were induced to as obtained pristine DWNTs by annealing in the furnace under an ambient environment at 500 °C. At next, the annealed DWNTs and Poly [(m-phenylenevinylene)-co-(2,5-dioctoxY-p-phenylenevinylene)] (PmPV) were added to 1, 2-dichloroethane and sonicated. During the sonication process, DWNTs starts unzipping and with the time it was unzipped to double-layer GNRs (dGNR) and as the sonication further

increases, the dGNRs were peeled off to the single-layer GNR (sGNR).[32] The AFM images of DWNT unzipped to sGNR is shown in **Figure 1.4** with the height profile of GNR.

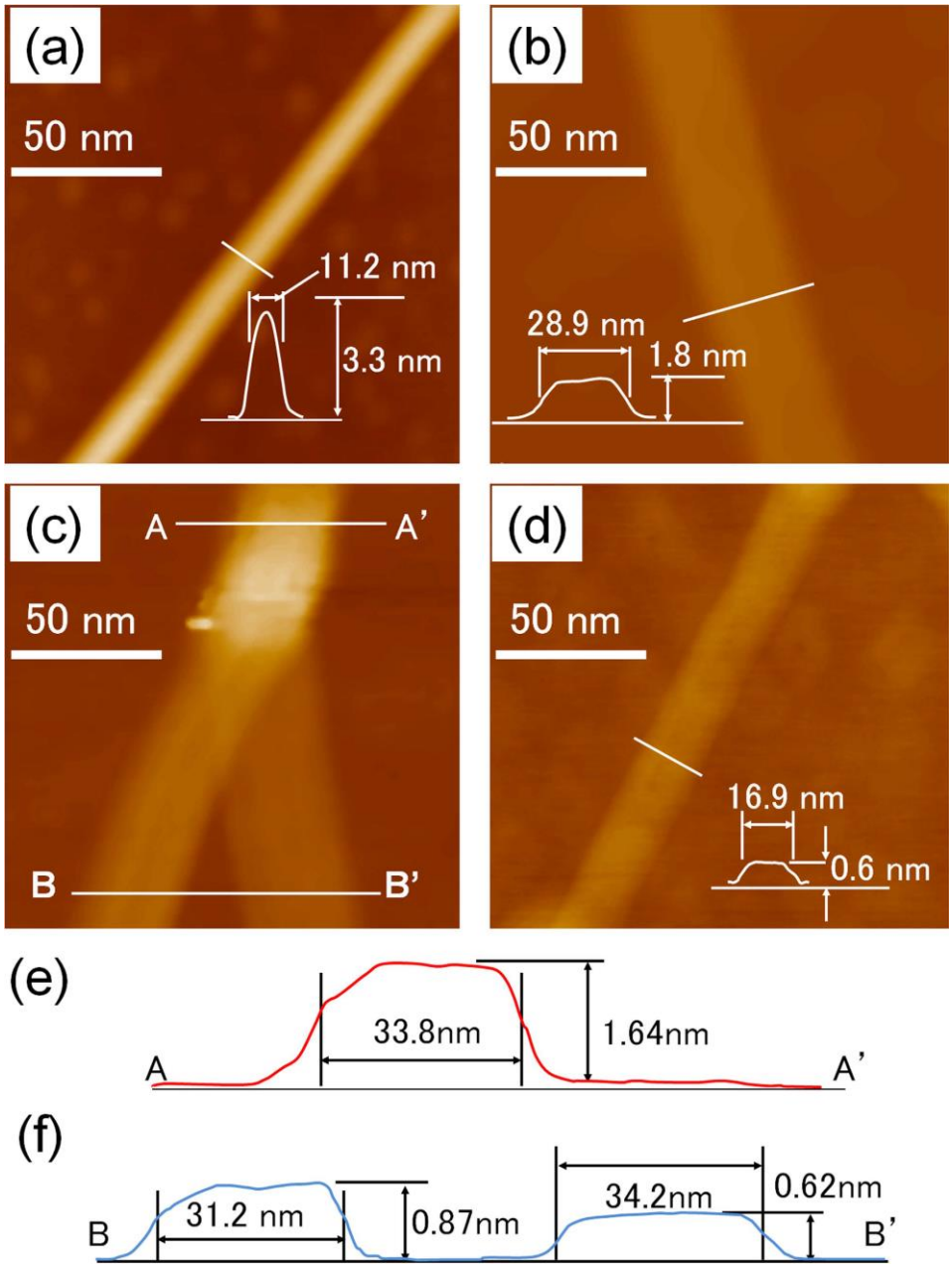

Figure 1.4 AFM images of unzipping DWNT. (a) DWNT as a starting material. (b) dGNR obtained by the unzipping. (c) Splitting region of dGNR to two sGNRs. (d) Obtained sGNR. (e) Height profile of the dGNR in fig. (c), obtained along the line A-A′. Height and width of the dGNR are 1.64 nm and 33.8 nm, respectively. (e) Height profile of the dGNR in (c), obtained along the line B-B′. (f) The height and width of sGNR in figure (c) on the left are 0.87 nm and 31.2 nm

respectively, and those of the sGNR on the right are 0.62 nm and 34.2 nm respectively. The insets in (a, b and d) show the height profile along the white line in each case. The images (a–d) correspond to different samples.[32]

There were no other unzipping methods reported so far to obtain sGNR from DWNTs in such a high percentage ratio. The percentage ratio of obtained sGNR was more than 90 %. It is the remarkable technique to obtain the sGNR which has better electrical property as compared to dGNR. It can be used for various applications like transistors, interconnects, wirings and many other.

1.4.1.2 Unzipping multi-walled carbon nanotubes

The unzipping of multi-walled carbon nanotubes (MWNTs) was reported by Jiao et al. with various methods in his several reports. One of his reports suggests that high-quality defect-free GNRs can be obtained by unzipping MWNT by sonication process using an organic solvent.[33] He reported that the obtained GNRs were atomically smooth and has width between 10-20 nm. They fabricated the field effect transistor (FET) device with the obtained GNR to measure the electrical property of GNR-FET device. The GNR-FET device with 14 nm GNR width shows high mobility of approximately 1500 cm^2/Vs and high electrical conductance of $5e^2/h$. Under low temperature, the GNR device shows phase-coherent transport and Fabry-Perot interference. This characteristic of the device suggests that the obtained GNR has minimum defects and edge roughness.

Furthermore, the unzipping of CNT by plasma etching was also suggested by the same group in which the nanotubes were partly embedded in a polymer film.[31] In this process, MWNTs were dispersed in tween 20 aqueous solution and sonicated for well dispersion followed by centrifuge to remove the aggregates. The obtained suspension was casted on SiO_2 substrate and

calcined to remove the Tween 20. Then PMMA was spin-coated over the pre-deposited MWNT on SiO_2, which results in MWNT-PMMA film and the film was peeled off with KOH solution.

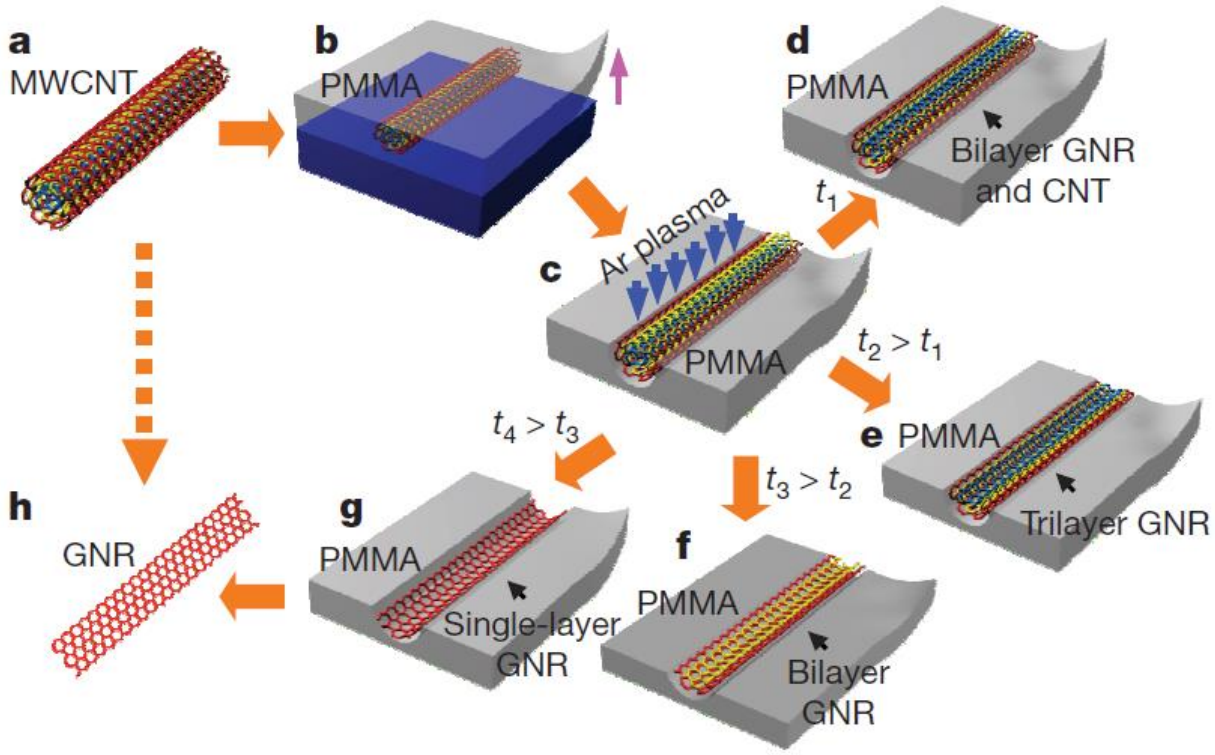

Figure 1.5 GNRs from MWNTs. (a) MWNT used as starting material. (b) MWNT deposited on Si substrate and coated with PMMA film. (c) PMMA–MWNT film peeled from the Si substrate, turned over and then exposed to an Ar plasma. (d) The products were obtained after etching for different times: GNRs with CNT cores were obtained after etching for a short time. (e-g) Tri-, bi- and single-layer GNRs produced after etching for variable times. (h) The PMMA was removed to obtain the GNR.[31]

Then the film was adhered to Si substrate and etched with Ar plasma to cut the MWNT. The synthesis approach of GNR was schematically represented in **Figure 1.5**. The GNR obtained through this method shows similar property obtained in a lithographically patterned GNRs. This method has a great advantage and can produce well aligned GNR array of controlled structure and

narrow width in sub 10 nm. Hence, suitable for the production of large-scale and high-quality GNR for electronics applications.

1.4.1.3 Chemical synthesis of GNR

The other method to synthesize the GNR was reported by Youpin Gong et al. He reported the fabrication of high-quality GNR through the chemical process by unzipping single-walled carbon nanotubes (SWNTs).[34] They used the CVD grown SWNT arrays with the density of 1-5 SWNT/um. The unzipping was processed through the chemical route in which 1-2 nm Zn film was deposited on SWNT array through magnetron sputtering followed by HCL dipping. This results in the well aligned GNR array which can be used for device integrations. The obtained GNR has height between 0.5 to 0.7 nm which was confirmed by AFM. Raman spectra and FET measurement were used to verify the intrinsic property of the GNR. Raman spectra show low Id/Ig ratio which confirms the GNR was of high quality and smooth edge. They also had confirmed that the obtained GNR through this process was chiral with low edge disorders.

1.4.1.4 Splitting MWNTs using potassium vapor

Moreover, Dmitry V. Kosynkin et al. investigated the opening of MWNT by using the potassium vapor.[35] They predicted that the alkali metal atom penetrates in the MWNT at an elevated temperature which opens the MWNT. In this process, potassium atom forms the intercalated compound within the MWNTs which was frequently observed in graphitic carbon.[36, 37] However, in this case splitting is supposed to be due to the generation of H_2 upon the quenching through the ethanol which results in 100% longitudinal splitting of MWNT as shown in **Figure 1.6**. Such a splitting of MWNT can form the narrow GNR with the few process steps.

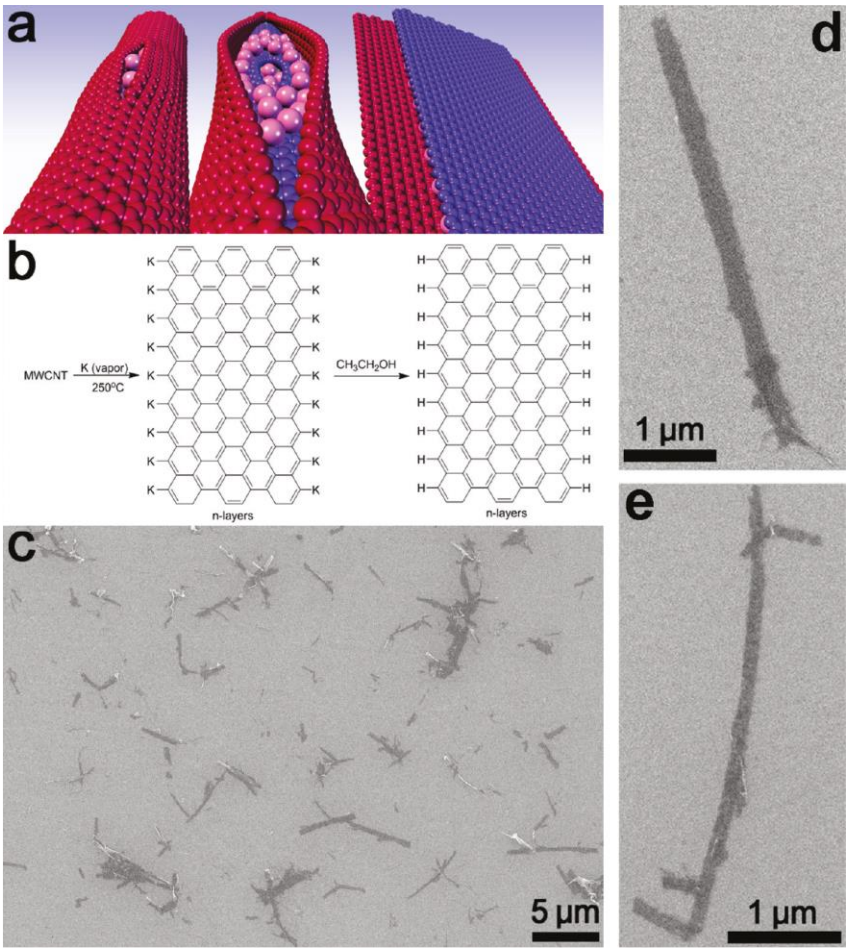

Figure 1.6 Schematic of the splitting process and SEM images of GNRs on Si/SiO_2 surface. (a) Schematic of potassium intercalation between the nanotube walls and sequential longitudinal splitting of the walls followed by unraveling to a nanoribbon stack. (b) Chemical schematic of the splitting processes where ethanol is used to quench the aryl potassium edges. (c) Overview of a large area showing complete conversion of MWCNTs to GNRs. (d, e) Images of isolated GNR stacks are demonstrating characteristic high aspect ratios and predominantly parallel edges.[35]

1.4.2 Bottom-up approach to obtain GNR

In spite of rapid development in top-down approach to synthesize GNRs, there is still lack of achievement to obtain the high-quality smooth edge GNR. In contrast, bottom-up approach utilizes the chemical properties of single molecules to obtain self-organized or self-assembled GNRs.

Through this approach, atomically smooth edge GNRs can be obtained. Some of the bottom-up synthesis methods to obtain GNRs are discussed below.

1.4.2.1 Chemical synthesis of GNR

Cai et al. reported that bottom-up chemical synthesis approach which has a great potential to synthesize the narrow width GNRs.[38] He reported the fabrication of nanoribbon on the surface of gold (111) or silver (111) single crystals by coupling molecular precursors into linear polyphenylenes followed by cyclodehydrogenation. The obtained nanoribbons were atomically smooth with armchair edges and have the width similar to few benzene ring. Furthermore, the researcher Timothy H. Vo. et al. demonstrated the bottom–up synthesis of narrow width atomically engineered GNRs.[39] He also reported that such an atomic scale GNR are currently unachieved by any top-down approaches.[40, 41] The obtained nanoribbons were approximately 1 nm wide and atomically smooth armchair edged. The achieved energy gap was approximately 1.3 eV which is significantly higher and have the potential applications for electronic device fabrications.

1.4.2.2 Organic synthesis of GNR in solution

The GNRs can be synthesized chemically with atomic precision from different types of monomers.[6, 26, 42] Such a GNR have a fine structure with narrow width and uniform edge in few nanometers. The reports also suggest the GNR with the length (L > 600 nm) have been achieved through bottom-up organic synthesis[43] and large-scale production can be achieved through this method.[39] In contrast to the ‘‘top-down’’ approach, ‘‘bottom-up’’ organic synthesis in solution can produce well-defined GNRs with uniform edge states. However, the transferring process to the suitable substrate is a bit challenging.

1.4.3 Lithographically cutting the graphene to GNR

In spite of unzipping CNT, there are various other methods reported to obtain monolayer GNR with the few layer of the graphene sheet. The lithographic approach is one of the popular approaches to cut the graphene sheet into narrow GNRs. But, there is a limitation in achieving the narrow width and smooth edge GNR. However, with the advancement in technology, there is an enormous progress in lithographic technology and can achieve the good quality of GNR. Some of the lithographic technique to obtain GNRs are discussed in following sections.

1.4.3.1 Helium ion beam lithography

Helium ion beam lithography (HIBL) is one of the finest technique to obtain the narrow width GNR from graphene. It has very fine resolution and small spot size as compared to electron beam (EB)-lithography. Since the mass of helium ions are over three orders of magnitude to that of electrons thus very low scattering around the apertures[44] which results in fine quality of patterning.[45] Through this technique, the graphene nanoribbon less than 10 nm width can be achieved.[46, 47] Moreover, the reports also suggests that the HIBL can create random defects in graphene lattice in order to create band gap.[48] Ahmad N. Abbas et al. reported the fabrication of FET with the GNR obtained through the HIBL. They can fabricate the dense GNR array up to 5 nm width and 2 um length.[16] Furthermore, the fabricated FET was measured to observe the band gap in GNR. They observed the activation energy and the band gap approximately 44 meV and 88 meV respectively. This finding suggests that the GNR obtained through HIBL has a good quality with low defects. The fabricated GNR arrays through HIBL technique is shown in **Figure 1.7**.

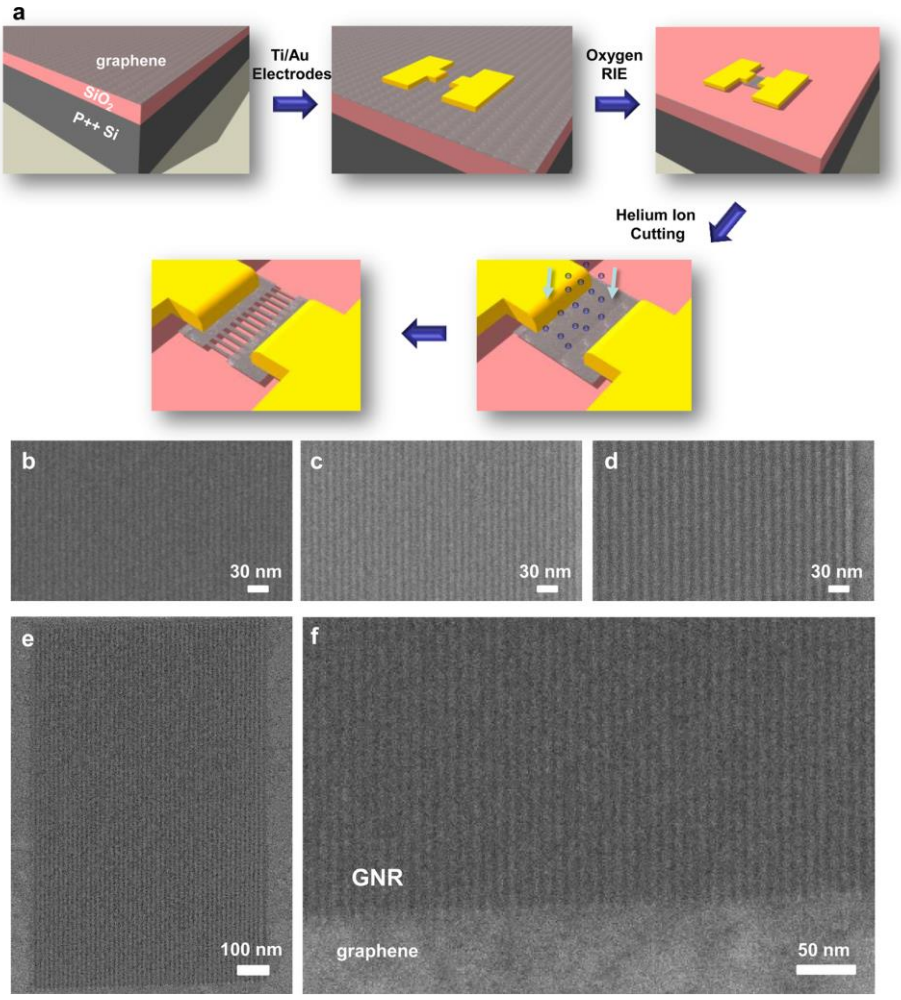

Figure 1.7 (a) Schematic of GNR arrays fabricated by HIBL. (b-d) Helium ion microscope images of (b) 5 nm, (c) 6 nm, and (d) 7.5 nm half-pitch arrays. (e) Helium ion microscope image of high aspect ratio GNRs (width length is 5 nm 1200 nm). (f) Helium ion microscope image shows the smooth interface between graphene and patterned GNRs. For all images, bright lines represent graphene.[16]

1.4.3.2 Electron beam lithography for patterning graphene

Various approaches have been made to lithographically pattern the graphene[18, 49] to achieve the nanostructure suitable for device fabrication, but there is still lack of control on the edge structure of GNR. The theoretical studies suggest that the control of edge state is important from

the perspective of energy gap since the energy gap is directly influenced by the atomic structure at the edge of GNR.[19, 50-54] Zhiwen shi et al. reported the controlled edge state GNR fabrication by the lithographic approach. He fabricated the GNR down to 10 nm width with low defect and zigzag edge structure.[55] The report suggests that the zigzag edged GNR has interesting characteristics like low edge scatting and phonon mode, semimetallic behavior independent of the GNR width, which makes it suitable for device fabrication. The other group also suggested about the graphene nanoribbon electronics.[21] They fabricated 20 nm GNR with the EB lithography technique. They described that unlike CNTs, GNRs has also defects which results in carrier scattering. It has the boundary conditions that has localized edge states[56] which affect the carrier transport phenomenon. In this aspect, Hoog's law suggests as the size of the material decreases the noise intensity increases.[57]

1.5 Objective of this study

The main objective of the research are:

1. The synthesis of graphene nanoribbon and altering its electrical property by adsorption of molecular nanoparticles.
2. Fabricating the sGNR-FET device and investigating the electrical property of sGNR-FET with and without the adsorption of molecular nanoparticles.
3. Fabricating the multi-layer GNR (mGNR) FET device and tailoring the electrical property of mGNR-FET with improved on/off current ratio.
4. Synthesizing the X-type, Y-type GNR and investigating the electrical property of the synthesized GNRs.

1.6 Research scope of this work

In this research work, the main aspects to be discussed are the synthesis of sGNR with DWNT, fabricating the sGNR-FET device and tuning the electrical property of sGNR-FET and mGNR-FET device with an adsorbent material. The scope of this study covers:

1. High percentage ratio synthesis of sGNR from DWNT by sonication process.
2. Stacked growth of mGNR by CVD process over the sGNR or dGNR template and investigate the electrical property.
3. Fabrication of FET device with single-layer and multi-layer GNR and investigating the electrical property of fabricated GNR device with and without the adsorption of molecular nanoparticle. Such a device could be promising candidate for next generation nanoelectronics as it has the device as well as interconnect in a single component.
4. Transition of metallic to semiconducting property of GNR by the adsorption of molecular nanoparticles.
5. The electrical property of GNR was analyzed with point contact current imaging (PCI-) AFM and the electrical measurements.

1.7 Outline of the thesis

This thesis consists of six chapters. Chapter one explains the introduction covering the research interest of graphene and graphene nanoribbon, Recent progress in GNR, synthesis methods of GNR, objectives of the research and scope of research.

Moreover, Chapter two deals with the preparation of sample, materials, chemicals used and synthesis of single-layer and multi-layer GNR. This chapter also includes the brief discussion about the fabrication of FET device and the process used in the device fabrication, like resist

coating, EB-lithography, metallization and lift-off. The characterization techniques, tools, and its working principle are also included in this chapter.

Chapter three explains the synthesis of sGNR, adsorption of molecular nanoparticle, the change in an electrical property of sGNR with and without nanoparticle adsorption. It also describes the details of fabricated FET and the obtained results. The characteristic of the device was also investigated at low temperature and are discussed in details. The device shows an interesting semiconducting property with the nanoparticles on it, which could be very interesting for future nanoelectronics industry

Chapter four focuses on altering the electronic property of multi-layer GNR. It briefly describes the growth of mGNR, the electrical property of mGNR and fabrication of FET device. This chapter also describes the change in an electrical property of mGNR after adsorption of molecular nanoparticle and its mechanism was also discussed.

Chapter five mainly emphasized on the fabrication of X,Y-type GNR cross junctions. It also includes the discussion about the change in an electrical property of GNR at the X,Y-cross junctions and the possible reasons for the change in property.

Finally, chapter six states the conclusion of the research work as well as some suggestions and recommendations.

1.8 References

[1] Wallace P R 1947 The band theory of graphite *Phys. Rev.* **71** 622

[2] Slonczewski J and Weiss P 1958 Band structure of graphite *Phys. Rev.* **109** 272

[3] Li L, Ruan G, Peng Z, Yang Y, Fei H, Raji A-R O, Samuel E L and Tour J M 2014 Enhanced cycling stability of lithium sulfur batteries using sulfur–polyaniline–graphene nanoribbon composite cathodes *ACS Appl. Mater. Interfaces* **6** 15033-9

[4] Allen M J, Tung V C and Kaner R B 2009 Honeycomb carbon: a review of graphene *Chem. Rev.* **110** 132-45

[5] Geim A K and Novoselov K S 2007 The rise of graphene *Nat.Mater.* **6** 183-91

[6] Wang X, Ouyang Y, Li X, Wang H, Guo J and Dai H 2008 Room-temperature all-semiconducting sub-10-nm graphene nanoribbon field-effect transistors *Phys. Rev. Lett.* **100** 206803

[7] Meyer J C, Geim A K, Katsnelson M I, Novoselov K S, Booth T J and Roth S 2007 The structure of suspended graphene sheets *Nature* **446** 60-3

[8] Cho S, Chen Y-F and Fuhrer M S 2007 Gate-tunable graphene spin valve *Appl. Phys. Lett.* **91** 123105

[9] Tombros N, Jozsa C, Popinciuc M, Jonkman H T and Van Wees B J 2007 Electronic spin transport and spin precession in single graphene layers at room temperature *Nature* **448** 571-4

[10] Ohno Y, Maehashi K, Yamashiro Y and Matsumoto K 2009 Electrolyte-gated graphene field-effect transistors for detecting pH and protein adsorption *Nano Lett.* **9** 3318-22

[11] Cohen-Karni T, Qing Q, Li Q, Fang Y and Lieber C M 2010 Graphene and nanowire transistors for cellular interfaces and electrical recording *Nano Lett.* **10** 1098-102

[12] Bunch J S, Van Der Zande A M, Verbridge S S, Frank I W, Tanenbaum D M, Parpia J M, Craighead H G and McEuen P L 2007 Electromechanical resonators from graphene sheets *Science* **315** 490-3

[13] Stoller M D, Park S, Zhu Y, An J and Ruoff R S 2008 Graphene-based ultracapacitors *Nano Lett.* **8** 3498-502

[14] Stankovich S, Dikin D A, Dommett G H, Kohlhaas K M, Zimney E J, Stach E A, Piner R D, Nguyen S T and Ruoff R S 2006 Graphene-based composite materials *Nature* **442** 282-6

[15] Lin Y-M, Dimitrakopoulos C, Jenkins K A, Farmer D B, Chiu H-Y, Grill A and Avouris P 2010 100-GHz transistors from wafer-scale epitaxial graphene *Science* **327** 662-

[16] Abbas A N, Liu G, Liu B, Zhang L, Liu H, Ohlberg D, Wu W and Zhou C 2014 Patterning, characterization, and chemical sensing applications of graphene nanoribbon arrays down to 5 nm using helium ion beam lithography *ACS nano* **8** 1538-46

[17] Pan M, Girao E C, Jia X, Bhaviripudi S, Li Q, Kong J, Meunier V and Dresselhaus M S 2012 Topographic and spectroscopic characterization of electronic edge states in CVD grown graphene nanoribbons *Nano Lett.* **12** 1928-33

[18] Han M Y, Özyilmaz B, Zhang Y and Kim P 2007 Energy band-gap engineering of graphene nanoribbons *Phys. Rev. Lett.* **98** 206805

[19] Son Y-W, Cohen M L and Louie S G 2006 Energy gaps in graphene nanoribbons *Phys. Rev. Lett.* **97** 216803

[20] Yang L, Park C-H, Son Y-W, Cohen M L and Louie S G 2007 Quasiparticle energies and band gaps in graphene nanoribbons *Phys. Rev. Lett.* **99** 186801

[21] Chen Z, Lin Y-M, Rooks M J and Avouris P 2007 Graphene nano-ribbon electronics *PHYSICA E* **40** 228-32

[22] Tapasztó L, Dobrik G, Lambin P and Biró L P 2008 Tailoring the atomic structure of graphene nanoribbons by scanning tunnelling microscope lithography *Nat. Nanotechnol.* **3** 397-401

[23] Ci L, Xu Z, Wang L, Gao W, Ding F, Kelly K F, Yakobson B I and Ajayan P M 2008 Controlled nanocutting of graphene *Nano Res.* **1** 116-22

[24] Campos-Delgado J, Romo-Herrera J M, Jia X, Cullen D A, Muramatsu H, Kim Y A, Hayashi T, Ren Z, Smith D J and Okuno Y 2008 Bulk production of a new form of sp2 carbon: crystalline graphene nanoribbons *Nano Lett.* **8** 2773-8

[25] Datta S S, Strachan D R, Khamis S M and Johnson A C 2008 Crystallographic etching of few-layer graphene *Nano Lett.* **8** 1912-5

[26] Li X, Wang X, Zhang L, Lee S and Dai H 2008 Chemically derived, ultrasmooth graphene nanoribbon semiconductors *Science* **319** 1229-32

[27] Bai J, Duan X and Huang Y 2009 Rational fabrication of graphene nanoribbons using a nanowire etch mask *Nano Lett.* **9** 2083-7

[28] Campos L C, Manfrinato V R, Sanchez-Yamagishi J D, Kong J and Jarillo-Herrero P 2009 Anisotropic etching and nanoribbon formation in single-layer graphene *Nano Lett.* **9** 2600-4

[29] Mohanty N, Moore D, Xu Z, Sreeprasad T, Nagaraja A, Rodriguez A A and Berry V 2012 NanotomY-based production of transferable and dispersible graphene nanostructures of controlled shape and size *Nat. Comm.* **3** 844

[30] Kosynkin D V, Higginbotham A L, Sinitskii A, Lomeda J R, Dimiev A, Price B K and Tour J M 2009 Longitudinal unzipping of carbon nanotubes to form graphene nanoribbons *Nature* **458** 872-6

[31] Jiao L, Zhang L, Wang X, Diankov G and Dai H 2009 Narrow graphene nanoribbons from carbon nanotubes *Nature* **458** 877-80

[32] Tanaka H, Arima R, Fukumori M, Tanaka D, Negishi R, Kobayashi Y, Kasai S, Yamada T K and Ogawa T 2015 Method for Controlling Electrical Properties of Single-Layer Graphene Nanoribbons via Adsorbed Planar Molecular Nanoparticles *Sci. Rep.* **5**

[33] Jiao L, Wang X, Diankov G, Wang H and Dai H 2010 Facile synthesis of high-quality graphene nanoribbons *Nat. Nanotechnol.* **5** 321-5

[34] Gong Y, Long M, Liu G, Gao S, Zhu C, Wei X, Geng X, Sun M, Yang C and Lu L 2013 Electronic transport properties of graphene nanoribbon arrays fabricated by unzipping aligned nanotubes *Phys. Rev. B* **87** 165404

[35] Kosynkin D V, Lu W, Sinitskii A, Pera G, Sun Z and Tour J M 2011 Highly conductive graphene nanoribbons by longitudinal splitting of carbon nanotubes using potassium vapor *ACS Nano* **5** 968-74

[36] Vallés C, Drummond C, Saadaoui H, Furtado C A, He M, Roubeau O, Ortolani L, Monthioux M and Pénicaud A 2008 Solutions of negatively charged graphene sheets and ribbons *J. Am. Chem. Soc.* **130** 15802-4

[37] Novikov Y N and Vol'pin M E 1971 Lamellar compounds of graphite with alkali metals *Russ. Chem. Rev.* **40** 733-46

[38] Cai J, Ruffieux P, Jaafar R, Bieri M, Braun T, Blankenburg S, Muoth M, Seitsonen A P, Saleh M and Feng X 2010 Atomically precise bottom-up fabrication of graphene nanoribbons *Nature* **466** 470-3

[39] Vo T H, Shekhirev M, Kunkel D A, Morton M D, Berglund E, Kong L, Wilson P M, Dowben P A, Enders A and Sinitskii A 2014 Large-scale solution synthesis of narrow graphene nanoribbons *Nat. Comm.* **5**

[40] Ruffieux P, Cai J, Plumb N C, Patthey L, Prezzi D, Ferretti A, Molinari E, Feng X, Mu¨ len K and Pignedoli C A 2012 Electronic structure of atomically precise graphene nanoribbons *ACS Nano* **6** 6930-5

[41] Koch M, Ample F, Joachim C and Grill L 2012 Voltage-dependent conductance of a single graphene nanoribbon *Nat. Nanotechnol.* **7** 713-7

[42] Linden S, Zhong D, Timmer A, Aghdassi N, Franke J, Zhang H, Feng X, Müllen K, Fuchs H and Chi L 2012 Electronic structure of spatially aligned graphene nanoribbons on Au (788) *Phys. Rev. Lett.* **108** 216801

[43] Narita A, Feng X, Hernandez Y, Jensen S A, Bonn M, Yang H, Verzhbitskiy I A, Casiraghi C, Hansen M R and Koch A H 2014 Synthesis of structurally well-defined and liquid-phase-processable graphene nanoribbons *Nat. Chem.* **6** 126-32

[44] Winston D, Cord B M, Ming B, Bell D, DiNatale W, Stern L, Vladar A, Postek M, Mondol M and Yang J 2009 Scanning-helium-ion-beam lithography with hydrogen silsesquioxane resist *J. Vac. Sci. Technol. B* **27** 2702-6

[45] Li W-D, Wu W and Williams R S 2012 Combined helium ion beam and nanoimprint lithography attains 4 nm half-pitch dense patterns *J. Vac. Sci. Technol. B* **30** 06F304

[46] Bell D C, Lemme M C, Stern L A, Williams J R and Marcus C M 2009 Precision cutting and patterning of graphene with helium ions *Nanotechnology* **20** 455301

[47] Lemme M C, Bell D C, Williams J R, Stern L A, Baugher B W, Jarillo-Herrero P and Marcus C M 2009 Etching of graphene devices with a helium ion beam *ACS Nano* **3** 2674-6

[48] Nakaharai S, Iijima T, Ogawa S, Suzuki S, Li S-L, Tsukagoshi K, Sato S and Yokoyama N 2013 Conduction tuning of graphene based on defect-induced localization *ACS Nano* **7** 5694-700

[49] Ponomarenko L, Schedin F, Katsnelson M, Yang R, Hill E, Novoselov K and Geim A 2008 Chaotic Dirac billiard in graphene quantum dots *Science* **320** 356-8

[50] Wakabayashi K, Fujita M, Ajiki H and Sigrist M 1999 Electronic and magnetic properties of nanographite ribbons *Phys. Rev. B* **59** 8271

[51] Son Y-W, Cohen M L and Louie S G 2006 Half-metallic graphene nanoribbons *Nature* **444** 347-9

[52] Ezawa M 2006 Peculiar width dependence of the electronic properties of carbon nanoribbons *Phys. Rev. B* **73** 045432

[53] Areshkin D A, Gunlycke D and White C T 2007 Ballistic transport in graphene nanostrips in the presence of disorder: importance of edge effects *Nano Lett.* **7** 204-10

[54] Ouyang Y, Yoon Y, Fodor J K and Guo J 2006 Comparison of performance limits for carbon nanoribbon and carbon nanotube transistors *Appl. Phys. Lett.* **89** 203107

[55] Shi Z, Yang R, Zhang L, Wang Y, Liu D, Shi D, Wang E and Zhang G 2011 Patterning Graphene with Zigzag Edges by Self-Aligned Anisotropic Etching *Adv. Mater.* **23** 3061-5

[56] Nakada K, Fujita M, Dresselhaus G and Dresselhaus M S 1996 Edge state in graphene ribbons: Nanometer size effect and edge shape dependence *Phys. Rev. B* **54** 17954

[57] Hooge F N 1969 1/*f* noise is no surface effect *Phys. Lett. A* **29** 139-40

CHAPTER 2

Methodology

2.1 Introduction

In spite of rapid development and advancement in technology, there is still a big challenge in synthesizing high-quality defect-free graphene nanoribbons (GNRs) and to fabricate the device using GNR. Thus, various process steps involved in the fabrication of GNR based devices are to be considered carefully, including GNR synthesis, GNR deposition on a substrate with appropriate density, electron beam lithography, developing resist, metal electrodes deposition, lift-off process, thermal annealing etc. Each and every process step has its own importance and uniqueness those are involved in good quality device fabrication. Moreover, once the devices are ready the credit goes to the measurement equipment. There may also various problems encounter during the experimental process, some of them might be common problems where some difficult to understand and analyze, hence the experimental process must be considered carefully. Furthermore, it should be worth to discuss the equipment's which were used in synthesizing and fabricating the device. It would be also worth to discuss the critical problems encountered during the experimental process. Electron beam (EB)-lithography and lift off process were important steps to discuss here in detail for the field effect transistor (FET) device fabrication.

2.2 Preparation of sample

In order to fabricate the best device for studying its electrical properties, it is important to obtain the best quality samples through an appropriate method. Preparation of sample plays an important role in understanding the fundamental properties of the device. It can be from any perspective,

either device fabrication or characterization. Considering an example, if good quality GNR samples are not achieved at starting point of device fabrication, it definitely would not have a good chance to obtain intrinsic physical properties. Moreover, the atomic force microscope (AFM) or scanning electron microscopy (SEM) images for the sample could not obtain the good quality of GNRs. The sections below describe the sample preparation for synthesizing GNRs and achieving single-layer GNR (sGNR), fabrication of multi-layer GNR on a single-layer or double-layer GNR (dGNR). Apart from this, the following section will also describe the equipment's used for device fabrication and their brief explanations. Moreover, the brief explanations of the characterization tools and measurement methods are also discussed in this chapter.

2.3 Raw materials and chemicals used in synthesizing GNR

The materials and chemicals used in this research are listed in Table 2.1.

Table 2.1 List of chemicals and materials used for this research work

Materials and Chemicals	Function	Supplier	Remarks
DWNT	To obtain GNR by unzipping	Tokyo Chem. Ind.	Purity : > 55 % Diameter : < 5 nm Length : 5-15 um
Ethanol	Cleansing Agent	Wako pure Chem. Ind.	Chemical Formula: C_2H_6O Molecular Weight : 46.07 g/mol
Acetone	Cleansing Agent	Wako pure Chem. Ind.	Chemical Formula: $(CH_3)_2CO$ Molecular Weight : 58.08 g/mol
1,2-Dichloroethane	Solvent for DWNT	Wako pure Chem. Ind.	Chemical Formula: $(CH_2)_2(Cl)_2$ Molecular Weight : 98.96 g/mol
PmPV	Surfactant Agent	Sigma-Aldrich	Poly [(m-phenylenevinylene)-co-(2,5-dioctoxY-p-phenylenevinylene)]

2.4 Synthesis of graphene nanoribbons

The GNRs used here for the experiments are synthesized by unzipping double-walled carbon nanotubes (DWNTs) with diameters of about 5 nm. We are the first in our group to synthesize the GNR by unzipping the DWNT with the high percentage ratio of sGNR, approximately 90 %.[1] In this process, the defects on the sidewalls of pristine DWNTs were induced by annealing the DWNTs in the furnace at 500 °C for 3 hours. The temperature profile for annealing DWNTs to induce the defects in the sidewalls of DWNTs is shown in **Figure 2.1 (a)**.

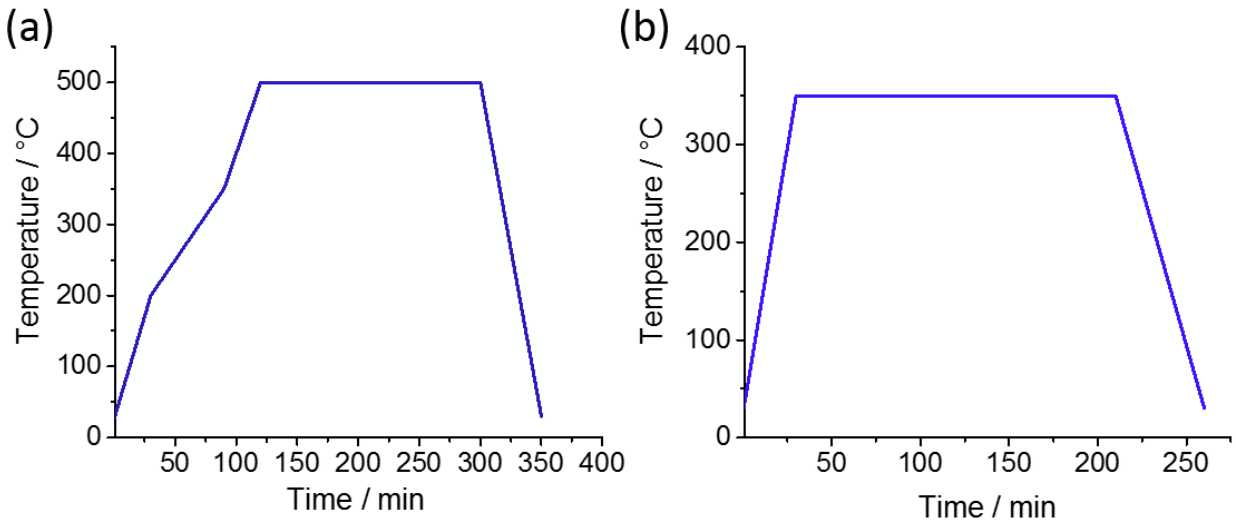

Figure 2.1 The temperature change profile of annealing (a) To induce the defect in pristine DWNT (b) Annealing the sample after casting of GNR to remove PmPV

The annealed DWNTs and 3 mg of Poly [(m-phenylenevinylene) -co-(2,5-dioctoxY-p-phenylenevinylene)] (PmPV) were added to 10 ml of 1, 2-dichloroethane for the sonication. The solution was sonicated for 4 hours at 37 kHz by a 600W sonicator, which unzips the DWNT to obtain GNRs. The PmPV in the solution works as a surfactant to stabilize the unzipped GNRs in solution. The obtained solution was centrifuged at 50000 G (20000 rpm ca; TOMY Suprema 23 High-Speed Centrifuge) for 5 hours to remove the remained nanotubes and amorphous carbon aggregates. Finally, the supernatant which contains GNR was extracted and cast on SiO_2 substrate.

The substrate was then annealed at 350 °C for 3 hours under air to remove the PmPV from the substrate and GNR. The temperature profile for annealing the sample to remove the PmPV on GNR is shown in **Figure 2.1 (b)**. Subsequently, AFM observation was carried out to confirm the GNR on the sample. The obtained GNR solution after all the process steps as described above is shown in **Figure 2.2**. There are three different solutions in the figure, which are synthesized at three different times. All the solutions are very clear and fine GNRs with a high percentage ratio of sGNR were obtained with these solutions. The AFM image of the casted GNR solution on SiO_2 substrate is also represented in **Figure 2.2** with the magnified image showing clear GNRs on the substrate with few bright spots of PmPV.

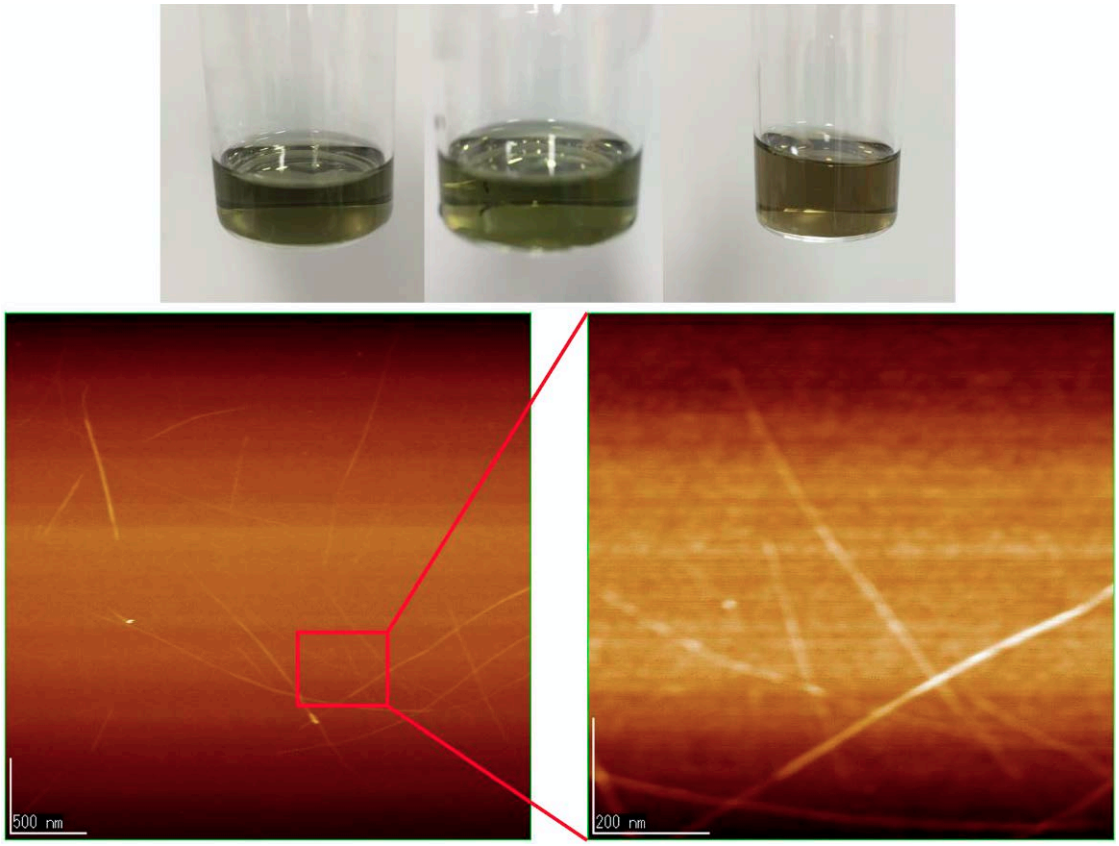

Figure 2.2 shows the solutions of GNR after sonication and centrifuge, followed by casting on SiO_2 substrate, annealing, and AFM imaging. The high-quality GNRs with few bright spots of PmPV are identified under AFM scanning.

Next, the acetone solution of 1,4,5,8,9,12-hexaazatriphenylene-hexacarbonitrile (HAT-CN6) was cast on the substrate. As the acetone evaporated, self-assembled nanoparticles of HAT-CN6 were adsorbed on the sGNRs through π-π stacking. The molecular structure of HAT-CN6 is shown in **Figure 2.3**. It is an acceptor molecule with LUMO energy level of - 4.4 eV.[2] The molecular nanoparticle played an important role in altering the electronic property of sGNR. To confirm the change in electric property, FET measurement was performed by the four-probe system (Pascal Co., Ltd) with semiconductor parameter analyzer as well as point contact current imaging (PCI-) AFM which was self-modified from general AFM (JEOL JSPM-5200).

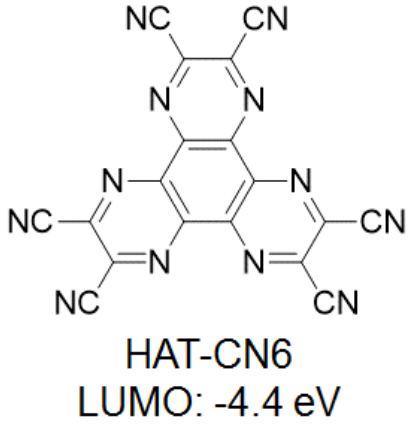

Figure 2.3 Molecular structure of HAT-CN6 used to alter the electronic property of GNR. The LUMO of this material is -4.4 eV

The electrodes of FET device were fabricated from Ti/Pt (6 nm / 24 nm) with the gap of 700 nm on SiO_2 substrate through EB-lithography. The width of sGNR for FET measurement was 23 nm. Finally, the temperature dependent property of a device was measured at different temperature by varying the *V*gs and fixed 0.5 V *V*ds.

2.5 Multi-layer GNR growth on sGNR or dGNR template

DWNTs were used as a starting material with the diameters about 5 nm. Defects were induced to pristine DWNTs by annealing at 500 °C. 3 mg of PmPV and the annealed DWNTs were added to

10 ml of 1, 2-dichloroethane solution. The solution was sonicated for 4 hours at 37 kHz by 600W sonicator to unzip the DWNT. The solution obtained with the sonication was centrifuged at 50000 G (20000 rpm ca; TOMY Suprema 23 high-Speed centrifuge) for 5 hours to remove the remained nanotubes and amorphous carbons or the agglomerated nanotubes. Finally, the supernatant was extracted in a clean bottle and obtained GNR solution was casted on SiO_2 substrate. The substrate was then annealed at 350°C for 3 hours under air to remove the PmPV from the substrate and GNR.

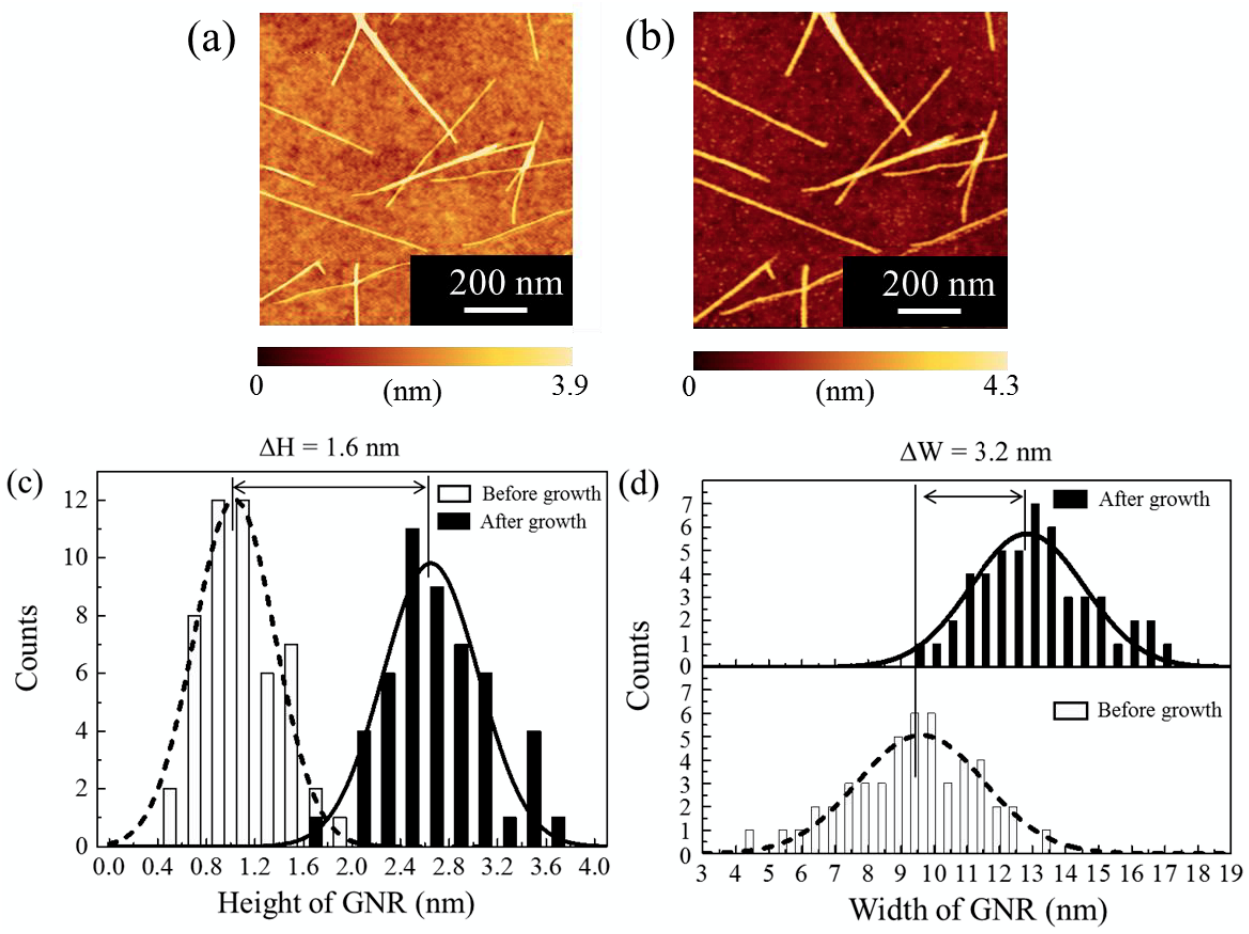

Figure 2.4 AFM images of GNRs. (a) GNRs obtained by unzipping DWNT. (b) Stacked layer of GNRs after CVD growth. (c) Change in height profile after growth of GNR. (d) Change in width profile after growth.[R. Negishi et al. submitted]

Next, the sample was further processed for the growth of stacked GNR layers through sloped-temperature CVD process. This makes the growth layer by layer on the pre-GNR deposited substrate. In this process, the carbon feedstock decomposition and graphene growth were separately controlled. [3-5] The control temperature in the furnace for the experiments was 900 °C for the carbon feedstock decomposition and 720-744°C for GNR growth. GNR samples before and after the CVD growth were characterized using AFM measurements. The height change can be clearly observed with the AFM images which confirm the number of layer grown on GNR template. The change in height and width profile of GNR with the AFM images is shown in **Figure 2.4**. Subsequently, gold electrode was deposited on the substrate containing multilayer GNR and the device can be used for electrical measurement.

Furthermore, the acetone solution of HAT-CN6 was cast on the substrate. As the acetone evaporated, self-assembled nanoparticles of HAT-CN6 were adsorbed on the multilayer GNRs through π-π stacking.[1] To confirm the change in electric property, FET measurement was performed by the low-temperature four-probe system (Pascal Co., Ltd) with semiconductor parameter analyzer. Gold electrode with Ti/Au (6 nm / 24 nm) with the gap of 1 um were deposited on SiO_2 substrate through EB-lithography. The width of multilayer GNR for FET measurement was 20 nm. Finally, the temperature dependence property of device was measured at different temperature by varying the gate-source voltage (Vgs) and fixed drain-source voltage 0.5 V.

2.6 Fabrication of FET device

The fabrication of FET device contains various process steps such as resist coating on the substrate, EB-lithography for drawing the electrode pattern and many other process steps. The flow chart for the fabrication of FET device is shown in **Figure 2.5.**

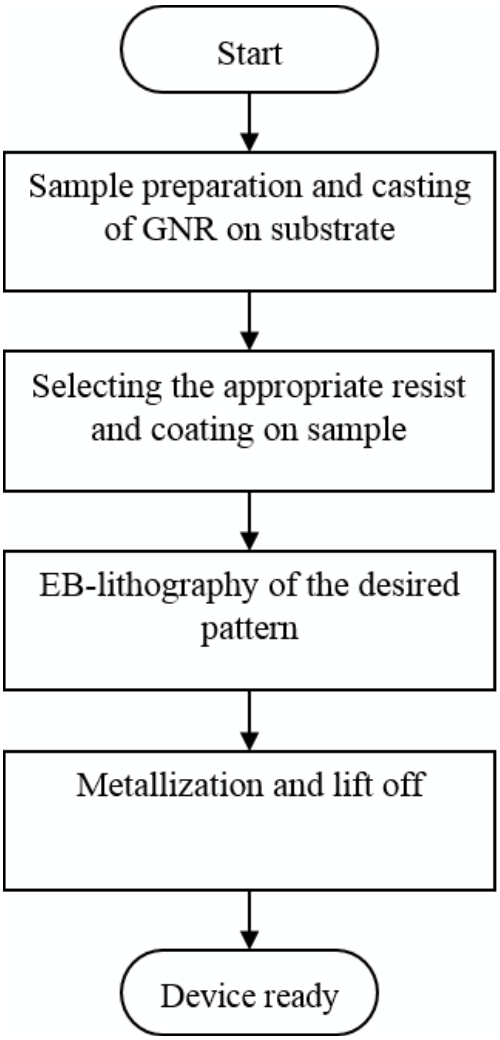

Figure 2.5 The flow chart for device fabrication

2.6.1 Electron beam (EB) resist

EB resist also known as photoresist is a resistant substance coated on the substrate to protect the surface of the sample during the various process of treatment. In general, there are two types of resist, namely positive type resist and a negative type resist. The basic difference between two types of resist is the effect on the exposed area, in the case of positive type resist the exposed area becomes soluble whereas, exposed area becomes insoluble in negative type of resist. Polymethylmethacrylate (PMMA) or GL-2000 are the positive resist used for e-beam lithography and can be easily removed by dimethyl sulfoxide.

2.6.2 EB resist used in this experiment

The selection of resist and finding the appropriate dose and current conditions of EB-lithography for the specific designed pattern are very important. This can be achieved by the expert operator in few repeated experiments and can be fixed accordingly. Moreover, it is important to avoid the excessive exposure to guarantee high-quality patterns.[6] The skilled operator can adjust the focus without taking long time which reduces the damage of sample with the electron beam. In this experiment, GL-2000-M (Gluon lab.) positive tone resist diluted with anisole was used as EB-resist in the concentration ratio of 1:1. The reason for diluting the as obtained resist is to achieve the required thickness of the resist on the substrate. The thickness profile of the resist with the rotation speed is shown in **Figure 2.6.**

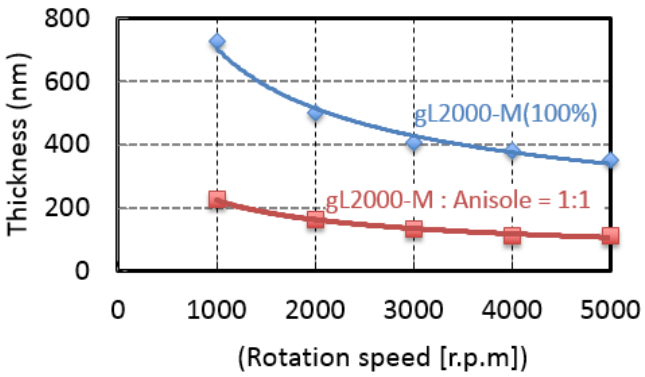

Figure 2.6 Thickness profile measured for the resist GL-2000-M, as obtained (blue curve), and resist diluted with anisole (red curve).

The resist was spin-coated on the substrate which had already GNR deposited on it. Depending on the required thickness of EB resist the rotation speed and time of spin coater can be adjusted. By repeated experiments, we found 160 nm resist thickness is appropriate for our device followed by 5 minutes baking on a hot plate at 180°C. After the resist coating, the sample was set to the sample holder in EB machine. At the next step, the designed pattern was loaded to the EB control software and checked properly to avoid any mistakes in design. The focus was adjusted with

respect to the mark at the corner of the substrate and dose was set to 167 uC / cm^2 with current around 30 nA to draw the pattern. Subsequently, after drawing the pattern the sample was dipped in N-amyl acetate (Zeon ZED-50) developer solution for 5 min to develop the pattern. The developed pattern was then ready for metal deposition.

2.6.3 Electron beam lithography

Photolithography is one of the most widely used lithographic technique in semiconductor industry if the pattern size is in the micrometer range. Photolithography is cheaper and more convenient as compared to other lithographic approaches. In the past few decades, there was great advancement in lithographic techniques and several methods are developed such as ion beam lithography, X-ray lithography, and EB-lithography. The diffraction limit is one of the important issues in the lithographic semiconductor technology to achieve a fine pattern of smaller size. Nowadays, EB-lithography is widely used in obtaining the nanostructures and are available with the very high resolutions. Although EB-lithography is a time-consuming process and costly, but it still has the advantage of forming the fine pattern of very small feature size which makes it widely acceptable.

In this experimental process, EB-lithography plays an important role to fabricate the FET device. The electrodes were patterned on the samples for the device fabrication through EB-lithography. The standard EB-lithography was used which is also equipped with SEM (Elionix ELS-7500) and has the range up to 50kV. The system for EB lithography is shown in **Figure 2.7** (left). The control panel interfaced with software control to draw the electrodes is shown in **Figure 2.7** (right). There are various factors to consider in designing and controlling the drawing of fine patterns, such as operator skill and the equipment accuracy, etc. The experienced operator on a specific system can achieve high accuracy and the best resolution, since each and every system has its own property and operating conditions, in spite of following the standard process.

Figure 2.7 EB-lithography system used in this experiment for drawing the pattern, equipped with the control panel (right) controlled by a computer interface.

2.6.4 Metal deposition for electrode

The selection of appropriate metal and deposition technique for the fabrication of the source-drain contact electrodes is very important. Some of the most widely used techniques for metal deposition are sputtering, CVD, thermal evaporation or electron beam evaporator. Here, we use the sputtering method to deposit the source-drain electrodes. Titanium followed by Platinum was sputtered to fabricate the electrodes on the developed pattern obtained from EB-lithography. The principle of deposition usually employ the magnetrons that utilize strong electric and magnetic fields to confine charged plasma particles close to the surface of the sputtering target.

Typically, the gas used for sputtering is an inert gas, mostly argon is used. The argon ions with high energy are injected and collide with each other which results in the displacement of the atoms from the target surface. In this process, the particles are ejected from the target in response to the bombardment of the target by energetic particles as shown in **Figure 2.8**.

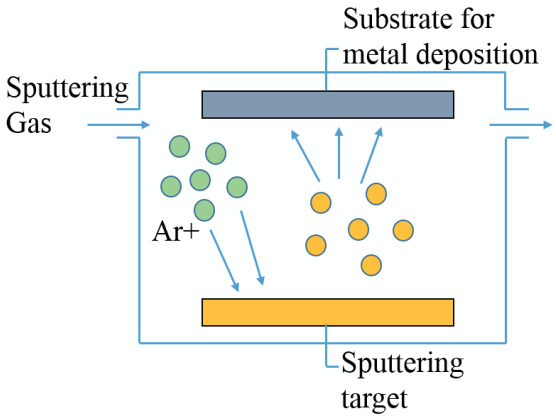

Figure 2.8 Schematic diagram of the sputtering system and its mechanism

The sputtering can take place only when the kinetic energy of the incoming particles is much higher than thermal energy. The deposition of metal takes place on the surface of the sample in high vacuum and was monitored by setting parameter in the display system. The setup of sputtering machine used for metal deposition is shown in **Figure 2.9.**

Figure 2.9 The set-up for metal deposition. Three targets are equipped with this sputtering system.

To deposit the required thickness and smooth dispersion of metal on the sample surface, some of the operation skills are required, such as adjusting the pressure of the chamber for deposition, the rate of the deposition and the rotation speed of the sample. The pressure inside the chamber for Pt and Ti deposition were 4 x 10^{-5} Pa and the deposition rate was 0.8 Å/s and 1 Å/s respectively. The thickness of the electrodes was 30 nm which contains 6nm of Ti and 24 nm Pt. Ar gas was injected in the chamber before the deposition to make the chamber free of any impurity or oxygen atoms.

2.6.5 Lift-off process and annealing

Once the metal was deposited on the patterned substrate, the lift-off is required to remove the extra deposited metal apart from the electrode. This is the crucial part to obtain a good device since over etching or less etching can result in a defective device. Over etching introduces the defect to GNR underneath the contact electrodes whereas less etching results in the remaining of resist over the GNR or reaming the metal on the GNR. The lift off was carried out in dimethylsulfoxide for 2 hours. After the lift-off process, the device was dried well in a vacuum desiccator to remove any humidity on the sample. Then, the device was annealed to achieve the good contact between the electrode and the GNR. The annealing was carried out for 2 hours at 350°C. The annealing furnace (Full-Tech Ft-101) was used to remove the impurities and improve the contact resistance of the GNR and deposited metal.

2.7 Characterization of the device

Various characterization tools are required to investigate the type, structure or morphology of the individual device. The selection of characterization tool depends on the property, for which the individual is interested in investigating. Here, we use the atomic force microscope (AFM) and scanning electron microscope (SEM) to study the height, length, and width of GNR and electrode

itself. The electrical characterization was carried out by semiconductor parameter analyzer coupled with the four probe system to measure electrical behavior. Our probe is also equipped with the low-temperature system which can measure the electrical characteristic at lower temperature up to 10K.

2.7.1 AFM observation

The AFM also known as scanning probe microscopy (SPM), is a powerful tool widely used in the nanoscale research. It has a high resolution of the order of a fraction of a nanometer, which can be used to precisely overserve the height, length or morphology of nanomaterials. Here, we used atomic contact mode AFM (JEOL JSPM-5200) to observe the GNR. The AFM setup is represented in **Figure 2.10.**

Figure 2.10 The AFM setup and software used to control the AFM (JEOL measurement) equipment.

The AFM system contains the optical microscope to align the laser and the cantilever for scanning. Most of the GNR observed was sGNR with the height of approximately 0.6 nm and a

length of 1 to 2 um. The quality of the image depends on the cantilever tip and the skill of the operator to control the software. In general, before scanning the sample the cantilever is set to auto tune and auto approaching in which the resonant frequency is adjusted automatically. Whereas, in some cases it is required to set manually, which requires the skill of operation to avoid the cantilever damage to obtain the finest quality images. Slow scanning rate and proper laser alignment are some of the parameters to obtain good quality of images. Vibrations or any type of noise can also affect the quality of the image. Hence, we need to observe the AFM in a vibration free environment with less noise.

2.7.2 Point-contact current imaging AFM (PCI-AFM)

PCI-AFM is one of the powerful tools to obtain the current images of the conductive material. This is self-modified AFM which use the conductive cantilever for measuring the current of samples containing conductive materials. It is different from general AFM, as AFM can perform contact or point contact mode measurement. But it can have some problems like loading force of tip can cause damage to sample, and piezoelectric actuators may results in inaccurate positioning due to the thermal drift of the tip in point-contact mode.[7] However, PCI-AFM is a combination of tapping mode and point-contact mode AFM. The tapping mode is used for topographic images whereas the point-contact mode is used for measuring the I-V characteristic.[8-11]

Thus, it can provide high-resolution topographic images and I-V characteristics simultaneously which is good for both the electrical property and structural images of the material. The schematic setup for the PCI-AFM is shown in the **Figure 2.11**. The figure also contains the AFM image and the current images obtained with the PCI-AFM. The current can be measured at any point with the obtained current topography and the electrical property of the material can be investigated.

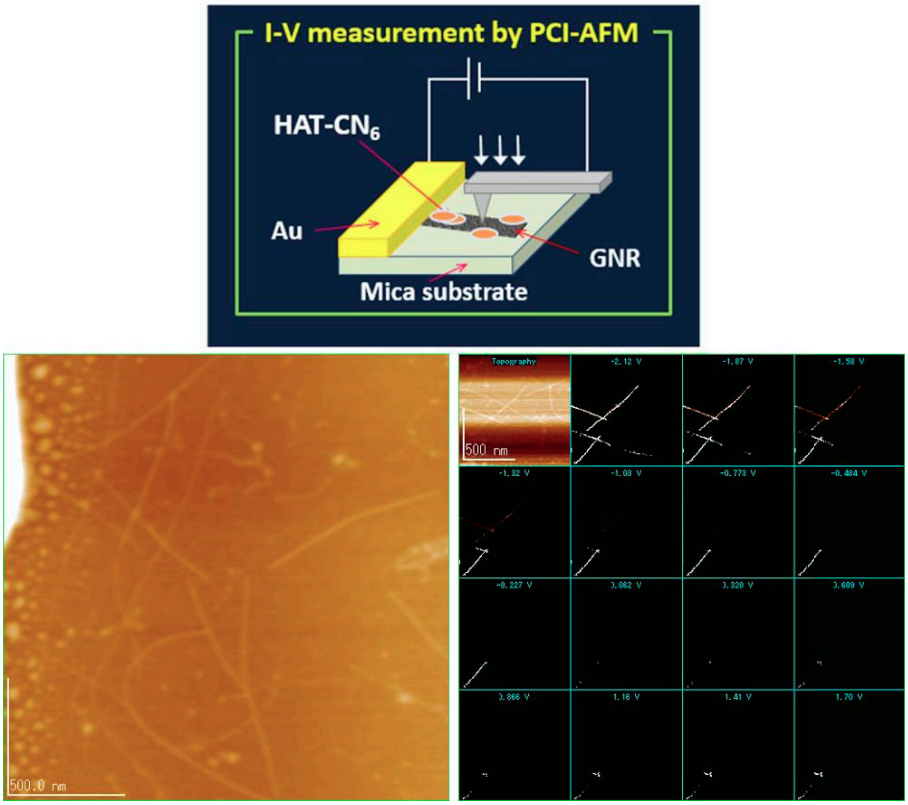

Figure 2.11 shows the schematic of PCI-AFM (top). The bottom left is the AFM image showing the GNR connected with the electrode and the bottom right is the current image obtained with PCI-AFM.

2.7.3 Scanning electron microscope measurement

Scanning electron microscope (SEM) in this experiment was used to observe the fabricated electrode and confirm the bridging of GNR between the electrodes. SEM is an electron microscope, which is used to produce the image of sample by focusing the electron beam and scanning the image of the sample. The SEM device used for characterization of fabricated sample is shown in **Figure 2.12**.

The focused electrons interact with atoms at the sample surface and produce various signals that contain the information about the sample composition and surface topography. The electrons

are generated by the electron gun and are accelerated by the application of high voltage. These electrons are injected on the sample surface and the obtained secondary electrons give the specimen image of the sample. The number of secondary electrons that can be detected depends upon various things like specimen topography, measurement environment, and sample type. The electron beam usually follows the raster scanning pattern, and the beam position combines with the detected signal to produce the image of the sample. It is easier as compared to AFM and less time consuming, but the resolution is not good as that of AFM. SEM can achieve resolution about 1 nm and the specimen sample can be observed in several conditions, namely, high vacuum, low vacuum, wet conditions, and even in a wide range of cryogenic or elevated temperatures. This is an efficient tool for obtaining the images of nanoscale devices or materials.

Figure 2.12 shows the SEM (HITACHI S-3400N) used in this work.

2.7.4 Electrical measurement of the device

Once the device is fabricated and the bridging between the electrodes is confirmed by SEM or AFM, the electrical measurement can be performed. I-V property of device was measured through

the four probe system (Pascal Co., Ltd) which is controlled through the semiconductor parameter analyzer (Hewlett-Packard HP-4156B). The semiconductor parameter analyzer was interfaced with the computer through the GPIB serial bus and the software through which the parameter analyzer controlled was Easy Expert. The setup for the electrical measurement is shown in the **Figure 2.13**, which includes the high vacuum chamber probe station having four probes inside. For the electrical measurement, the specimen sample was put inside the vacuum chamber and the probes were carefully adjusted with the electrodes on the sample with the help of microscope before closing chamber. Various other things should have to be considered carefully as the temperature inside the chamber is very low. Hence, the probes must be handled carefully to avoid any damage. It should be kept clean to avoid humidity or moisture inside the chamber. The contact between the sample and the probe must be verified before creating the vacuum inside the chamber, as bad contact can alter the I-V characteristic of the device.

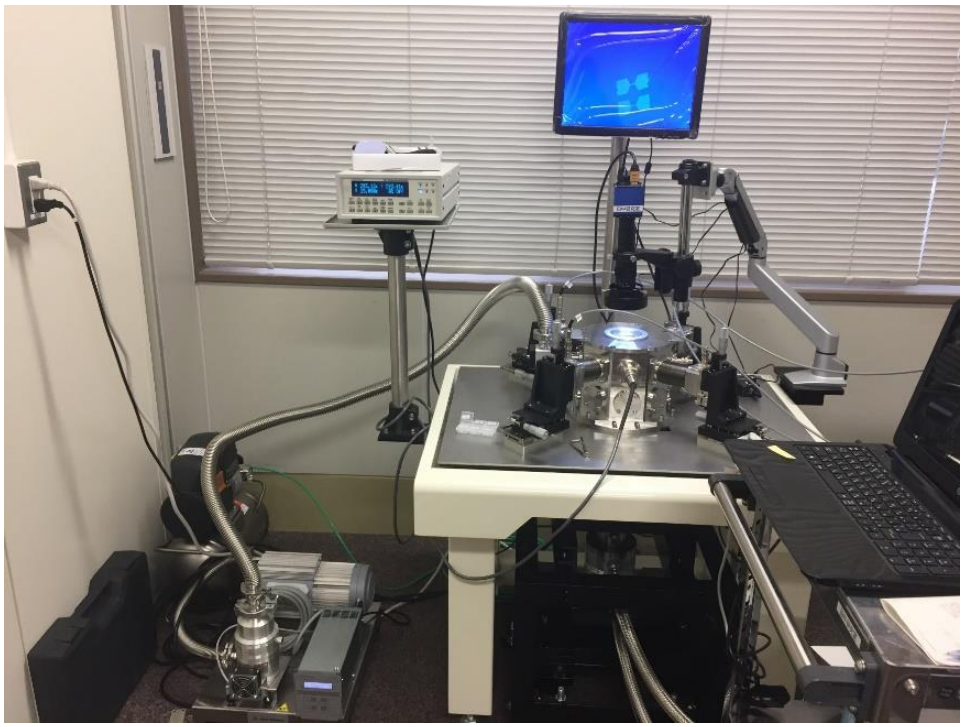

Figure 2.13 High vacuum four probe system equipped with the temperature control up to 10 K.

2.8 Conclusion

The materials used in the synthesis process of sGNR, mGNR are discussed. All the characterization tools used in the experiments were also explained. Fabrication of the electrode through EB-lithography is discussed in detail. With the above-discussed details, we can follow the procedures to synthesize the GNRs and fabricate the GNR based FET devices.

2.9 References

[1] Tanaka H, Arima R, Fukumori M, Tanaka D, Negishi R, Kobayashi Y, Kasai S, Yamada T K and Ogawa T 2015 Method for controlling electrical properties of single-layer graphene nanoribbons via adsorbed planar molecular nanoparticles *Sci.Rep.* **5** 12341

[2] Chifotides H T, Schottel B L and Dunbar K R 2010 The π-Accepting Arene HAT (CN) 6 as a Halide Receptor through Charge Transfer: Multisite Anion Interactions and Self-Assembly in Solution and the Solid State *Angew. Chem. Int. Ed.* **49** 7202-7

[3] Negishi R, Hirano H, Ohno Y, Haehashi K, Matsumoto K and Kobayashi Y 2011 Thickness Control of Graphene Overlayer via Layer-bY-Layer Growth on Graphene Templates by Chemical Vapor Deposition *Jpn. J. Appl. Phys.* **50** 06GE4

[4] Negishi R, Hirano H, Ohno Y, Maehashi K, Matsumoto K and Kobayashi Y 2011 Layer-bY-layer growth of graphene layers on graphene substrates by chemical vapor deposition *Thin Solid Films* **519** 6447-52

[5] Negishi R, Ohno Y, Maehashi K, Matsumoto K and Kobayashi Y 2012 Carrier Transport Properties of the Field Effect Transistors with Graphene Channel Prepared by Chemical Vapor Deposition *Jpn. J. Appl. Phys.* **51** 06FD3

[6] Kang S, Movva H C, Sanne A, Rai A and Banerjee S K 2016 Influence of electron-beam lithography exposure current level on the transport characteristics of graphene field effect transistors *J. Appl. Phys.* **119** 124502

[7] Otsuka Y, Naitoh Y, Matsumoto T and Kawai T 2003 Point-contact current-imaging atomic force microscopy: Measurement of contact resistance between single-walled carbon nanotubes in a bundle *Appl. Phys. Lett.* **82** 1944-6

[8] De Pablo P, Gómez-Navarro C, Colchero J, Serena P, Gómez-Herrero J and Baró A 2002 Nonlinear resistance versus length in single-walled carbon nanotubes *Phys. Rev. Lett.* **88** 036804

[9] De Pablo P, Moreno-Herrero F, Colchero J, Herrero J G, Herrero P, Baró A, Ordejón P, Soler J M and Artacho E 2000 Absence of dc-Conductivity in λ-DNA *Phys. Rev. Lett.* **85** 4992

[10] Cui X, Primak A, Zarate X, Tomfohr J, Sankey O, Moore A, Moore T, Gust D, Harris G and Lindsay S 2001 Reproducible measurement of single-molecule conductivity *Science* **294** 571-4

[11] Bietsch A, Schneider M A, Welland M E and Michel B 2000 Electrical testing of gold nanostructures by conducting atomic force microscopy *J. Vac. Sci. Technol. B* **18** 1160-70

CHAPTER 3

Tuning the electrical property of single-layer graphene nanoribbon by adsorption of planar molecular nanoparticles

This chapter mainly emphasizes on the synthesis and the approach of band gap formation in single-layer graphene nanoribbon (sGNR), which was obtained using Hexaazatriphenylenehexacarbonitrile (HAT-CN6) as an adsorbent. sGNRs were successfully synthesized through the unzipping of double-walled carbon nanotube followed by casting HAT-CN6 in acetone solution. Then, the electric property of sGNR was measured using a field effect transistor structure and observed by point-contact current imaging atomic force microscopy. The results demonstrate the formation of electron trapping sites with the nanoparticles and the neck structure of sGNR near the adsorbed region of the molecule. Therefore, the charge carriers on sGNR can only pass through the neck region, which works similarly to narrow sGNR. Such a narrow sGNR has lateral confinement of charge carrier around the neck region; hence, the device turns to semiconducting. The fabricated semiconducting sGNR could be widely used in electronic devices.

3.1 Introduction

Graphene has emerged as a promising two-dimensional material due to its high carrier mobility and high spin conduction rendering for nanoscale devices.[1] In particular, graphene-based electronics are proposed due to its excellent switching speed and high electrical conductivity.[2] However, low on/off current ratio limits the application of graphene for field effect transistor (FET) based devices.[3] Thus, the scaling down of graphene becomes important for transistors and

wiring applications, such a narrow width graphene, is known as graphene nanoribbon (GNR). Hence, several methods are investigated to obtain GNR, including the unzipping of carbon nanotubes (CNTs),[4, 5] etching of graphene to GNR,[6] and chemical synthesis.[7, 8] However, precise control of the width, aspect ratio, density, and alignment of GNR still remain as challenging topics.

Furthermore, the pristine GNR with a width of more than 10 nm shows semimetallic behavior (zero bandgap semiconductor) that cannot be used as transistors at room temperature. Previous reports have highlighted that the GNR with less than 10 nm width has quasi-one-dimensional charge carrier confinement, which results in a finite band gap opening with high carrier mobility and on/off ratio.[9] Due to high carrier mean free path (MFP) and mobility, GNR has become a suitable candidate for interconnects and transistors.[10, 11] In this regard, previous studies have reported on the band-gap engineering of graphene[12] such as chemical modification,[13, 14] dual gate structure,[15] and defect induced band gap tuning.[16] Single-layer GNR (sGNR) has particularly attracted wide attention for its application in semiconductor device technology. Hence, the synthesis of sGNR and altering the property of sGNR device still remains the challenging topic. There are few reports suggest the opening of band gap with the unzipping of CNTs.[17] However, to the best of our knowledge, there has been no published work on a well-improved method for band gap extraction of sGNR obtained by unzipping DWNT.

In the present work, a high existence ratio of sGNR synthesized from DWNT was successfully achieved by sonication process. The devices were then fabricated by electron beam lithography (EBL) for electrical measurement. Next, the acetone solution of Hexaazatriphenylenehexacarbonitrile (HAT-CN6) was casted on the fabricated devices to alter the electric property of sGNR. The obtained data confirmed a band gap opening of sGNR in the narrow

width region near the adsorbed HAT-CN6 nanoparticles. This molecular nanoparticle is a strong acceptor with -4.4 eV of lowest unoccupied molecular orbital (LUMO) energy level.[18]

3.2 Experimental procedures

The experimental process to obtain sGNR from DWNT and fabrication of the sGNR-FET device is discussed in this section. It consists of brief explanations about the synthesis procedures and casting of GNR for the sample fabrication.

3.2.1 Synthesis of sGNR from DWNT

DWNTs with diameters of 3–15 nm were used as a starting material. The defect was induced to pristine DWNTs by annealing at 500 °C. Approximately 3 mg of Poly [(m-phenylenevinylene)-co-(2,5-dioctoxY-p-phenylenevinylene)] (PmPV) and the annealed DWNT was then added to 10 ml of 1, 2-dichloroethane. The solution was sonicated for 4 h at 37 kHz by a 600W sonicator, which unzips the DWNT to obtain GNRs. The obtained solution was centrifuged at 50000 G (20000 rpm ca; TOMY Suprema 23 high-speed centrifuge) for 5 h to remove the remained nanotubes and amorphous carbons. Finally, the supernatant was extracted which contains a large percentage of sGNR some of the double-layer GNRs. The synthesis process of GNR is illustrated in **Figure 3.1**.

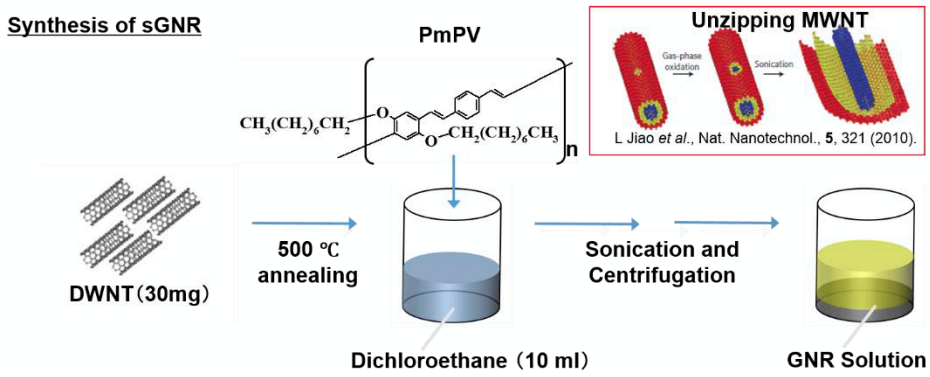

Figure 3.1 Schematic representation of synthesis process of GNR from DWNT

3.2.2 Casting the GNR solution on the substrate

The obtained GNR solution was casted on SiO_2 substrate. The substrate was then annealed at 350 °C for 3 h under air to remove the PmPV from the substrate and GNR. The annealed substrate containing GNR was then taken for AFM measurement to confirm the GNR on the substrate. Subsequently, gold electrode was deposited on the substrate containing sGNR. The casting and annealing process of GNR is illustrated in **Figure 3.2**.

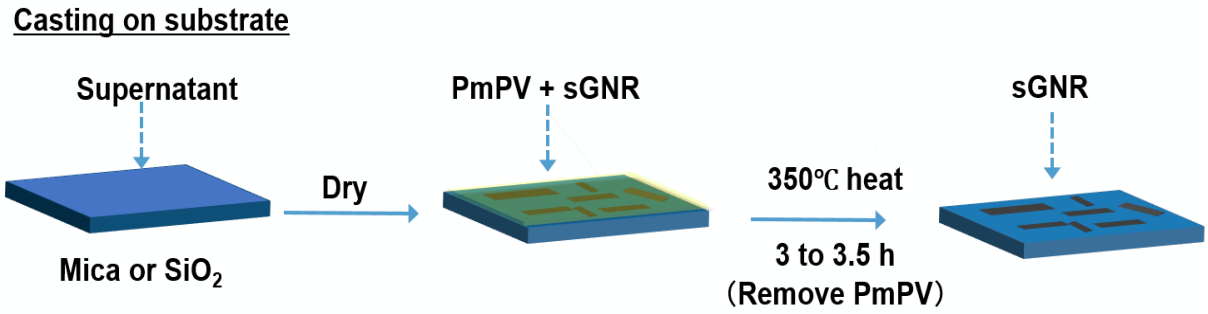

Figure 3.2 Casting and annealing of sample to obtain pure sGNR

3.2.3 FET device fabrication and measurement

To confirm the electric property of synthesized sGNR, FET device was fabricated. The electrode of Ti/Pt (6 nm / 24 nm) with the gap of 700 nm were deposited on SiO_2 substrate through EBL. The width of sGNR for FET measurement was 23 nm. The device was measured with the four-probe system (Pascal Co., Ltd) coupled with semiconductor parameter analyzer (HP 4156B). The electrical property was also measured by point contact-current imaging (PCI-) AFM which is home modified from general AFM (JEOL JSPM-5200). Finally, the temperature dependence property of a device was measured at different temperature by varying the *V*gs and fixed 0.5 V *V*ds. Next, the acetone solution of HAT-CN6 was cast on the substrate to verify the change in electrical properties of sGNR with the adsorption of the nanoparticle. As the acetone evaporated, self-assembled nanoparticles of HAT-CN6 were adsorbed on the sGNRs through π-π stacking.[19]

3.3 Results and Discussion

Figure 3.3 shows the atomic force microscopy (AFM) images observed to verify HAT-CN6 nanoparticles adsorbed on sGNR. The height of pristine sGNR was observed between 0.54 nm to 0.62 nm. The reason for the change of sGNR height was presumably due to the roughness of the substrate. Furthermore, HAT-CN6 in acetone with different concentration was casted on the sGNR to clarify the effect of adsorbed amount of HAT-CN6 nanoparticles on the electric property of sGNR. The AFM images in **Figure 3.3** (a), (b) (c), and (d) were observed with the samples containing HAT-CN6 concentration of 10^{-7}, 10^{-6}, 10^{-5}, and 10^{-4} mol/L, respectively.

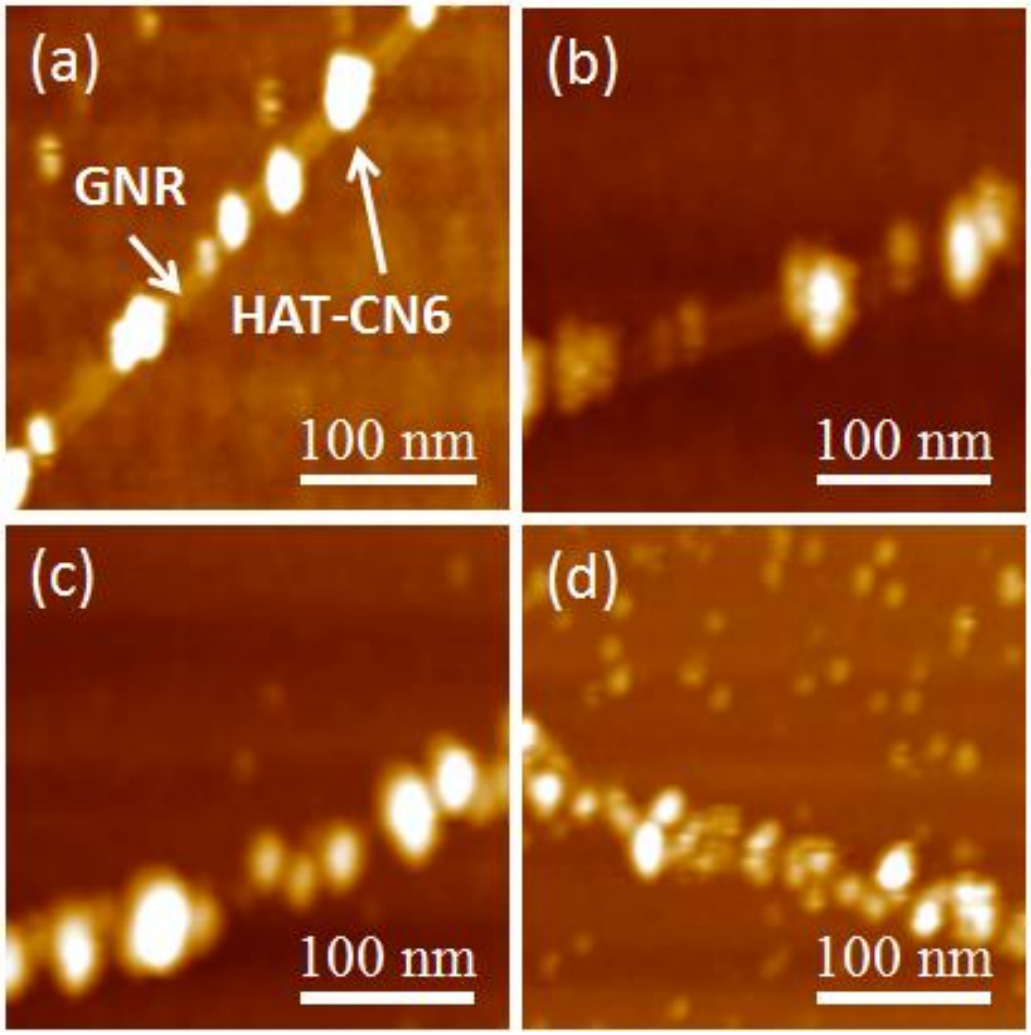

Figure 3.3 AFM image representing the adsorption of nanoparticles on sGNR. (a) HAT-CN6 in solvent (10^{-7}) casted on GNR forming nanoparticles with diameter larger than GNR width. (b)

Increase in the concentration of HAT-CN6 in solvent (10^{-6}) forming smaller nanoparticle. (c) The concentration of HAT-CN6 in solvent (10^{-5}). (d) Large number of adsorbed nanoparticle per unit length with higher concentration of HAT-CN6 in solvent (10^{-4}).

The bright spots in the AFM images are the adsorbed nanoparticles on sGNR. The results of AFM clearly confirmed that as the concentration of HAT-CN6 in acetone is increased, the number of adsorbed nanoparticles per unit length also increases. Due to the strong π-π interaction of sGNR with HAT-CN6, nanoparticles can be easily adsorbed on sGNR to make a complex of self-assembled molecular nanoparticles and sGNR.[18]

In the next step, the nanoparticle-sGNR samples for PCI-AFM[20] measurement was prepared with four different concentrations. The schematic setup of sample for PCI-AFM measurement is shown in **Figure 3.4**

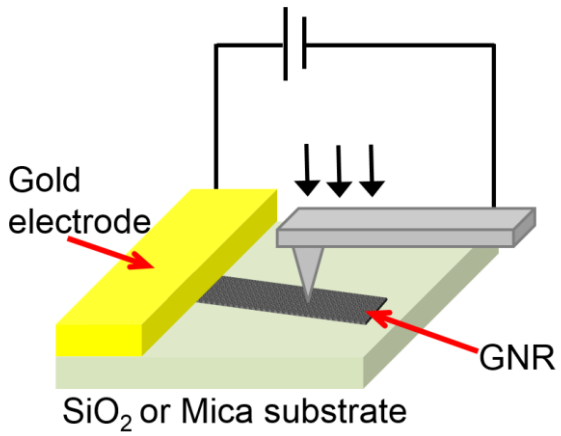

Figure 3.4 The setup for the PCI-AFM measurement.

The PCI-AFM results obtained from the samples at room temperature with different HAT-CN6 concentrations deposited on sGNR are shown in **Figure 3.5 (a)**. According to the current-voltage (I-V) results obtained from the device with HAT-CN6 concentration of 10^{-7} mol/L, the device still shows metallic property, while the other devices containing 10^{-6}, 10^{-5} and 10^{-4} mol/L HAT-CN6 concentration are semiconducting.

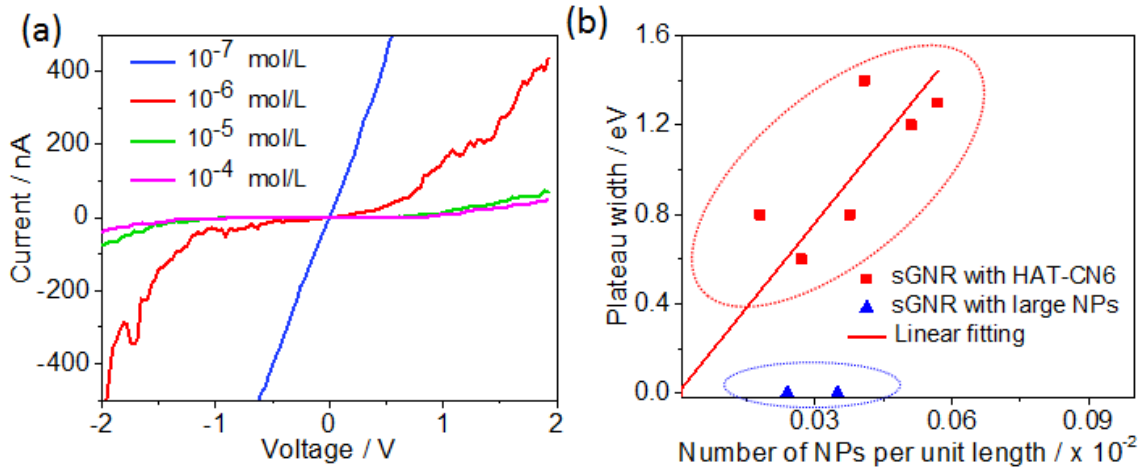

Figure 3.5 Obtained characteristic with PCI-AFM. (a) I-V curve obtained from the PCI-AFM with varied concentration of HAT-CN6. (b) Plateau width obtained by sGNR device adsorbed with HAT-CN6 nanoparticles.

The transition from metallic to semiconducting property is due to the formation of strong electron trapping sites at the adsorbed region of molecular nanoparticles on sGNR.[19] The semiconducting property of the device is also confirmed by the plateau width extracted from the I-V curves, as shown in **Figure 3.5 (b)**. The plateau width was extracted from the obtained I-V curve by plotting dI/dV-V curve. The flat area of dI/dV-V curve is defined as plateau width as shown in **Figure 3.6.** For simple and fair comparison with an activation energy, the plateau width is converted to the energy and the unit of the vertical axis is in eV in **Figure 3.5 (b).**

According to the results, the plateau width is directly proportionate to the number of adsorbed nanoparticles per unit length, which is due to the formation of electron trapping sites and lateral confinement of charge carrier at the neck region.[19] As the number of nanoparticle per unit length on sGNR increases, the electron trapping becomes stronger. This suggests that there is less conduction at the trapped region of sGNR. However, the conduction occurred through the neck region of sGNR, which showed similar behavior as graphene nanomesh.[12] In other words the

presence of the neck region, the narrow conduction pass region turns to the sGNR into semiconducting.[21] In contrast, no plateau width is observed for low concentration (10^{-7} mol/L) of the HAT-CN6 device (blue plots in **Figure 3.5 (b)**).

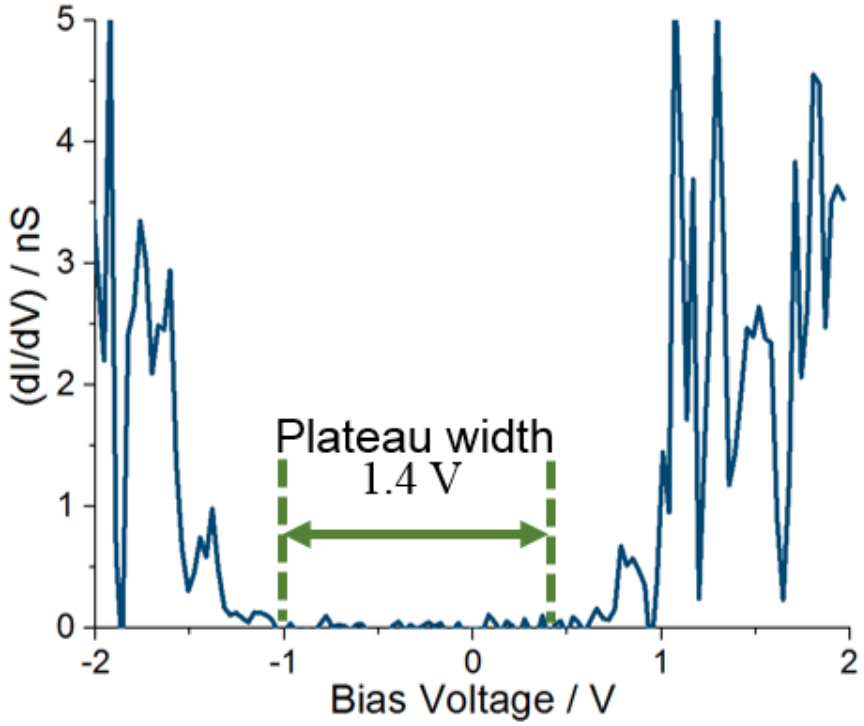

Figure 3.6 The extracted plateau width from dI/dV-V curve

The result of the extracted plateau width is also compared with our previous report where naphthalenediimide (C15-NDI) molecule was used for altering the property of sGNR and is shown in **Figure 3.7**.[19] Vertical axis of the plateau width in **Figure 3.7** was converted to eV for easy and fair comparison in with the activation energy or band gap. The molecular structures of both the molecule are shown in **Figure 3.8.**

Based on the comparative results extracted from both adsorbed HAT-CN6 and C15-NDI nanoparticle on sGNR, it can be concluded that HAT-CN6 is a strong acceptor with a larger plateau width than C15-NDI, which is due to its stronger interaction with sGNR and higher LUMO energy level.[18]

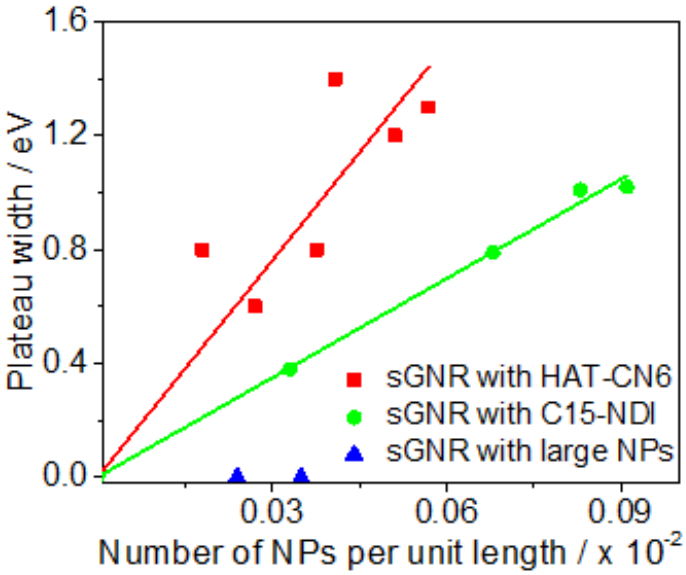

Figure 3.7 Comparison of plateau width obtained by sGNR device with C15-NDI and HAT-CN6 nanoparticles.

Figure 3.9 (a) presents the schematic of the complex formation mechanism of HAT-CN6 nanoparticle with sGNR. Due to the deposited HAT-CN6 nanoparticles, the lateral confinement of charge carriers occurred at the neck of sGNR. Around the neck of the sGNR, screening effect causes high resistance in the small area, which results in a Zener-like tunneling conduction.[19]

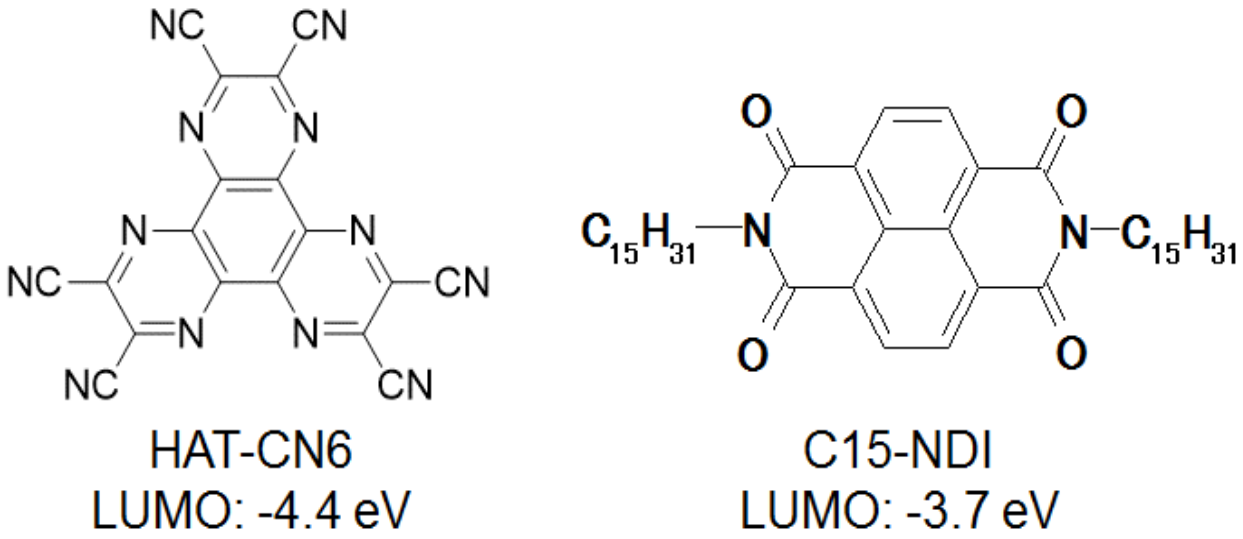

Figure 3.8 Molecular structure of the used molecule to alter the electronic property

In contrast, as shown in **Figure 3.9 (b)**, where the nanoparticle is larger than the sGNR width, carriers are completely trapped on the sGNR. Thus, the conduction occurred only by electron hopping, which resulted in no plateau width (blue plots in **Figure 3.5 (b)**).

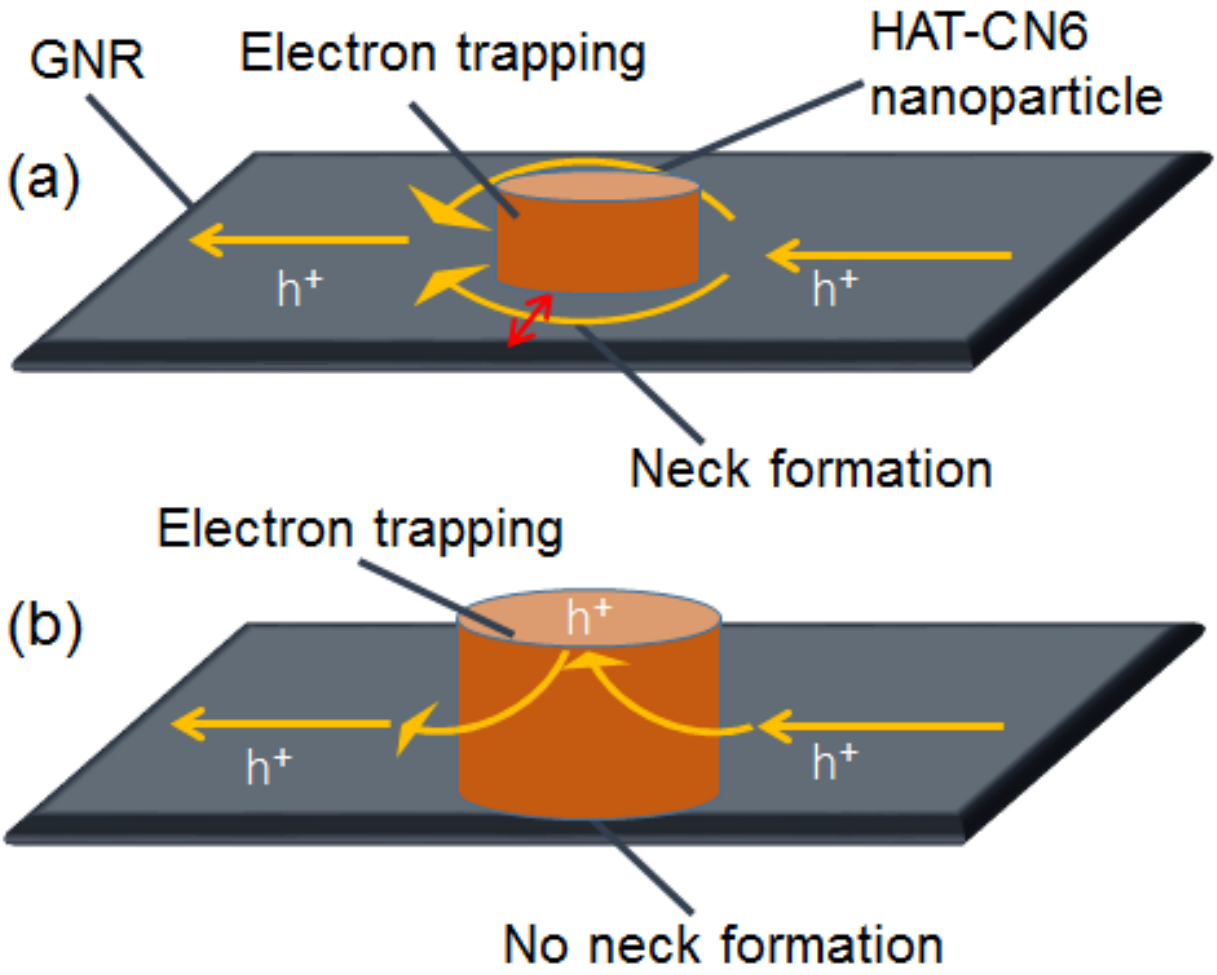

Figure 3.9 Formation of neck structure. (a) Schematic representation of HAT-CN6 nanoparticle on GNR and carrier transport. (b) Schematic with larger nanoparticle than sGNR width, all the carriers are trapped with the nanoparticle.

Furthermore, the semiconducting property of sGNR after the adsorption of nanoparticles is also confirmed with the field effect transistor (FET) measurement. The AFM image of synthesized sGNR and the fabricated FET device is shown in **Figure 3.10.**

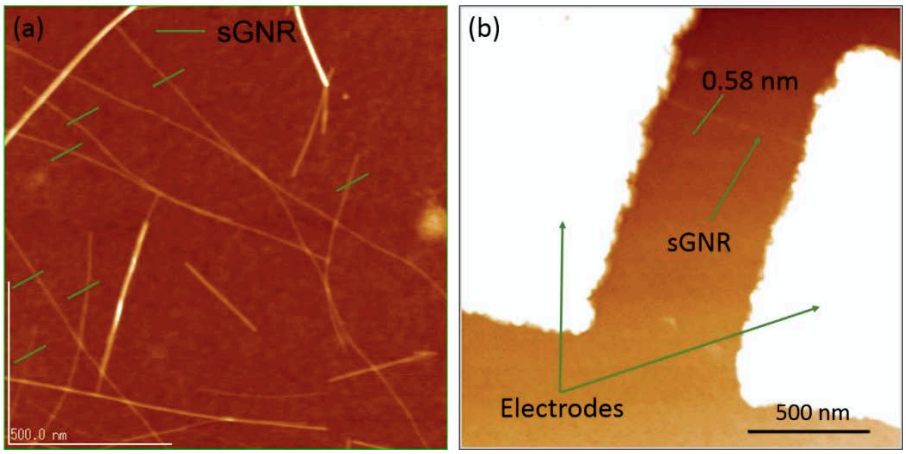

Figure 3.10 The AFM images (a) the synthesized sGNR obtained on substrate, (b) the fabricated sGNR device

The schematic diagram of the back-gate FET measurement is shown in **Figure 3.11 (a)**. The characterization of the FET device was performed at room temperature using I_{ds}-V_{ds} measurement for the devices with and without HAT-CN6 adsorption as shown in **Figure 3.11 (b)**. From the obtained I-V curves, it can be seen that the current is suppressed after adsorption of HAT-CN6 nanoparticles, which is due to the formation of electron trapping sites at the sGNR as described earlier.[19] The transfer characteristic of the device is also obtained in order to confirm the on/off ratio and semiconducting property caused by the HAT-CN6 molecule on sGNR as shown in **Figure 3.11 (c)**. The device with pristine sGNR showed a metallic behavior with electron doped from SiO_2 substrate, while the device with HAT-CN6 transformed to clear p-type semiconductor. The mobility of the sGNR device at room temperature with the HAT-CN6 is about 17 cm^2/Vs which was obtained from the slope obtained in **Figure 3.11 (c)**. The mobility of the device was calculated in linear region with the equation

$$u = mlin\frac{L}{W}\frac{1}{Vds}\frac{1}{Ci}$$

Where u is mobility of the device, m_{lin} is the slope of the plot, L is the channel length and W the width, C_i the gate capacitance and Vds is drain-source voltage.

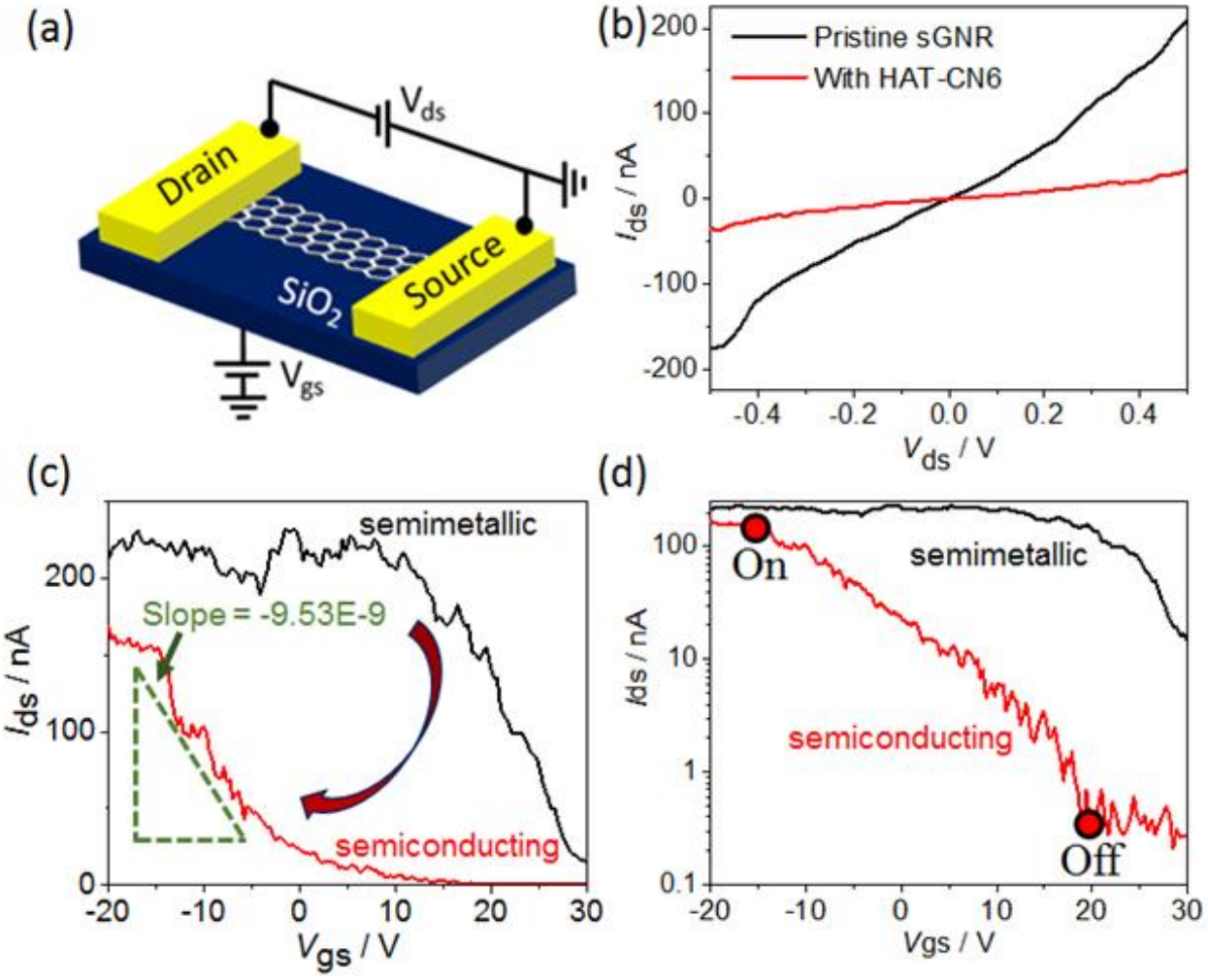

Figure 3.11 Electric property of pristine device and the device with HAT-CN6, (black plot and curve are from the pristine device whereas red is from the device with HAT-CN6). (a) Schematic of back-gate FET measurement. (b) I-V characteristic. (c) The transfer characteristic of sGNR-FET device at linear scale. (d) Logarithmic scale transfer characteristic of sGNR-FET device.

The on/off ratio of the device at room temperature with the HAT-CN6 is in the order of 10^2 which can be clearly seen on a logarithmic scale plot in **Figure 3.11 (d).** Such a high on/off ratio was reported in in sub 10 nm GNR,[12] whereas the used GNR for this experiment has width of

23 nm. The improvement in on/off ratio was supposed to be due to the adsorbed nanoparticles, resulting in a neck like structure which works similar to narrow width GNR. The on off ratio of the device highly depend on the width of GNR, previous reports suggests that as the width of GNR decreases the on/off current ratio increases.[22] Maintaining the on/off ratio in narrow width GNR devices is highly required in advanced digital electronics applications.[23] Since the device with HAT-CN6 on sGNR has high on/off ratio, such device can be used for high-speed switching applications.[24] It was also observed that the transfer characteristic of the device with HAT-CN6 showed a sudden rise in current in negative gate voltage, which might be also due to the Zener-like tunneling in the device.[19] According to the Zener-like tunneling, there was no current observed when $V_{gs} > + 17$ V, and the current started to rise as the gate voltage was decreased towards the negative bias followed by sudden increase at about -5 V.

The temperature dependent electrical transport of the device was also measured to identify the carrier transport mechanism as shown in **Figure 3.12**. The carrier transport occurring in the device was mainly due to two phenomena, namely tunneling and hopping, which is divided into two sections of plot **Figure 3.12 (a)**. Tunneling phenomenon was observed in the low-temperature region, whereas, hopping conduction in the high-temperature region (above 150°C). The Arrhenius plot for the activation energy was plotted in **Figure 3.12 (b)**. According to the obtained results, the pristine sGNR-based FET device shows that the conductivity decreases as the temperature was lowered until 150 K.

Furthermore, the fluctuation in conductivity was observed around 100 K in both the device (pristine and the device with HAT-CN6), possibly due to the acoustic phonon in the metallic region of sGNR.[25] The trend line in **Figure 3.12 (a)** shows the Arrhenius plot of the activation energy for sGNR with HAT-CN6.[26] The activation energy of pristine sGNR device and the device with

HAT-CN6 was calculated about 0.15 meV and 52 meV respectively. Activation energy is the probability to excite the carrier with the thermal energy which is approximately half of the band gap energy.[27] The pristine sGNR device has low activation energy as compared to the device with HAT-CN6. Thus, the device with HAT-CN6 has a large transition from semimetallic to semiconducting property. The activation energy was calculated in linear region with the equation

$$Slope = -\frac{Ea}{R}$$

Where Ea is the activation energy, R is the ideal gas constant in joules per mole Kelvin, and the slope is the temperature dependent slope.

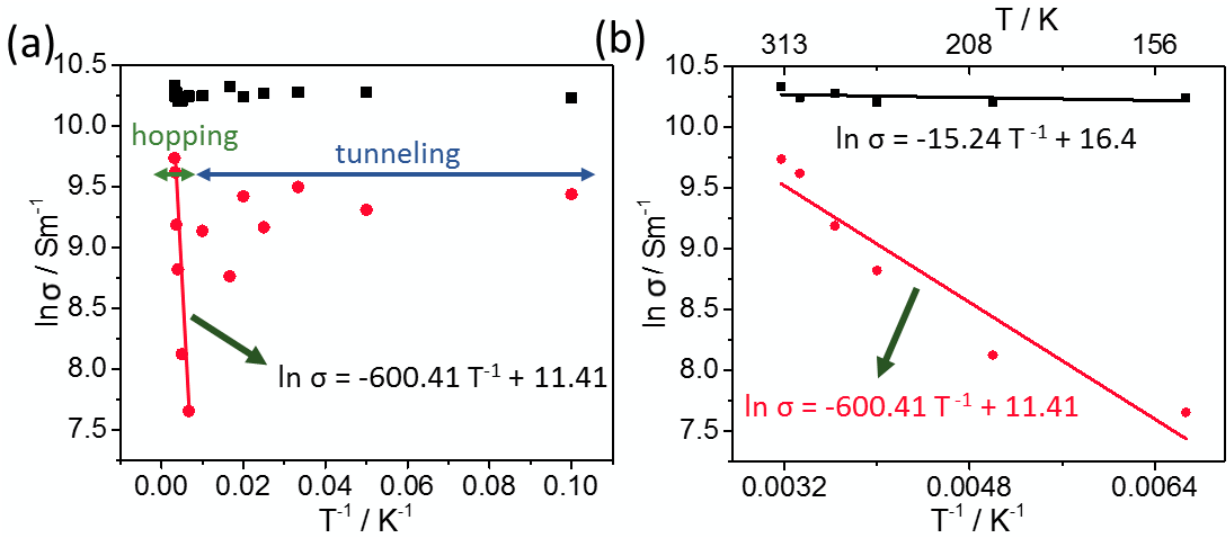

Figure 3.12 Temperature dependent conductivity of the sGNR-FET device (black plot and curve are from pristine device whereas red is from the device with HAT-CN6). (a) Carrier transport occurring in the device with tunneling and hopping which is divided. (b) Arrhenius plot for the activation energy.

The activation energy is much lower than the measured plateau width, which implies that the plateau width is originated with carrier hopping conduction among the nanoparticles. As the temperature increases, the device with HAT-CN6 followed a semiconducting behavior with increasing conductivity. However, at a temperature of around 100 K, the fluctuation in conductivity was observed in the device, which is mostly due to the domination of metallic property. The fluctuations could also be due to the adsorption of HAT-CN6 molecule on narrow width sGNR, which suppressed the current conductivity. There could also be fluctuation in the conductivity due to Anderson localization effect which was frequently observed in narrow width GNRs. As the width of GNRs decreased the Anderson localization could be more prominent due to edge defects, local defects or the backscattering effects.[28, 29] The nanoparticles on GNR can be similar to local defect as it forms the carrier trapping site and could also be one of the possible reason of appearance of activation energy in our device.

There could also be a possibility to improve the performance of GNR based FET device by the surface treatment of SiO_2 substrate, which will be introduced in the next step of research. As there are the reports suggesting a substrate induced effect on change in an intrinsic property of GNR based FET devices. The charge impurities on SiO_2 substrate during the experimental process could induce charge puddles or ionized impurities which can alter the property of device.[30] These impurities could also be in the form of adsorbed molecules or residue of resist during the fabrication process and can induce asymmetry in electron-hole conduction.[31-33] The hydrophilic layer of silanol (SiOH) is easy to form at the surface of SiO_2 with the hydroxyl (-OH) group.[34] This SiOH group can easily attract the polar adsorbates like water molecule and induce the carrier doping on the SiO_2 substrate which can affect the intrinsic property of GNR devices.[35, 36]

Self-assembled monolayers (SAMs) is one of the well-known technique reported to improve the device performance with the SiO_2 surface treatment.[37, 38] The other process is coating hexamethyldisilazane (HMDS) on the surface of SiO_2 which results in hydrophobic substrate by preventing the formation of SiOH, thus, reducing the attachment of polar molecules.[33] The ionized impurities which induce electron puddles could also be reduced by the coating of HMDS, as the distance between GNR and substrate is increased.[30]

The specific surface treatment of SiO_2 was not performed in this experimental process. However, the annealing of substrate was performed which can reduce the impact of charge impurities and hence it was supposed that the GNR device has its own property.[39] The other some other surface treatment will be considered in next step to compare the device performance. Boron nitride is also one of the suitable substrates to obtain the intrinsic property of GNR based FET devices.[40]

3.4 Conclusion

We have successfully controlled metal p-type semiconductor transition by adsorption of flat organic molecule HAT-CN6. According to the results obtained by FET measurement and the PCI-AFM, we can confirm the transition in electric property of sGNR. In addition, it was found that the HAT-CN6 is the stronger molecular nanoparticle to open the band gap in GNRs that are wider than 10 nm. We have also suggested the possible reason of opening the band gap in sGNR. The plateau width is in proportion to the number of nanoparticles adsorbed on sGNR. The activation energy is also obtained by temperature dependence measurement. This technique of opening bandgap could be promising for future semiconductor electronics applications.

3.5 References

[1] Weiss N O, Zhou H, Liao L, Liu Y, Jiang S, Huang Y and Duan X 2012 Graphene: an emerging electronic material *Adv. Mater.* **24** 5782-825

[2] Yung K, Wu W, Pierpoint M and Kusmartsev F 2013 Introduction to graphene electronics–a new era of digital transistors and devices *Contemp. Phys.* **54** 233-51

[3] Zhan B, Li C, Yang J, Jenkins G, Huang W and Dong X 2014 Graphene Field-Effect Transistor and Its Application for Electronic Sensing *Small* **10** 4042-65

[4] Wei D, Xie L, Lee K K, Hu Z, Tan S, Chen W, Sow C H, Chen K, Liu Y and Wee A T S 2013 Controllable unzipping for intramolecular junctions of graphene nanoribbons and single-walled carbon nanotubes *Nat. Commun.* **4** 1374

[5] Xie L, Wang H, Jin C, Wang X, Jiao L, Suenaga K and Dai H 2011 Graphene nanoribbons from unzipped carbon nanotubes: atomic structures, Raman spectroscopy, and electrical properties *J. Am. Chem. Soc.* **133** 10394-7

[6] Abramova V, Slesarev A S and Tour J M 2013 Meniscus-mask lithography for narrow graphene nanoribbons *ACS Nano* **7** 6894-8

[7] Ruffieux P, Cai J, Plumb N C, Patthey L, Prezzi D, Ferretti A, Molinari E, Feng X, Mu¨ len K and Pignedoli C A 2012 Electronic structure of atomically precise graphene nanoribbons *ACS Nano* **6** 6930-5

[8] Cai J, Ruffieux P, Jaafar R, Bieri M, Braun T, Blankenburg S, Muoth M, Seitsonen A P, Saleh M and Feng X 2010 Atomically precise bottom-up fabrication of graphene nanoribbons *Nature* **466** 470-3

[9] Li X, Wang X, Zhang L, Lee S and Dai H 2008 Chemically derived, ultrasmooth graphene nanoribbon semiconductors *Science* **319** 1229-32

[10] Naeemi A and Meindl J D 2007 Conductance modeling for graphene nanoribbon (GNR) interconnects *IEEE ELECTR DEVICE L* **28** 428-31

[11] Lemme M C, Echtermeyer T J, Baus M and Kurz H 2007 A graphene field-effect device *arXiv preprint cond-mat/0703208*

[12] Bai J, Zhong X, Jiang S, Huang Y and Duan X 2010 Graphene nanomesh *Nat. Nanotechnol.* **5** 190-4

[13] Chang C-K, Kataria S, Kuo C-C, Ganguly A, Wang B-Y, Hwang J-Y, Huang K-J, Yang W-H, Wang S-B and Chuang C-H 2013 Band gap engineering of chemical vapor deposited graphene by in situ BN doping *ACS Nano* **7** 1333-41

[14] Balog R, Jørgensen B, Nilsson L, Andersen M, Rienks E, Bianchi M, Fanetti M, Lægsgaard E, Baraldi A and Lizzit S 2010 Bandgap opening in graphene induced by patterned hydrogen adsorption *Nature materials* **9** 315-9

[15] Zou K, Zhang F, Clapp C, MacDonald A and Zhu J 2013 Transport studies of dual-gated ABC and ABA trilayer graphene: band gap opening and band structure tuning in very large perpendicular electric fields *Nano Lett.* **13** 369-73

[16] Nakaharai S, Iijima T, Ogawa S, Suzuki S, Li S-L, Tsukagoshi K, Sato S and Yokoyama N 2013 Conduction tuning of graphene based on defect-induced localization *ACS Nano* **7** 5694-700

[17] Shimizu T, Haruyama J, Marcano D, Kosinkin D, Tour J, Hirose K and Suenaga K 2011 Large intrinsic energy bandgaps in annealed nanotube-derived graphene nanoribbons *Nat. Nanotechnol.* **6** 45-50

[18] Aragay G, Frontera A, Lloveras V, Vidal-Gancedo J and Ballester P 2013 Different Nature of the Interactions between Anions and HAT (CN) 6: From Reversible Anion− π Complexes to Irreversible Electron-Transfer Processes (HAT (CN) 6= 1, 4, 5, 8, 9, 12-Hexaazatriphenylene) *J. Am. Chem. Soc.* **135** 2620-7

[19] Tanaka H, Arima R, Fukumori M, Tanaka D, Negishi R, Kobayashi Y, Kasai S, Yamada T K and Ogawa T 2015 Method for Controlling Electrical Properties of Single-Layer Graphene Nanoribbons via Adsorbed Planar Molecular Nanoparticles *Sci. Rep.* **5**

[20] Yajima T, Tanaka H, Matsumoto T, Otsuka Y, Sugawara Y and Ogawa T 2007 Refinement of conditions of point-contact current imaging atomic force microscopy for molecular-scale conduction measurements *Nanotechnology* **18** 095501

[21] Jiao L, Zhang L, Wang X, Diankov G and Dai H 2009 Narrow graphene nanoribbons from carbon nanotubes *Nature* **458** 877-80

[22] Bai J, Duan X and Huang Y 2009 Rational fabrication of graphene nanoribbons using a nanowire etch mask *Nano Lett.* **9** 2083-7

[23] Lu Y, Goldsmith B, Strachan D R, Lim J H, Luo Z and Johnson A 2010 High-On/Off-Ratio Graphene Nanoconstriction Field-Effect Transistor *Small* **6** 2748-54

[24] Schwierz F 2010 Graphene transistors *Nat. Nanotechnol.* **5** 487-96

[25] Jiao L, Wang X, Diankov G, Wang H and Dai H 2010 Facile synthesis of high-quality graphene nanoribbons *Nat. Nanotechnol.* **5** 321-5

[26] Chen Z, Lin Y-M, Rooks M J and Avouris P 2007 Graphene nano-ribbon electronics *Physica E* **40** 228-32

[27] Dyalsingh H and Kakalios J 1996 Thermopower and conductivity activation energies in hydrogenated amorphous silicon *Phys. Rev. B* **54** 7630

[28] Mucciolo E R, Neto A C and Lewenkopf C H 2009 Conductance quantization and transport gaps in disordered graphene nanoribbons *Phys. Rev. B* **79** 075407

[29] Cresti A, Nemec N, Biel B, Niebler G, Triozon F, Cuniberti G and Roche S 2008 Charge transport in disordered graphene-based low dimensional materials *Nano Res.* **1** 361-94

[30] Fan X, Nouchi R and Tanigaki K 2011 Effect of charge puddles and ripples on the chemical reactivity of single layer graphene supported by SiO2/Si substrate *J. Phys. Chem. C* **115** 12960-4

[31] Hwang E, Adam S and Sarma S D 2007 Carrier transport in two-dimensional graphene layers *Phys. Rev. Lett.* **98** 186806

[32] Martin J, Akerman N, Ulbricht G, Lohmann T, Smet J v, Von Klitzing K and Yacoby A 2008 Observation of electron–hole puddles in graphene using a scanning single-electron transistor *Nature Phys.* **4** 144-8

[33] Lafkioti M, Krauss B, Lohmann T, Zschieschang U, Klauk H, Klitzing K v and Smet J H 2010 Graphene on a hydrophobic substrate: doping reduction and hysteresis suppression under ambient conditions *Nano Lett.* **10** 1149-53

[34] Asay D B and Kim S H 2005 Evolution of the adsorbed water layer structure on silicon oxide at room temperature *J. Phys. Chem. B* **109** 16760-3

[35] Wehling T, Katsnelson M and Lichtenstein A 2009 Adsorbates on graphene: Impurity states and electron scattering *Chem. Phys. Lett.* **476** 125-34

[36] Wehling T O, Lichtenstein A I and Katsnelson M I 2008 First-principles studies of water adsorption on graphene: The role of the substrate *Appl. Phys. Lett.* **93** 202110

[37] Mayorov A S, Gorbachev R V, Morozov S V, Britnell L, Jalil R, Ponomarenko L A, Blake P, Novoselov K S, Watanabe K and Taniguchi T 2011 Micrometer-scale ballistic transport in encapsulated graphene at room temperature *Nano Lett.* **11** 2396-9

[38] Kobayashi S, Nishikawa T, Takenobu T, Mori S, Shimoda T, Mitani T, Shimotani H, Yoshimoto N, Ogawa S and Iwasa Y 2004 Control of carrier density by self-assembled monolayers in organic field-effect transistors *Nat. Mater.* **3** 317-22

[39] Nagashio K, Yamashita T, Nishimura T, Kita K and Toriumi A 2011 Electrical transport properties of graphene on SiO2 with specific surface structures *J. Appl. Phys.* **110** 024513

[40] Dean C R, Young A F, Meric I, Lee C, Wang L, Sorgenfrei S, Watanabe K, Taniguchi T, Kim P and Shepard K 2010 Boron nitride substrates for high-quality graphene electronics *Nat. Nanotechnol.* **5** 722-6

CHAPTER 4

Fabrication of turbostratic multi-layer graphene nanoribbon field effect transistor and investigating the electrical property with the adsorption of HAT-CN6

Graphene nanoribbon (GNR) is a narrow strip of carbon atoms composed with various intrinsic properties required to explore. This study demonstrates the fabrication of multi-layer graphene nanoribbon (mGNR) field effect transistor (FET) (mGNR-FET) and controlling its electrical property with the adsorption of the flat molecular nanoparticle. The stacked mGNR device shows the performance similar to single-layer GNR (sGNR) device which is due to the lower inter layer interaction. Inter layer interaction was supposed to be lower since the turbostratic stacking of GNR was formed by chemical vapor deposition (CVD) growth process. Furthermore, Hexaazatriphenylenehexacarbonitrile (HAT-CN6) were casted on the mGNR-FET device to alter the electronic property of mGNR-FET device. The solution of HAT-CN6 forms the self-assembled molecular nanoparticles and adsorbed on the mGNR. These adsorbed nanoparticles works as a charge carrier trapping sites and the remaining small area without nanoparticle are defined as neck region. Thus, the carriers pass only through the neck region, which shows similar behavior to narrow width GNR. Hence, at the neck region due to lateral charge carrier confinement, the GNR device shows the semiconducting property. The on/off ratio of the mGNR-FET device was also improved with the adsorption of nanoparticle on mGNR. The fabricated mGNR-FET device can have a wide area of semiconductor electronics applications in the semiconductor industry.

4.1 Introduction

The discovery of graphene ignited intense research to explore the electronics property of 2D materials.[1] It opens the wide range of applications in the area of electronics engineering and is a good contender to replace the silicon technology in near future. However, the pristine graphene (width > 10nm) shows semimetallic behavior (zero bandgap semiconductor) and the device has low on/off ratio which hinders the application of graphene-based nano- and micro-electronic devices.[2] Hence, various efforts have been made to open the band gap in graphene,[3] but the devices performance were not well improved due to lack of charge transport and complex structure. However single-layer graphene has enormous potential with various properties,[4] and offering near ballistic transport[5] which enables a wide range of graphene-based field effect transistor (FET) applications[6] and electronics device applications.

Further, with the advancement in technology, the researchers tried to scale down the width of graphene to open the band gap,[7] and the scaled graphene is known as graphene nanoribbon (GNR). Both the single-layer and multi-layer GNR (mGNR) has the fascinating electronic property for transistor and interconnects due to high carrier mean free path and large current carrying capacity.[8] It was supposed that the resistance of mGNR decreases as the number of layer increases but the impact of interlayer resistance was ignored.[9] Furthermore, it was also reported that the mGNR has lower conductivity as compared to single-layer GNR (sGNR) due to inter layer electron hopping.[10] So far, there are various groups reported the synthesis of mGNR by unzipping multi-walled carbon nanotubes (MWNTs).[11-13] But the width of GNR obtained is too wide to observe the transistor property and quantum effects as MWNTs are significantly large in diameters.

Here, we are interested in investigating the electrical property of mGNR grown on the sGNR or double-layer GNR (dGNR) template. The narrow width single-layer and double-layer GNRs were successfully synthesized from double-walled carbon nanotubes (DWNT),[14] which was further grown to mGNR by chemical vapor deposition (CVD) process.[15, 16] The obtained mGNRs through this process forms the turbostratic structure. According to reported theoretical calculations, mGNR with turbostratic structures has a band structure similar to that of single-layer graphene with a linear dispersion (Dirac cone structure) due to very weak interaction between graphene layers. The mGNR field effect transistor (mGNR-FET) device was fabricated and the Hexaazatriphenylenehexacarbonitrile (HAT-CN6) nanoparticle was used as an adsorbate molecules to tune the electrical property of mGNR. The device with HAT-CN6 shows improved on/off ratio with that of the pristine device which is due to narrowing the width of mGNR by adsorption of nanoparticles. The reports suggest, the gap opening due to carrier confinements and edge effects in very narrow GNRs (~10 nm) which leads to their future applications in transistors and interconnects.[17, 18] The turbostratic stacking of graphene has still various unexplored property required to understand. This feature is ideal for high-performance FETs with both high carrier mobility and high on/off ratio.

4.2 Experimental procedures

DWNTs were used as a starting material with the diameters between 3–15 nm. Defects were induced to pristine DWNTs by annealing at 500°C. 3 mg of Poly [(m-phenylenevinylene) -co- (2,5-dioctoxY-p-phenylenevinylene)] (PmPV) and the annealed DWNT was added to 10 ml of 1, 2-dichloroethane solution. The solution was then sonicated for 4 h at 37 kHz by a 600W sonicator, to unzip the DWNT. The solution obtained with the sonication was centrifuged at 50000 G (20000 rpm ca; TOMY Suprema 23 high-speed centrifuge) for 5 h to remove the remained nanotubes and

amorphous carbons or the agglomerated nanotubes. Finally, the supernatant was extracted in a clean bottle. This is the obtained GNR solution and casted on SiO_2 substrate. The substrate was then annealed at 350°C for 3 h under air to remove the PmPV from the substrate and GNR.[19]

Next, the sample was further processed for the growth of stacked GNR layers through sloped-temperature CVD process. This makes the growth layer by layer on the pre-GNR deposited substrate. In this process, the carbon feedstock decomposition and graphene growth were separately controlled.[15, 16, 20] The control temperature in the furnace for the experiments were 900°C for the carbon feedstock decomposition and 720-744°C for GNR growth. GNR samples before and after the CVD growth were characterized using AFM measurements.

Subsequently, gold electrode was deposited on the substrate containing multilayer GNR. The device is ready for electrical measurement. Furthermore, the acetone solution of HAT-CN6 was casted on the substrate. As the acetone evaporated, self-assembled nanoparticles of HAT-CN6 were adsorbed on the multilayer GNRs through π-π stacking.[14] To confirm the change in electric property, FET measurement was performed by the low-temperature four-probe system (Pascal Co., Ltd) with semiconductor parameter analyzer (HP 4156B). Gold electrode with Ti/Au (6 nm / 24 nm) having the gap of 1 um were deposited on SiO_2 substrate through EBL. The width of multilayer GNR for FET measurement was 20 nm. Finally, the temperature dependence property of device was measured at different temperature by varying the Vgs and fixed 0.5 V Vds.

4.3 Results and Discussion

The AFM images of mGNR device and the mGNR with adsorbed molecular nanoparticles are shown in **Figure 4.1.** The channel formation between the source and drain electrodes was confirmed with the AFM image as in **Figure 4.1 (a).** The electrodes were fabricated with a

conventional photolithography technique.[21] Moreover, the AFM images of mGNR with different concentration of HAT-CN6 solution casted on mGNR are shown in **Figure 1 (b), (c)** and the concentration of solutions were $1x10^{-4}$ and $2x10^{-4}$ mol/L respectively. It can be clearly observed from the AFM images that, as the concentration of HAT-CN6 increased the number of adsorbed nanoparticles were also increased.

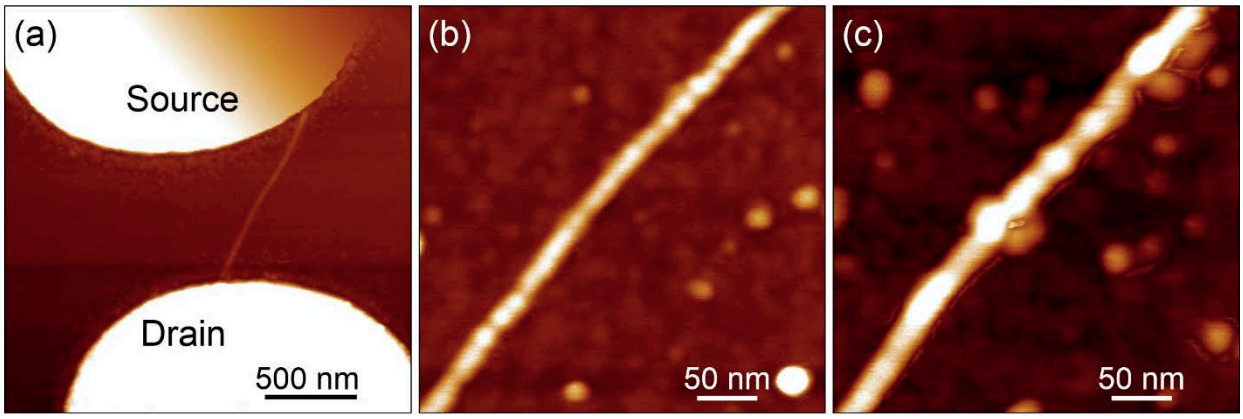

Figure 4.1 AFM images. (a) The fabricated mGNR-FET device. (b) mGNR adsorbed with HAT-CN6 concentration $1x10^{-4}$. (c) mGNR adsorbed with HAT-CN6 concentration $2x10^{-4}$

Figure 4.2 shows the schematic representation of HAT-CN6 nanoparticle adsorbed on mGNR. Stronger π-π interaction of GNR with HAT-CN6 makes it suitable for altering the electrical property of GNR based devices. It has been reported that HAT-CN6 is a strong acceptor with higher LUMO energy level.[22] Here the device is fabricated with mGNR as a channel and the nanoparticles can be adsorbed at the top most layer of the mGNR and at the edge of successive layers. Thus, it changes the electronic property of the top most layer whereas other layer has no or very low impact of HAT-CN6 adsorption due to adsorption at sidewalls. However, the overall conductivity of the GNR device is affected by the adsorption of the nanoparticle. The nanoparticles on GNR results in lateral confinement of charge carriers occurred around the neck region of mGNR

and the nanoparticles form the trapping sites, hence, the carriers can pass only through the neck region at the top layer of the mGNR. (shown in **Figure 4.2**). Thus, the current will be suppressed due to high resistance at the neck region and charge carrier screening effect was supposed to be observed.[14] In contrast, the bottom layers of GNRs have a conduction similar to pristine turbostratic GNR because no nanoparticles adsorbed.

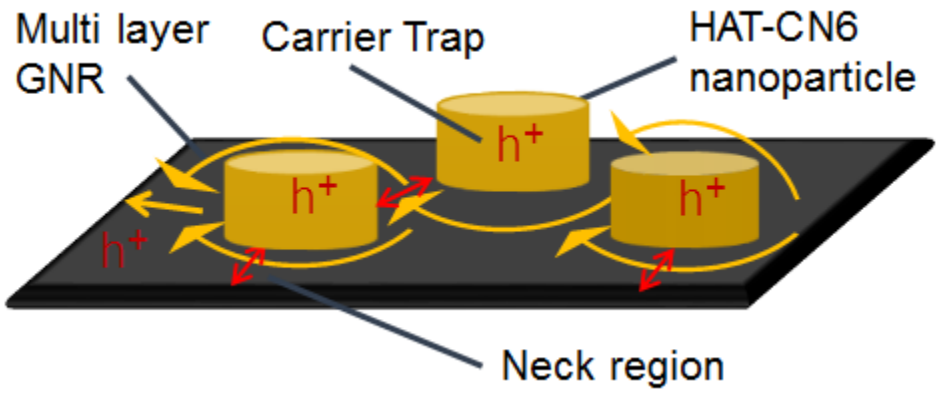

Figure 4.2 Adsorption of nanoparticle on multilayer GNR and forming the charge carrier trapping sites and neck structures

Furthermore, the schematic of the turbostratic structure of GNR is shown in **Figure 4.3.** The mGNR used in this study were grown on GNR template through the CVD process and forms turbostratic structure. The turbostratic property of the obtained mGNR was confirmed by Raman spectroscopy. [R. Negishi et al. Synthesis of very narrow multilayer graphene nanoribbon with turbostratic stacking] It is supposed that mGNRs grown by CVD process on GNR template have different lattice orientations and are stacked layer by layer on GNR which results in turbostratic structure. The change in lattice structure stacking between the layers of graphene can make the possible way to open the band gap in graphene-based electronics device. It was also reported that the graphene grown on carbon faces has higher mobility and forms the turbostratic structure

because of the rotational disorder.[23] Thus, multilayer graphene can achieve the electronic property of single-layer graphene by a relevant change in the stacking structure of graphene.[24]

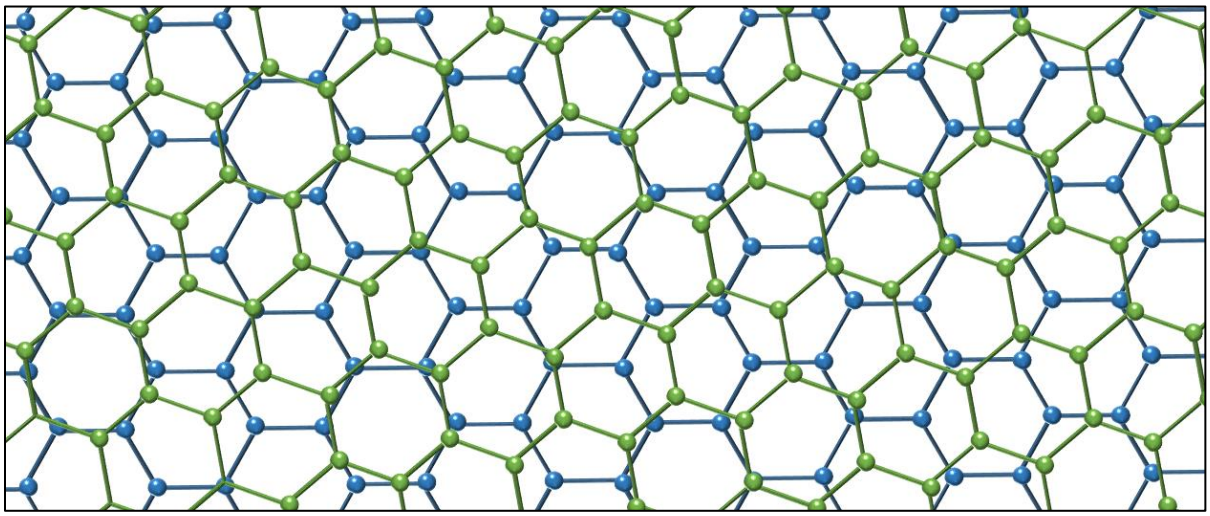

Figure 4.3 Schematic representation of turbostratic stacked multilayer GNR, showing rotation of lattice stacking and thus reduced interlayer interaction

Next, the electrical property of pristine mGNR-FET device and the device with adsorption of nanoparticles were investigated with the FET measurement. The schematic diagram of the back-gate FET device is shown in **Figure 4.4 (a).** The electrical characteristic of the device was observed using current-voltage measurement (I_{ds}-V_{ds}) for both the device with and without HAT-CN6 nanoparticles as shown in **Figure 4.4 (b)**. The obtained I-V curve indicates that the current is suppressed with the adsorption of nanoparticle and was suppressed due to the electron trapping sites formed on the GNR.[14] The gate dependent transfer characteristic of the device was also measured to observe the device behavior with the back-gate FET. The transfer curve of the device indicates the improved on/off ratio with the adsorption of HAT-CN6 molecular nanoparticle on mGNR as shown in **Figure 4.4 (c).** The phenomenon of improvement in on/off ratio was also reported by the theoretical calculations in the turbostratic structure of mGNR.[25] The

improvement in on/off ratio is supposed due to the adsorption of nanoparticles on the mGNR-FET device.

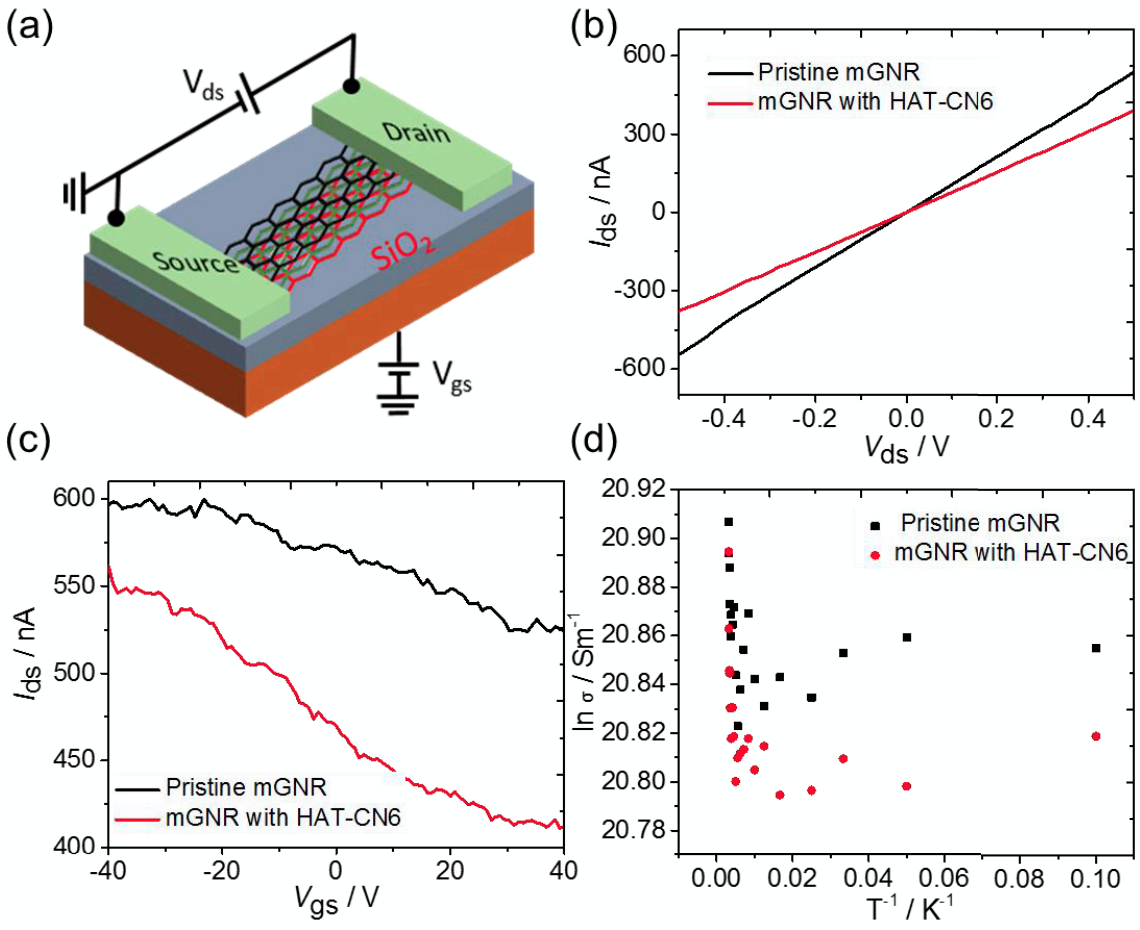

Figure 4.4 Electrical characteristic of a FET device for stacked multilayer GNR. (a) Schematic of the back-gate FET device. (b) Comparison of the I-V curve with and without HAT-CN6 nanoparticle. (c) Transfer curve obtained using back gate measurement. (d) Temperature dependent conductivity measurement.

The channel width is narrowed due to adsorbed nanoparticle and works similar to narrow width GNR. Whereas the pristine mGNR device showed the pure metallic behavior with electron doped from SiO_2 substrate and the device with HAT-CN6 is shifting towards p-type semiconductor. The

on/off ratio of the device with HAT-CN6 at room temperature is about 2.5 times to that of the pristine device. The mobility of the device with HAT-CN6 was also calculated and was obtained about 22 cm^2/Vs. Improved on/off ratio in narrow width GNR device is highly appreciable for advanced digital electronics applications.[26]

The device adsorbed with HAT-CN6 have high on/off ratio, which makes it suitable for high-speed switching applications.[27] The reason of improved on/off ratio of the device with HAT-CN6 is supposed to be due to the carrier trapping sites formed at top layer of the mGNR. Thus, some of the charge carriers are trapped with the nanoparticle on GNR and conduction path becomes narrow at the top most layer due to nanoparticles on it. Thus, the device with nanoparticles has narrower channel as compared to pristine device which improves the on/off current ratio of the device.[28, 29] This results in the suppression of current flow and shifts towards the semiconductor property. From the transfer curve, it can be observed that the device is in the transition state from metallic to semiconducting. The reason for not fully transforming to semiconductors is supposed due to an inner layer of device that has not any effect or just a few effects from the adsorption of nanoparticle at the sidewalls.

At next step, carrier transport mechanism of the device was also studied with the temperature dependent electrical measurement as shown in **Figure 4.4 (d)**. The obtained results of the temperature dependent curve suggest that in the high-temperature region the conductivity is due to electron hopping and as the temperature increases the conductivity of the device also increases. The increase in conductivity at the higher temperature is due to charge carrier hopping conduction in the mGNR-FET device. It was also observed that at a temperature around 200 K there is a slight fluctuation in the conductivity. Such a fluctuations could be due to two possible reasons, the acoustic phonon vibrations in the metallic region of mGNR[19] or due to suppressed carrier flow

resulting in lower conductivity with the adsorbed nanoparticle on mGNR. The activation energy of the device was calculated with the Arrhenius plot in **Figure 4.5.**

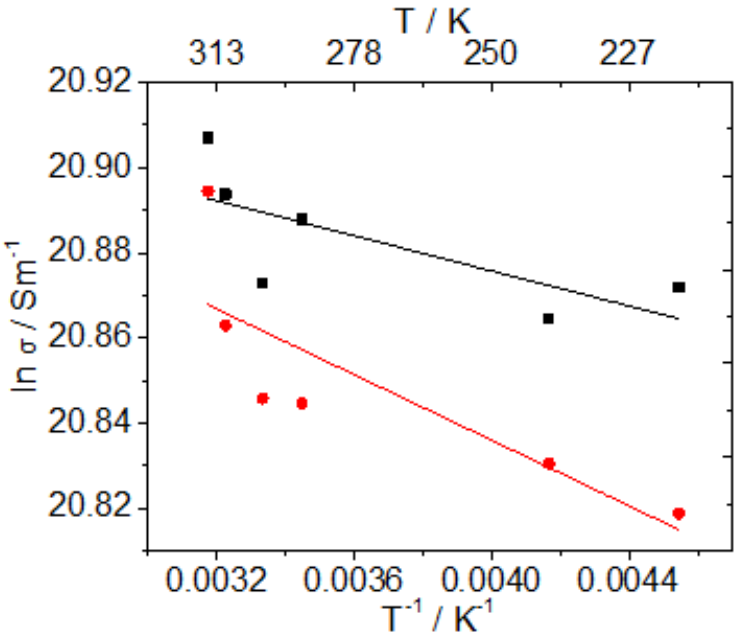

Figure 4.5 Arrhenius plot to obtain the activation energy, pristine mGNR (black plot), mGNR with HAT-CN6 (red plot).

The slope obtained at trend line as shown in **Figure 4.5** and the activation energy was calculated according to the equation given below.[30]

$$Slope = -\frac{Ea}{R}$$

Where Ea is the activation energy, R is the ideal gas constant in joules per mole Kelvin, and the slope is the temperature dependent slope.

The calculated activation energy for the pristine mGNR device is about 1.81 meV whereas the device with HAT-CN6 was about 3.45 meV. The change in activation energy of the device with the HAT-CN6 could be due to Anderson localization effect at the top most layer of mGNR resulted

with the adsorption of nanoparticles.[31, 32] The obtained activation energy is very low which shows that device is in a transition state and not fully tuned to semiconducting. This is due to the nanoparticles only adsorbed at the topmost layer.

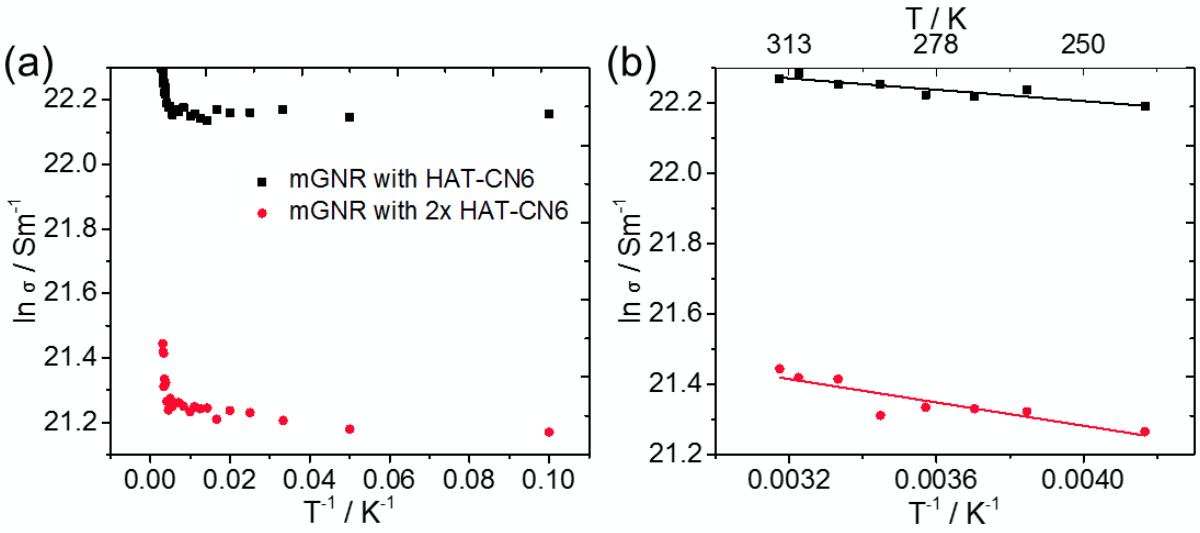

Figure 4.6 **(a)** Comparison of temperature dependent conductivity by varying the concentration of HAT-CN6 nanoparticle. (b) The Arrhenius plot to obtain the activation energy.

Moreover, the mGNR device with varying concentration of HAT-CN6 nanoparticle was also observed to verify the effect of nanoparticle on mGNR. The temperature dependent conductivity was measured in **Figure 4.6 (a)** to compare the change in conductivity by adsorption of molecular nanoparticles. It can be observed from as the concentration of HAT-CN6 was increased the conductivity of the device was suppressed due to large number of nanoparticles on mGNR. These nanoparticles forms the strong carrier trapping sites. Furthermore, the activation energy of the device was calculated from the Arrhenius plot in **Figure 4.6 (b).** The obtained activation energy was 7.0 meV black plot, whereas once the concentration was twice the activation energy was about 14.3 meV. It was observed that the activation energy of the device was increased with the higher concentration of the HAT-CN6 nanoparticle. This increase in activation energy confirms that the

device is more emphasized towards the semiconductor property resulting in the band gap opening with the increase in nanoparticle concentration. Since the increased concentration of nanoparticle results in large number of adsorption sites thus large traps and hence much confinement of charge carriers. The device is still transition state from semimetal to semiconductor as the activation energy is very small.

The drastic change in activation energy was observed in the sGNR device with the adsorption of molecular nanoparticles as described in Chapter 3, whereas mGNR device has very small change. This change in activation energy confirms the finite opening of band gap in sGNR device and tuning it to semiconductor but, the mGNR device just shows the transition state with small change. The reason for small change in activation energy is due to nanoparticles can only adsorb at topmost layer. However, the mGNR device with HAT-CN6 showed the improved on/off ratio, which is due to the narrow conduction path at top layer of GNR from the adsorbed nanoparticles. The conductivity of the mGNR device was increased as compared to sGNR as the conduction path becomes stronger with the multilayer turbostratic stacking.

4.4 Conclusion

The turbostratic stacked mGNR were grown on the GNR template, obtained by unzipping DWNT via sonication process. mGNR-FET device shows the reasonable gate dependence modulation in the transfer curve with the nanoparticle adsorbed on it. The device shows the transition from semimetallic to p-type semiconducting with improved on/off ratio after the adsorption of flat organic molecule HAT-CN6. The obtained results suggest the formation of neck with HAT-CN6 nanoparticle on GNR thus, the GNR device works similar to the narrow width GNR device. In addition, it was found that the HAT-CN6 is the strong acceptor molecular nanoparticle to alter the electrical property of GNR and noticeable band gap can be achieved in GNR device that is wider

than 10 nm. The possible reason of opening the band gap in GNR device was also discussed. The concentration of nanoparticle has a great impact on opening the band gap in GNR device. The activation energy was also calculated with the temperature dependence measurement. Such a technique could be promising for next generation semiconductor electronics industry.

4.5 References

[1] Tahy K, Xing H and Jena D 2013 Graphene nanoribbon FETs for digital electronics: experiment and modeling *Int. J. Circuit Theory Appl.* **41** 603-7

[2] Xia F, Farmer D B, Lin Y-m and Avouris P 2010 Graphene field-effect transistors with high on/off current ratio and large transport band gap at room temperature *Nano Lett.* **10** 715-8

[3] Jariwala D, Srivastava A and Ajayan P M 2011 Graphene synthesis and band gap opening *J. Nanosci. Nanotechnol.* **11** 6621-41

[4] Zhu Y, Murali S, Cai W, Li X, Suk J W, Potts J R and Ruoff R S 2010 Graphene and graphene oxide: synthesis, properties, and applications *Adv. Mater.* **22** 3906-24

[5] Du X, Skachko I, Barker A and Andrei E Y 2008 Approaching ballistic transport in suspended graphene *Nat. Nanotechnol.* **3** 491-5

[6] Meric I, Han M Y, Young A F, Ozyilmaz B, Kim P and Shepard K L 2008 Current saturation in zero-bandgap, top-gated graphene field-effect transistors *Nat. Nanotechnol.* **3** 654-9

[7] Wang X, Ouyang Y, Li X, Wang H, Guo J and Dai H 2008 Room-temperature all-semiconducting sub-10-nm graphene nanoribbon field-effect transistors *Phys. Rev. Lett.* **100** 206803

[8] Naeemi A and Meindl J D 2009 Compact physics-based circuit models for graphene nanoribbon interconnects *IEEE Trans. Electron Devices* **56** 1822-33

[9] Kumar V, Rakheja S and Naeemi A 2011 Modeling and optimization for multi-layer graphene nanoribbon conductors: IEEE) p 1-3

[10] Benedict L X, Crespi V H, Louie S G and Cohen M L 1995 Static conductivity and superconductivity of carbon nanotubes: Relations between tubes and sheets *Phys. Rev. B* **52** 14935

[11] Jiao L, Zhang L, Wang X, Diankov G and Dai H 2009 Narrow graphene nanoribbons from carbon nanotubes *Nature* **458** 877-80

[12] Kosynkin D V, Higginbotham A L, Sinitskii A, Lomeda J R, Dimiev A, Price B K and Tour J M 2009 Longitudinal unzipping of carbon nanotubes to form graphene nanoribbons *Nature* **458** 872-6

[13] Higginbotham A L, Kosynkin D V, Sinitskii A, Sun Z and Tour J M 2010 Lower-defect graphene oxide nanoribbons from multiwalled carbon nanotubes *ACS Nano* **4** 2059-69

[14] Tanaka H, Arima R, Fukumori M, Tanaka D, Negishi R, Kobayashi Y, Kasai S, Yamada T K and Ogawa T 2015 Method for Controlling Electrical Properties of Single-Layer Graphene Nanoribbons via Adsorbed Planar Molecular Nanoparticles *Sci. Rep.* **5**

[15] Negishi R, Hirano H, Ohno Y, Maehashi K, Matsumoto K and Kobayashi Y 2011 Layer-bY-layer growth of graphene layers on graphene substrates by chemical vapor deposition *Thin Solid Films* **519** 6447-52

[16] Negishi R, Hirano H, Ohno Y, Haehashi K, Matsumoto K and Kobayashi Y 2011 Thickness Control of Graphene Overlayer via Layer-bY-Layer Growth on Graphene Templates by Chemical Vapor Deposition *Jpn. J. Appl. Phys.* **50** 06GE4

[17] Li X, Wang X, Zhang L, Lee S and Dai H 2008 Chemically derived, ultrasmooth graphene nanoribbon semiconductors *Science* **319** 1229-32

[18] Xu C, Li H and Banerjee K 2009 Modeling, analysis, and design of graphene nano-ribbon interconnects *IEEE Trans. Electron Devices* **56** 1567-78

[19] Jiao L, Wang X, Diankov G, Wang H and Dai H 2010 Facile synthesis of high-quality graphene nanoribbons *Nat. Nanotechnol.* **5** 321-5

[20] Negishi R, Ohno Y, Maehashi K, Matsumoto K and Kobayashi Y 2012 Carrier Transport Properties of the Field Effect Transistors with Graphene Channel Prepared by Chemical Vapor Deposition *Jpn. J. Appl. Phys.* **51** 06FD3

[21] Negishi R and Kobayashi Y 2014 Extraordinary suppression of carrier scattering in large area graphene oxide films *Appl. Phys. Lett.* **105** 253502

[22] Aragay G, Frontera A, Lloveras V, Vidal-Gancedo J and Ballester P 2013 Different nature of the interactions between anions and HAT (CN) 6: from reversible anion− π complexes to irreversible electron-transfer processes (HAT (CN) 6= 1, 4, 5, 8, 9, 12-Hexaazatriphenylene) *J. Am. Chem. Soc.* **135** 2620-7

[23] Tiberj A, Huntzinger J-R, Camassel J, Hiebel F, Mahmood A, Mallet P, Naud C and Veuillen J-Y 2011 Multiscale investigation of graphene layers on 6H-SiC (000-1) *Nanoscale Res. Lett.* **6** 1-8

[24] Dos Santos J L, Peres N and Neto A C 2007 Graphene bilayer with a twist: Electronic structure *Phys. Rev. Lett.* **99** 256802

[25] Ouyang Y, Dai H and Guo J 2010 Projected performance advantage of multilayer graphene nanoribbons as a transistor channel material *Nano Res.* **3** 8-15

[26] Lu Y, Goldsmith B, Strachan D R, Lim J H, Luo Z and Johnson A 2010 High-On/Off-Ratio Graphene Nanoconstriction Field-Effect Transistor *Small* **6** 2748-54

[27] Schwierz F 2010 Graphene transistors *Nat. Nanotechnol.* **5** 487-96

[28] Bai J, Duan X and Huang Y 2009 Rational fabrication of graphene nanoribbons using a nanowire etch mask *Nano Lett.* **9** 2083-7

[29] Bai J, Zhong X, Jiang S, Huang Y and Duan X 2010 Graphene nanomesh *Nat. Nanotechnol.* **5** 190-4

[30] Chen Z, Lin Y-M, Rooks M J and Avouris P 2007 Graphene nano-ribbon electronics *PHYSICA E* **40** 228-32

[31] Mucciolo E R, Neto A C and Lewenkopf C H 2009 Conductance quantization and transport gaps in disordered graphene nanoribbons *Phys. Rev. B* **79** 075407

[32] Cresti A, Nemec N, Biel B, Niebler G, Triozon F, Cuniberti G and Roche S 2008 Charge transport in disordered graphene-based low dimensional materials *Nano Res.* **1** 361-94

CHAPTER 5

Fabrication of X- and Y-type graphene nanoribbon cross junction and study the electrical transport property

Double-walled carbon nanotubes (DWNTs) were used as a starting material to synthesize graphene nanoribbon (GNR) via lengthwise unzipping method and the obtained GNRs were used to form X-type or Y-type nanostructures. The electrical transport properties of X- and Y-type GNRs were successfully investigated using point contact current imaging (PCI-) AFM. According to the obtained results, semiconducting property of GNRs was observed at the junction whereas other parts were semimetallic. Moreover, the obtained results suggest the stacking angle dependent semiconducting property of X-type GNR. Semiconductor property of the junction located at the center of X-type GNR was supposed to be due to changes in lattice stacking. If the stacking angle between two GNRs differs the electrical transport properties also changes. The results also indicate that only one ribbon is behaving as semimetal but the conjunction of two ribbon works as semiconductor at the junction. Therefore, the electrical behavior of X- and Y-type GNRs were investigated which shows an important phenomenon in nanowire-based GNR junctions.

5.1 Introduction

Nowadays, graphene nanoribbon (GNR) as a two-dimensional material gained a huge interest due to its high carrier mobility and high-performance in graphene-based electronics.[1, 2] Several fabrication methods for GNR has been reported. However, lengthwise unzipping and subsequent chemical reduction of the nanoribbons still remains an attractive topic by the researchers in this area to restate the electrical conductivity of GNR.[3] Carbon nanotubes (CNTs) are considered to

be GNRs rolled up into seamless tubes, and the greatest challenge in converting CNTs to GNRs is cleaving CNTs in the longitudinal direction without rapid etching along the circumference.[4] Therefore, controlled unzipping of the CNTs is an essential to obtain GNR based devices.[5]

The career mobility of graphene is known to be much higher than present semiconductor material,[6] thus, many researchers are trying the substitute of present semiconductor devices to GNR device. These properties place GNR as one of the most attractive materials for electronic applications. However, graphene is a zero gap semiconductor[7] and consequently cannot be directly introduced as a material for mainstream logic electronic devices. The absence of an electronic gap makes it a poor candidate to achieve a sufficiently large on/off ratio needed for practical logic device operation.[8] Moreover, the gap can be induced in a number of ways such as structural alterations of the two-dimensional (2D) graphene sheet which can effectively reduce the system's dimensionality and lead to one-dimensional (1D) GNRs, a material with appealing electronic properties.[9, 10]

In this research, we have unzipped double-walled carbon nanotubes (DWNTs) to synthesize graphene nanoribbon.[11] The obtained nanoribbons were in a random pattern and depending on the number of casting and waiting time we had tried to control the structure to X- and Y-type. The electrical property of synthesized X- and Y-type GNRs were investigated from the point contact current imaging (PCI-) AFM. It was observed that depending on the angle of X, Y junction, the electrical property was different. Although the cross structure of GNR has been reported previously, the electrical property, however, has not reported yet. Study on electrical properties of X- and Y-type GNR structures could be interesting for fabricating nanowire-based GNR devices.

5.2 Experimental procedures

The systematic explanation of the GNR synthesis is presented in this section. It comprises of unzipping process, sample preparation, and the technique to obtain the X- and Y-type GNRs.

5.2.1 Unzipping DWNT

DWNT were used as starting material to synthesize GNR. First DWNTs were annealed at 500°C for 180 minutes to induce the defects on DWNTs surface. After annealing, DWNTs will have some defects on the surface of the tube. Then 3 mg of PmPV in dichloroethane solution with the annealed DWNTs were sonicated for 4 hours at 600 W. Thus, the DWNTs were unzipped as the sonication proceeds. The schematic representation of the unzipping process of DWNT is shown in **Figure 5.1**. From the schematic diagram, it can be seen as the sonication time increased the DWNT was unzipped and form the double-layer GNR (dGNR) and subsequently it forms the Y-type GNR and sGNR.

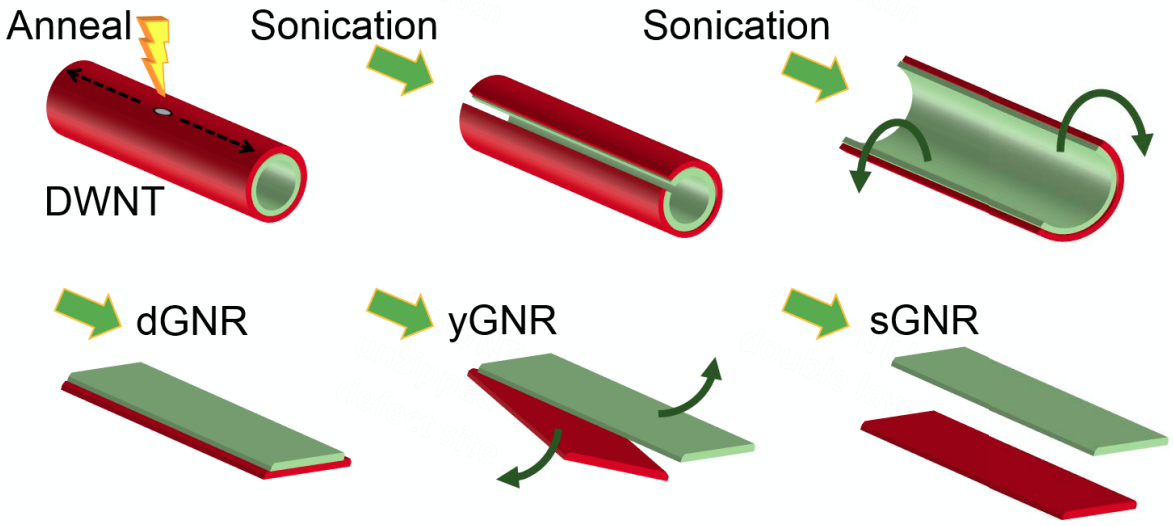

Figure 5.1 Synthesis of yGNR and sGNR from DWNT. DWNTs were annealed to induce defects followed by sonication. As the sonication time increases DWNTs were unzipped to double-layer GNR (dGNR), Y-type GNR (yGNR) and sGNR subsequently.

5.2.2 Sample preparation for X- and Y-type GNR

Moreover, 1 to 2 hours sonication will lead to the formation of Y-type GNR, while more than 2 hours sonication will make all the GNR to be single-layer. After sonication, the centrifugation was carried out at 5000 G for 4 hours to separate the impurities and PmPV. The remained unzipped DWNTs were at the sediment due to its heavier mass and GNRs remains on the top of the solution as supernatant. The supernatant solution was extracted and then was used to cast on the substrate. By casting twice, the X-type GNR were obtained on the substrate with some of the PmPV. The steps for sample preparation with the obtained GNR solution is shown in **Figure 5.2**.

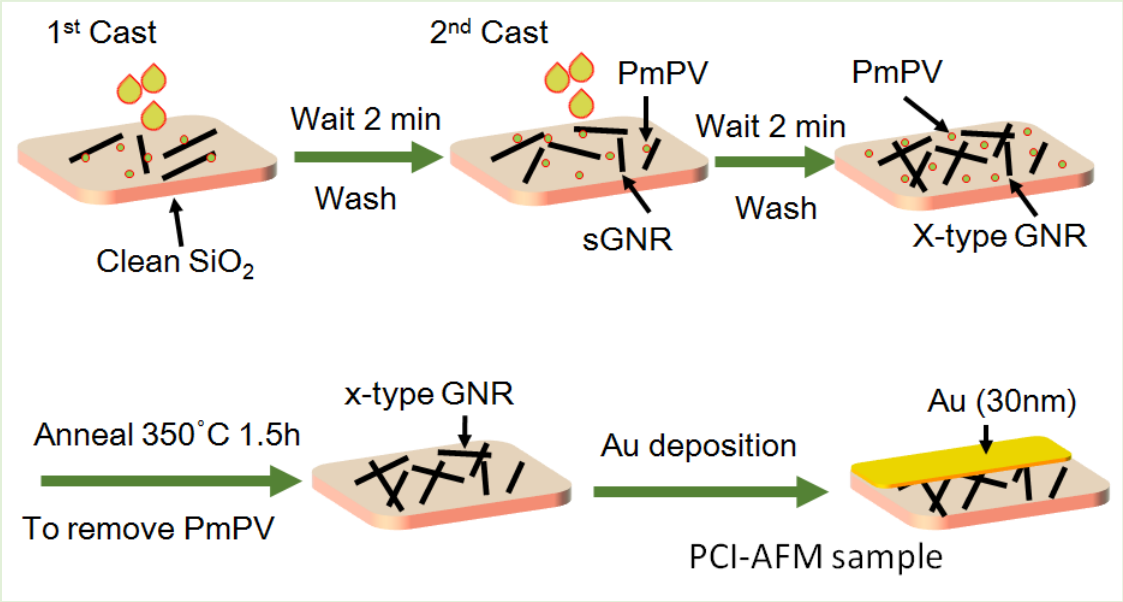

Figure 5.2 The process of sample preparation to obtain X- and Y-type GNR, subsequently the electrode deposition for PCI-AFM measurement.

After annealing the substrate with GNRs/PmPV at 350 C at 90 minutes the complete removal of the PmPV was obtained. Next, the sample for PCI-AFM was prepared by depositing the gold electrode on the silicon substrate which contains the GNR on it. The PCI-AFM measurement was performed to obtain the electrical property of X- and Y-type GNRs.

5.3 AFM characterization of X- and Y-type GNR

The AFM image of synthesized X- and Y-type GNR obtained from DWNTs are shown in **Figure 5.3.** Y-type structure was obtained just after 1-2 hours of sonication since both the layers of GNR starts splitting within 1-2 hours. If the sonication time was further increased around to 4 hours, the sGNR were obtained. Moreover, by adjusting the casting, waiting time and the number of casting the X-type structures were obtained as can be seen from the AFM image. The AFM images were obtained to confirm the formation of X- and Y-type GNRs. Once the X- and Y-type structure were confirmed the sample were set for the electrode deposition to prepare the sample for PCI-AFM measurement.

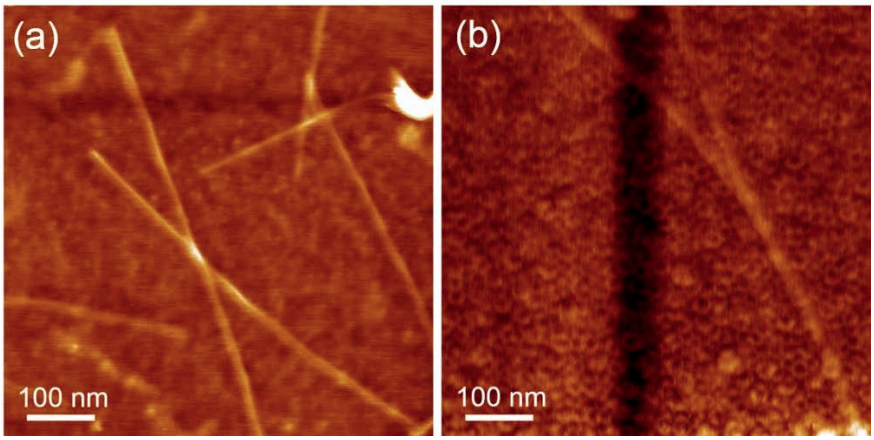

Figure 5. 3 The AFM images of synthesized GNR (a) X-type GNR (b) Y-type GNR

5.4 PCI-AFM characterization of the obtained structures

To investigate the electrical property of synthesized GNR, PCI-AFM measurement was carried out. PCI-AFM is a typical AFM in which the electrical property of conductive nanomaterials can be measured together with the image of the nanomaterial. This is the combination of tapping mode and point contact mode in which the topography of the material can be obtained with the tapping mode whereas the electrical property with the point-contact mode. It was developed by Prof. T.

Matsumoto and his co-workers in 2002.[12] PCI-AFM can provide high-resolution topographic image and I-V characteristic of the nanomaterial at every pixel of the topographic image.

In this experiment, PCI-AFM measurement was conducted by a scanning probe microscope controlled by two function generators. The platinum-coated cantilever was used for the I-V topographic measurement. Gold electrode was deposited on the substrate to form the conductive electrode with respective connected GNRs.

The schematic representation of PCI-AFM measurement is shown in **Figure 5.4.** The topography of the sample was obtained by tapping mode AFM, whereas current at each pixel was measured by point-contact mode AFM. By setting the optimized parameters, the resolution of the topographic image could be high enough to distinguish each and every GNRs on the sample and the images can be obtained at the specific area.

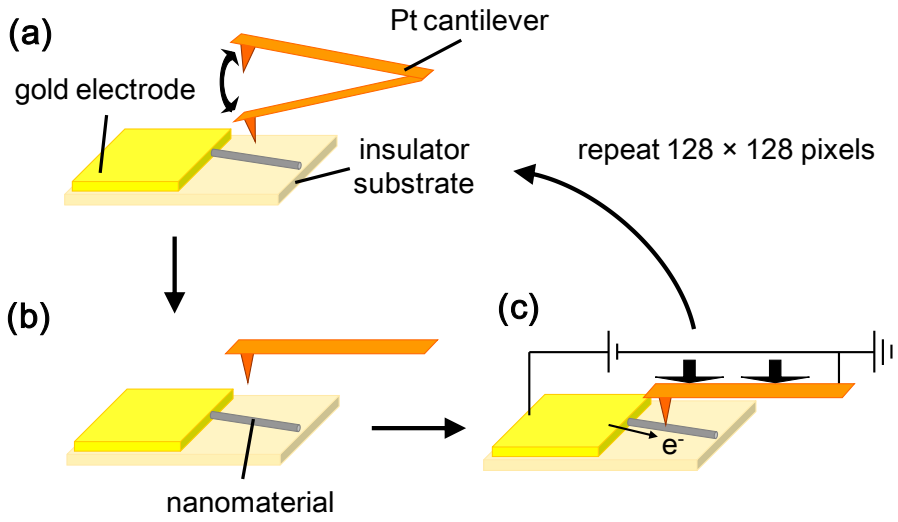

Figure 5.4 Schematic representation of PCI-AFM measurement. (a) Topographic image is obtained by tapping-mode AFM. (b) Vibration of cantilever stopped during I-V measurement. (c) Pt cantilever is pressed to make electrical contact with the GNR to obtain I-V curve. All the steps (a) – (c) repeated for each 128 × 128 pixels of the AFM measurement.

5.5 Results and discussion

The electrical property of synthesized X- and Y-type GNR cross junctions were measured with the PCI-AFM. The topographic current image of X-type GNR obtained from the PCI-AFM measurement is shown in **Figure 5.5 (a)**. This image shows the current obtained from the conductive material. If the GNR is not connected to the electrode or the tapping is not enough to pass the current between the cantilever and the GNR, no current image appears. Thus, it is very important to consider the tapping force on the cantilever during the PCI-AFM measurement.

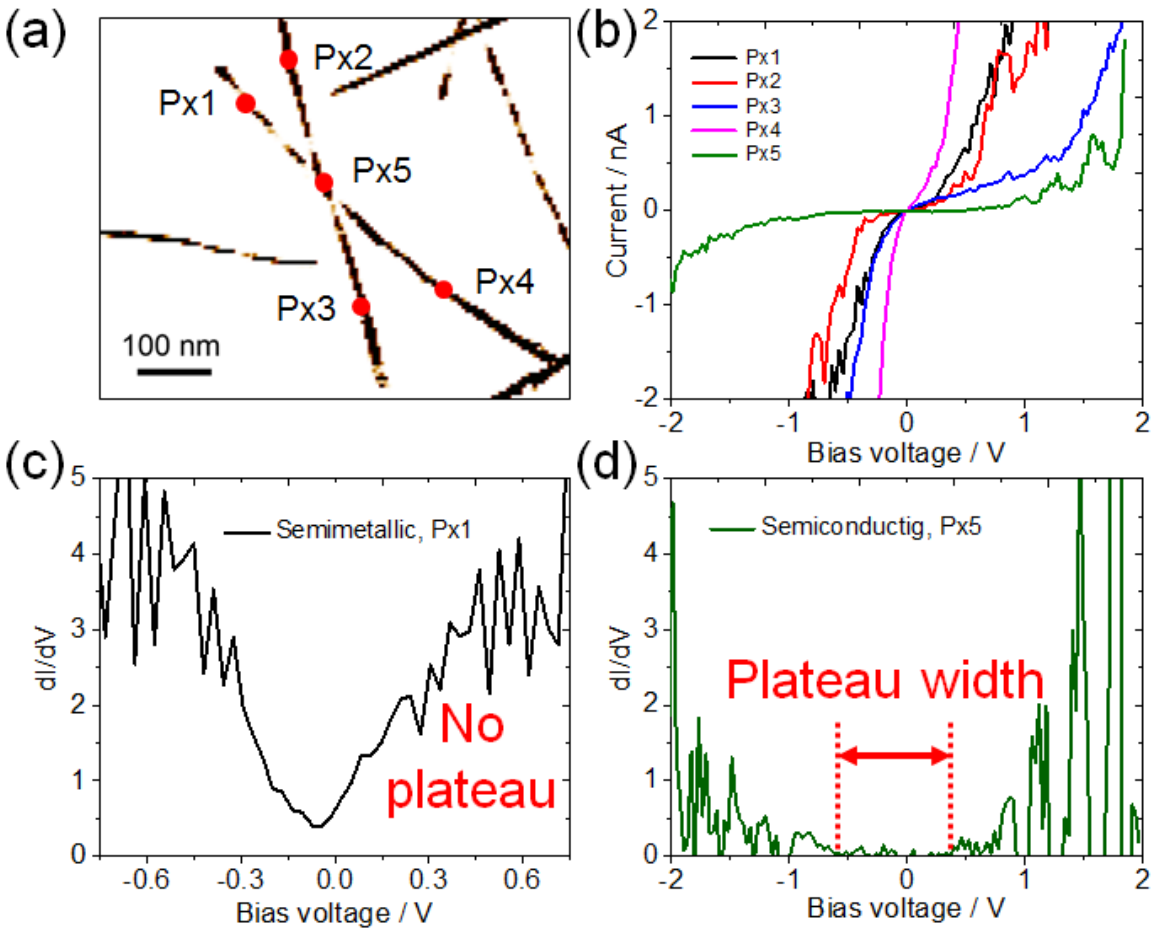

Figure 5.5 Electrical property of X-type GNR obtained from PCI-AFM. (a) Topographic current image. (b) I-V curve obtained at the different point of X-type GNR. (c) Extracted plateau width of semimetallic GNR. (d) Plateau width of semiconducting GNR at the X-type junction

Moreover, the electrical property of the GNR at the junction of X-type GNR and at different points of GNR was measured to investigate how the electrical behavior of GNR changes at the junction. The typical I-V curve extracted from the topographic image at different points of X-type GNR are shown in **Figure 5.5 (b)**.

I-V curves extracted at the different point in the topographic image on the X-type structure are indicated by Px1, Px2, Px3, Px4, and Px5. The semiconducting property of GNR was observed at the junction of X-type GNR at point Px5. Semiconducting property at the junction was supposed to be due to the turbostratic stacking of GNR was formed at the junction. If the stacking between the cross junctions is out-of-plane it shows an important electron transfer property.[13] The electrical property of stacked GNR changes depending on the type of stacking of GNR. It is similar to the stacking of few layer GNRs which resembles the property of single-layer GNR due to lower interlayer interaction[14] and thus the turbostratic stacking at the junction shows the semiconducting property. Moreover, the point Px1, Px2, Px3 and Px4 shows the semimetallic property of the GNR. This was due to synthesized GNR have the width between 15-25 nm, and it shows the semimetallic property.[Reetu raj et al. nanotechnology submitted] The semimetallic property of GNR with the width greater than 10 nm was also verified by various researchers.[15] The semimetallic and semiconducting property of GNR were confirmed by extracting the plateau width from the obtained I-V curve. The plot in **Figure 5.5 (c)** was extracted from the I-V curve Px1 and indicates no plateau. Thus, it confirms the semimetallic property of GNR. Whereas the plateau width extracted from the I-V curve at point Px5 in **Figure 5.5 (d)** shows the finite plateau, thus, confirms the semiconducting property at the junction.

To confirm the electrical property of GNR at junction several X-type GNR cross junctions were synthesized. The electrical transport property of X-type GNRs was investigated at the

junction. Many of the X-type GNRs at the junction shows semiconducting property with the different plateau width. The different plateau width with the different X-type GNR was supposed to be due to the varied stacking angle of the X-structure.[13] The plateau width was extracted from the obtained I-V curve by plotting dI/dV-V curve. The flat area of dI/dV-V curve is defined as plateau width as shown in **Figure 5.5 (d)**. More the plateau width, stronger the semiconducting property of the GNR. It was observed from the comparison with several X-type GNR by the varying angle of x structure the plateau width was varying. This variation is plateau width was supposed due to change in the lattice structure at the stacking with the different angles and thus results in different plateau width. However, the change in the plateau width is very small which confirms the semiconducting property at the junction of X-type GNR.

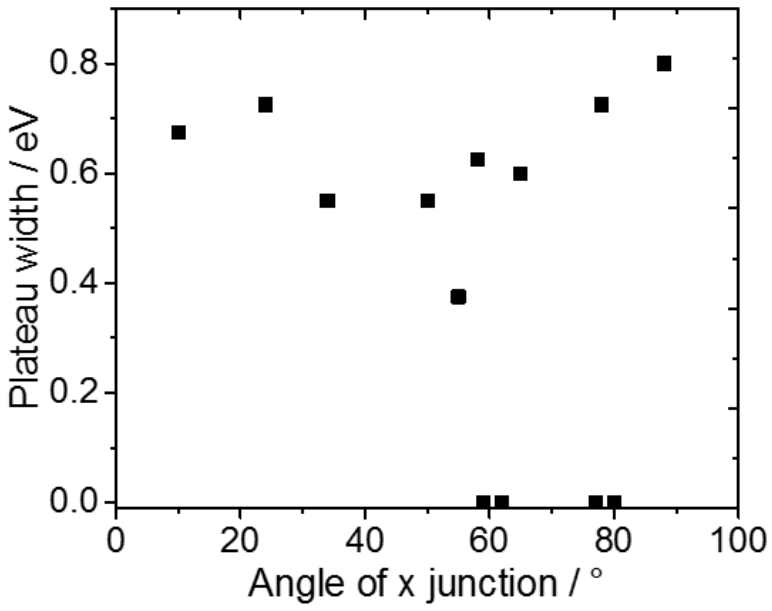

Figure 5.6. Plateau width obtained from the different stacking angle at X-type junction

However, some of the X-type GNRs shows the semimetallic property at the junction. This can be due to AB stacking of GNR at the junction and in-plane electron transmission.[16, 17] To verify the property of X-type GNR at the junction, several x structures of GNR were synthesized and the

electrical property at the junction was measured. Furthermore, the plateau width was also extracted. The plateau width obtained from the I-V curve at X-type junction are plotted with the angle of stacking at X-type junction in **Figure 5.6.** The obtained data suggest as the angle of junction changes the electrical property of GNR at the junction is also changed, which was confirmed by plateau width.

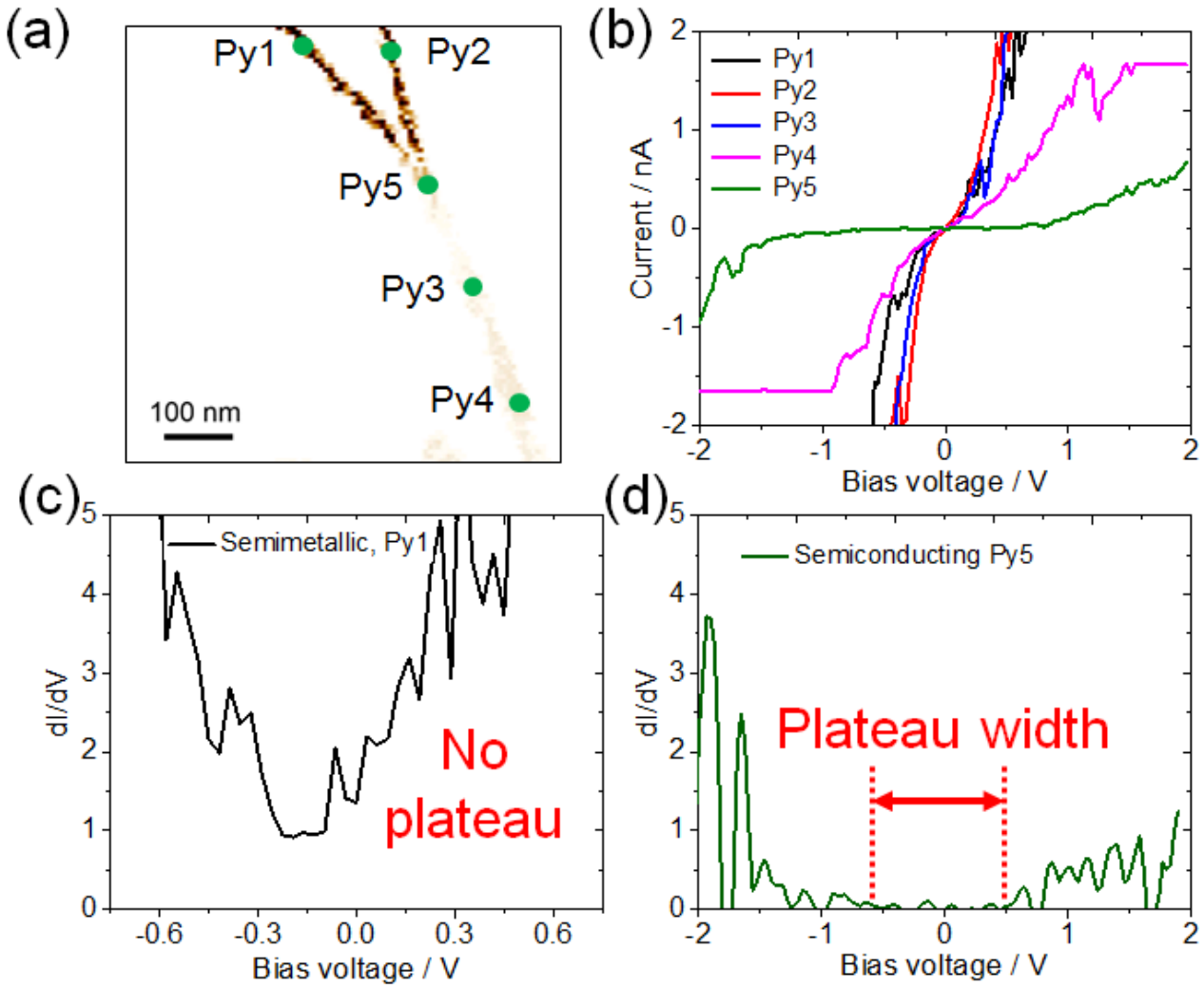

Figure 5.7 Electrical property of Y-type GNR obtained from PCI-AFM. (a) Topographic current image. (b) I-V curve obtained at the different point of Y-type GNR. (c) Extracted plateau width of semimetallic GNR. (d) Plateau width of semiconducting GNR at the junction.

Next, the electrical property of Y-type GNR was also investigated. The topographic image of the Y-type GNR is shown in **Figure 5.7 (a).** I-V curve was observed at several points as indicated in the topographic image. All the points Py1, Py2, Py3, and Py4 shows the semimetallic property except the junction point Py5 as shown in **Figure 5.7 (b).** The phenomenon is similar to X-type junction. The lattice stacking at the junction is changed thus, the property of GNR changed at the junction. Hence, it is confirmed that the x and Y-type junction has semiconducting property and the rest part of GNR is semimetallic.

Furthermore, the plateau width of the Y-type junction and the plateau width of a metallic GNR was also extracted to confirm electrical transport property of Y-type GNR as shown in **Figure 5.7 (c and d)**. **Figure 5.7 (c)** has no plateau width which confirms there is no any bandgap in the GNR is semimetallic. However, **Figure 5.7 (d)** has the plateau width, suggesting there is a finite band gap at the junction of Y-type GNR and has semiconducting property at the junction. Thus, the nanoribbons having over 10 nm width are considered to be semimetallic as reported from some of the theoretical and experimental calculations. It is also well-known that if it would be smaller than 10 nm, the GNR will be semiconductor due to charge carrier confinement, and edge of the nanoribbon also has effect on the property of GNR.

5.6 Conclusion

The synthesis of X- and Y-type GNRs were successfully performed. Electrical transport property of GNR at different points of X and Y cross junctions were investigated. It was observed that the property of GNR at the junction is different as compared to other part of the GNR. The semiconducting property at the junction was obtained and confirmed by extracting the plateau width. The obtained plateau width suggests the finite opening of bandgap at the junction of X, Y-type GNR whereas other parts have no bandgap. Different plateau width was observed at different

X-type junction and the variation in plateau width was supposed to be due to changes in lattice stacking angles at the different X-type junction of GNR. However, some junction shows no plateau width, the reason for this is supposed the AB stacking of GNR at those junctions and in-plane electron transmission.

5.7 References

[1] Chen D, Tang L and Li J 2010 Graphene-based materials in electrochemistry *Chem. Soc. Rev.* **39** 3157-80

[2] Dean C R, Young A F, Meric I, Lee C, Wang L, Sorgenfrei S, Watanabe K, Taniguchi T, Kim P and Shepard K 2010 Boron nitride substrates for high-quality graphene electronics *Nat. Nanotechnol.* **5** 722-6

[3] Kosynkin D V, Higginbotham A L, Sinitskii A, Lomeda J R, Dimiev A, Price B K and Tour J M 2009 Longitudinal unzipping of carbon nanotubes to form graphene nanoribbons *Nature* **458** 872-6

[4] Jiao L, Zhang L, Wang X, Diankov G and Dai H 2009 Narrow graphene nanoribbons from carbon nanotubes *Nature* **458** 877-80

[5] Shinde D B, Debgupta J, Kushwaha A, Aslam M and Pillai V K 2011 Electrochemical unzipping of multi-walled carbon nanotubes for facile synthesis of high-quality graphene nanoribbons *J. Am. Chem. Soc.* **133** 4168-71

[6] Geim A K 2009 Graphene: status and prospects *Science* **324** 1530-4

[7] Geim A K and Novoselov K S 2007 The rise of graphene *Nat. Mater.* **6** 183-91

[8] Nguyen V H, Nguyen H-V and Dollfus P 2014 Improved performance of graphene transistors by strain engineering *Nanotechnol.* **25** 165201

[9] Ni Z H, Yu T, Lu Y H, Wang Y Y, Feng Y P and Shen Z X 2008 Uniaxial strain on graphene: Raman spectroscopy study and band-gap opening *ACS Nano* **2** 2301-5

[10] Terrones M, Botello-Méndez A R, Campos-Delgado J, López-Urías F, Vega-Cantú Y I, Rodríguez-Macías F J, Elías A L, Munoz-Sandoval E, Cano-Márquez A G and Charlier J-

C 2010 Graphene and graphite nanoribbons: Morphology, properties, synthesis, defects and applications *NANO TODAY* **5** 351-72

[11] Tanaka H, Arima R, Fukumori M, Tanaka D, Negishi R, Kobayashi Y, Kasai S, Yamada T K and Ogawa T 2015 Method for controlling electrical properties of single-layer graphene nanoribbons via adsorbed planar molecular nanoparticles *Sci. Rep.* **5** 12341

[12] Otsuka Y, Naitoh Y, Matsumoto T and Kawai T 2002 A nano tester: a new technique for nanoscale electrical characterization by point-contact current-imaging atomic force microscopy *Jpn. J. Appl. Phys.* **41** L742

[13] Botello-Méndez A R, Cruz-Silva E, Romo-Herrera J M, López-Urías F, Terrones M, Sumpter B G, Terrones H, Charlier J-C and Meunier V 2011 Quantum transport in graphene nanonetworks *Nano Lett.* **11** 3058-64

[14] Latil S, Meunier V and Henrard L 2007 Massless fermions in multilayer graphitic systems with misoriented layers: Ab initio calculations and experimental fingerprints *Phys. Rev. B* **76** 201402

[15] Wang X, Ouyang Y, Li X, Wang H, Guo J and Dai H 2008 Room-temperature all-semiconducting sub-10-nm graphene nanoribbon field-effect transistors *Phys. Rev. Lett.* **100** 206803

[16] Jayasekera T and Mintmire J 2007 Transport in multiterminal graphene nanodevices *Nanotechnol.* **18** 424033

[17] Areshkin D A and White C T 2007 Building blocks for integrated graphene circuits *Nano Lett.* **7** 3253-9

CHAPTER 6

Conclusion

This work mainly emphasizes on investigating the electrical property of graphene nanoribbon (GNR). Furthermore, the electrical property of GNR was tuned to semiconducting by the adsorption of molecular nanoparticle. Great effort was made in tuning the electrical property of GNR to open the band gap in synthesized GNR. In this step, the synthesis of high-quality GNR has an important role, in investigating the physical and electrical property of GNR. The single-layer GNR (sGNR) was successfully synthesized with the high percentage ratio of GNR, which was approximately 90 %. The electrical property of pristine GNR was investigated which shows semimetallic behavior since the GNR has width was more than 10 nm. Previous reports have highlighted that the GNR with less than 10 nm width has quasi-one-dimensional charge carrier confinement, which results in a finite band gap opening with high carrier mobility and on/off ratio.[1] Based on this theory the electrical property of sGNR was altered by the adsorption of the HAT-CN6 molecular nanoparticle. It is an acceptor[2] type molecule in nature forming the carrier trapping site at the GNR and thus, the formation of the neck region. The neck region works similar to narrow width GNR and hence the semiconducting behavior in our device was observed. Metal to p-type semiconductor transition was observed by adsorption of flat organic molecule HAT-CN6. The results obtained by field effect transistor (FET) measurement and the point contact current imaging (PCI-) AFM confirms the transition in electric property of sGNR. In addition, it was also confirmed that the HAT-CN6 is the strong contender molecular nanoparticle to open the band gap in GNRs that are wider than 10 nm. The possible reason for opening the band gap in sGNR was also suggested. The observed plateau width was in proportion to the number of nanoparticles

adsorbed on sGNR. The activation energy was also investigated by temperature dependent electrical measurement. The technique of opening bandgap could be promising for next generation semiconductor industry.

Moreover, the multi-layer GNR (mGNR) was also synthesized and the electrical property was investigated. The GNR layers were grown by CVD process[3, 4] on the pre-synthesized GNR unzipped from double-walled carbon nanotubes (DWNTs). The synthesized mGNR has turbostratic structure and hence the reduced inter layer coupling.[5] Thus, there were low inter layer interaction and the device can achieve property of sGNR with higher conductivity and on/off ratio.[6] The fabricated FET device shows the reasonable gate dependence modulation in the transfer curve. The device was changed to clear p-type with improved on/off ratio after the adsorption of flat organic molecule HAT-CN6. The obtained results suggest the formation of the neck and the clear change in an electrical property of mGNR-FET device was observed with HAT-CN6. The concentration of nanoparticle has a great impact in opening the band gap in GNR device. The activation energy was also calculated with the temperature dependence measurement. Such a technique could be used for a high-speed switching device in near future.

The work also has a brief description of the various other techniques used to synthesize the GNR. In addition, the other 2D materials beyond the carbon-based materials are also attracting great interest in the research fields which could be one of the candidates for the next generation of electronics. It still needs the intensive research and study for unveiling the fundamental and physical properties and applications of 2D materials.

Moreover, the fabrication of X- and Y-type GNR cross junction were also successfully performed. The electrical property of GNR at different points of x and y cross junctions was investigated. It was observed that the property of GNR at the junction is different as compared to

other part of the GNR. The semiconducting property at the junction was obtained with the varying plateau width. The variation in plateau width was supposed to be due to changes in lattice stacking at the different angles of GNR. However, some junction shows no plateau width, the reason for this is supposed the AB stacking of GNR and in-plane conduction at those junctions.[7]

6.1 Scope of the thesis

The electrical property of the pristine sGNR synthesized from DWNT was investigated which shows semimetallic behavior since the GNR has width more than 10 nm. The property was tuned to semiconducting by use of molecular nanoparticles. This makes the great scope of such a GNRs in the semiconductor industry, which could be used in future for semiconductor device applications. The on/off ratio of mGNR-FET device was also improved with the use of molecular nanoparticles, which can be applied for high-speed switching devices.

Moreover, the X- and Y-type junctions were also fabricated with the GNRs obtained from DWNTs. The junction shows the semiconducting property, which could be used for wiring applications as well as the device semiconducting device at the junctions.[8]

6.2 References

[1] Li X, Wang X, Zhang L, Lee S and Dai H 2008 Chemically derived, ultrasmooth graphene nanoribbon semiconductors *Science* **319** 1229-32

[2] Chifotides H T, Schottel B L and Dunbar K R 2010 The π-Accepting Arene HAT (CN) 6 as a Halide Receptor through Charge Transfer: Multisite Anion Interactions and Self-Assembly in Solution and the Solid State *Angew. Chem. Int. Ed.* **49** 7202-7

[3] Negishi R, Hirano H, Ohno Y, Maehashi K, Matsumoto K and Kobayashi Y 2011 Layer-bY-layer growth of graphene layers on graphene substrates by chemical vapor deposition *Thin Solid Films* **519** 6447-52

[4] Negishi R, Hirano H, Ohno Y, Haehashi K, Matsumoto K and Kobayashi Y 2011 Thickness Control of Graphene Overlayer via Layer-bY-Layer Growth on Graphene Templates by Chemical Vapor Deposition *Jpn. J. Appl. Phys.* **50** 06GE4

[5] Kumar V, Rakheja S and Naeemi A 2011 Modeling and optimization for multi-layer graphene nanoribbon conductors: IEEE) p 1-3

[6] Dos Santos J L, Peres N and Neto A C 2007 Graphene bilayer with a twist: electronic structure *Phys. Rev. Lett.* **99** 256802

[7] Botello-Méndez A R, Cruz-Silva E, Romo-Herrera J M, López-Urías F, Terrones M, Sumpter B G, Terrones H, Charlier J-C and Meunier V 2011 Quantum transport in graphene nanonetworks *Nano Lett.* **11** 3058-64

[8] Awano Y 2009 Graphene for VLSI: FET and interconnect applications: IEEE) p 1-4

ACHIEVEMENTS AND AWARDS

1. KDDI Foundation Scholarship (April 2016- March 2017), Japan
2. Kyutech 100 Anniversary Scholarship (April 2015- March 2016), Japan
3. Junior Specialist (February 2015- March 2015), Univ. of California, USA
4. JASSO Scholarship (April 2014- March 2015), Japan

LIST OF PUBLICATIONS

Paper publications

1 R. R. Pandey, M. Fukumori, A. TermehYousefi, M. Eguchi, D. Tanaka, T. Ogawa and H. Tanaka: Tuning the electrical property of single-layer graphene nanoribbon by adsorption of planar molecular nanoparticles (Published online Nanotechnology 2017)

2 M. Fukumori, R. R. Pandey, T. Fujiwara, A. TermehYousefi, R. Negishi, Y. Kobayashi, H. Tanaka, T. Ogawa: Diameter dependence of longitudinal unzipping of single-walled carbon nanotube to obtain graphene nanoribbon (Published online JJAP 2017)

3 A. TermehYousefi, M. Fukumori, R. R. Pandey, P. Liu, L. Fu, S. Bagheri, H. Tanaka: Progress on nanoparticle-based carbon nanotube complex: fabrication and potential application, Rev. Inorg. Chem. 4, 83–201 (2016).

4 R. R. Pandey, R. Negishi, A. TermehYousefi, Y. Kobayashi, H. Tanaka: Fabrication of turbostratic multi-layer graphene nanoribbon field effect transistor and investigating its electrical property with the adsorption of HAT-CN6 (Under submission)

5 R. R. Pandey, T. Fujiwara, P. Liu, A. TermehYousefi, H. Tanaka: Fabrication of X- and Y-type graphene nanoribbon cross junction and investigating it's electrical transport properties (Under submission)

6 A. TermehYousefi, R. R. Pandey, F. Budiman, Hadiyawarman, H. D. G. Hernowo, H. Tanaka: Nanomaterial Based Neuromorphic Engineering: Toward Fabrication of Memristive Devices with High Speed Signal Processing and Low Power Consumption (Submitted, Nanotechnology 2017)

Conferences

1. R. R. Pandey, H. Tanaka: (2016) "Fabrication of single-layer graphene nanoribbon field effect transistor and controlling its property using planar molecules" 4th International Symposium on Applied Engineering and Sciences (SAES2016), Kyushu Institute of Technology, Tobata, Japan

2. R. R. Pandey, A. TermehYousefi, H. Tanaka: (2016) "Altering the electronics property of graphene nanoribbon by adsorption of molecular nanoparticles" conference paper on 77th JSAP, Niigata city, Japan

3. R. R. Pandey, A. TermehYousefi, H. Tanaka: (2016) "High yield synthesis of single-layer graphene nanoribbon and controlling its electronic property" conference paper on Molarch 5th meeting, Kyushu University, Fukuoka, Japan.

4. R. R. Pandey, P. Liu, H. Tanaka: (2016) "Extraction of bandgap in graphene nanoribbon by adsorption of molecular nanoparticle" conference paper on 29th International Microprocesses and Nanotechnology Conference (29^{th}-MNC) Kyoto, Japan.

5. R. R. Pandey, G. R. Abel Jr, Tao Ye, H. Tanaka: (2015) "Self-assembly of precise gold nanoparticle arrays on DNA origami tiles for nanophotonics and nanoelectronics" Conference paper on India-Japan expert group meeting on biomolecular electronics and organic nanotechnology for environment preservation (IJEGMBE), Tobata, Japan.

6. R. R. Pandey, G. R. Abel Jr, T. Ye, H. Tanaka: (2015) "High yield fabrication of gold nanoparticle assemblies on DNA origami templates" an international conference paper on PACIFICHEM-2015, Hawaii, USA.

7. R. R. Pandey, H. Tanaka: (2015) "Electrical circuit model for neuron firing device by negative differential resistance junctions components" conference paper on 62nd JSAP, Nagoya, Japan.